Charles University
Faculty of Science

STUDY PROGRAMME: INORGANIC CHEMISTRY (4XANOR)

Mgr. Peter Urbanovský

COMPLEXES OF CYCLEN-BASED MACROCYCLIC LIGANDS WITH A PHOSPHINATE PENDANT ARM

(Komplexy makrocyklických ligandů odvozených od cyklenu mající fosfinátovou pendantní skupinu)

Doctoral Thesis

Supervisor: prof. RNDr. Petr Hermann, PhD

Prague, 2020

Prohlášení

Tímto prohlašuji, že jsem tuto závěrečnou práci vypracoval samostatně a že jsem uvedl všechny použité literární zdroje. Tato práce a ani její část nebyla použita k získání žádného jiného nebo stejného akademického titulu.

Declaration

Hereby I declare that this Thesis is my original work and that I have properly cited all the information resources. This work or its any part has not been submitted for any other or for the same academic degree.

_____

In Prague, July 2020 Peter Urbanovský

Content

Abstract

Lanthanide(III) complexes of DOTA derivatives are utilized in the medical imaging techniques such as magnetic resonance imaging (MRI), magnetic resonance angiography (MRA), and magnetic resonance spectroscopy (MRS), nuclear imaging (PET and SPECT), or optical methods (luminescence).

It has been shown that relaxometric parameters of the Gd(III) complexes of DOTA derivatives with a phosphinic acid pendant arm (Gd–DO3AP^{R}) can reach optimal values (*e.g.* water residence time, τ_M, being close to ~10 ns). The relaxometric parameters can be further modified through the phosphorus substituents. It is also known that the complexes possess a high thermodynamic stability and they are kinetically inert. The main goal of this Thesis is an investigation of the effect of pendant amino group protonation in substituents bound to the phosphorus atom on properties of the complexes. Thus in this Thesis, DOTA derivatives with the phosphinic acid pendant arm with an amino group and their complexes were prepared and characterized. The complexes are intended as contrast agents for molecular imaging techniques (mainly for MRI and ^{31}P MRS).

The first part of the Thesis introduces two new versatile "phospha-Mannich" protocols performed under mild conditions. Amino-*H*-phosphinic acids (AHPAs) were synthesized with excess of the appropriate aldehyde and equimolar amounts of secondary amine and hypophosphorous acid utilizing acetic acid as a solvent (Figure A1). Secondary amines with pK_A > ~8 showed very high conversions to AHPAs which were mostly purified only by a simple ion-exchange chromatography and were isolated in high yields. A small library (~40 compounds) of *α*-aminoalkyl-*H*-phosphinic acids was prepared. For a less nucleophilic secondary amines (pK_A < ~7) and polyamines with the ethylene-diamine fragment, reductive *N*-methylation coupled with hypophosphorus acid oxidation were observed as the main reactions. A mechanism of the AHPA synthesis was proposed. It involves initial *N*-hydroxymethylation of the secondary amine and esterification of the hydroxogroup with acetic acid. It is probably followed by trans-esterification with H_3PO_2 and re-arrangement of the hypophosphorous acid ester to the final product with P–C bond, AHPA.

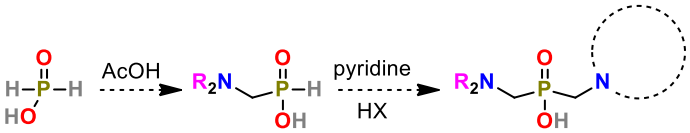

Figure A1

The target cyclen-based ligands with phospho(i)nate pendant arms were prepared by a new variant of Kabachnik–Fields reaction of a cyclen derivative, an

alkyl *H*-phosphinate / H–P(O)(OEt)$_2$ and formaldehyde in anhydrous pyridine as a solvent (Figure A1). The reaction requires a strong acid (*e.g.* HBr) as a catalyst and proceeds with almost quantitative conversion. Reaction was successfully tested on several model compounds. Reaction mechanistic investigations suggested an initial formation of an aminal (>N–CH$_2$–N<) and its fast acid-catalyzed decomposition to iminium species ((>N=CH$_2$)$^+$ X$^-$) which reacted with the phosphorus acid ester with the P–H bond, likely in its tautomeric trivalent form.

Lanthanide(III) complexes of the macrocyclic ligands of the DO3AP^R type with phosphorus-bound group containing a hydrophobic amine were investigated as contrast agents (CAs) for MRA whose properties are altered with (de)protonation of the pendant amino group (Figure A2). Based on TSA / SA isomer abundance in the Ln(III) complexes, the Gd(III) complexes coordinate one water molecule regardless of pH. The Gd(III) complexes have a high TSA isomer abundance (~50–70 %) which is dependent on protonation of the pendant amino group (pK_A 5–7). The Gd(III) complexes with the deprotonated pendant amino group (*i.e.* at pH > 7–8) have an extraordinary short water residence time (τ_M down to ~5 ns at 25 °C) because of it easily accessible octa-coordinated transient state. In the presence of human serum albumin (HSA), relaxivity of the Gd(III) complexes is significantly increased (5–10-times, the highest observed relaxivity was r_{1p} ~55 mM^{-1} s^{-1}; 20 MHz, 37 °C, pH = 7.4) due to the formation of a supramolecular adducts of the complexes with HSA. Strength of the complex–HSA interaction depends on pH and the complexes with the protonated pendant amino group have 1–2 orders of magnitude lower affinity to HSA than that of the deprotonated complexes. Surprisingly, relaxivity of the protonated and deprotonated complexes if theoretically fully bound to HSA (*i.e.* relaxivity of the "pure" CA–HSA conjugate) is almost identical. The concept of the binding / release of molecules to / from its conjugate with HSA triggered by their protonation is an interesting new approach to altering drug pharmacokinetics.

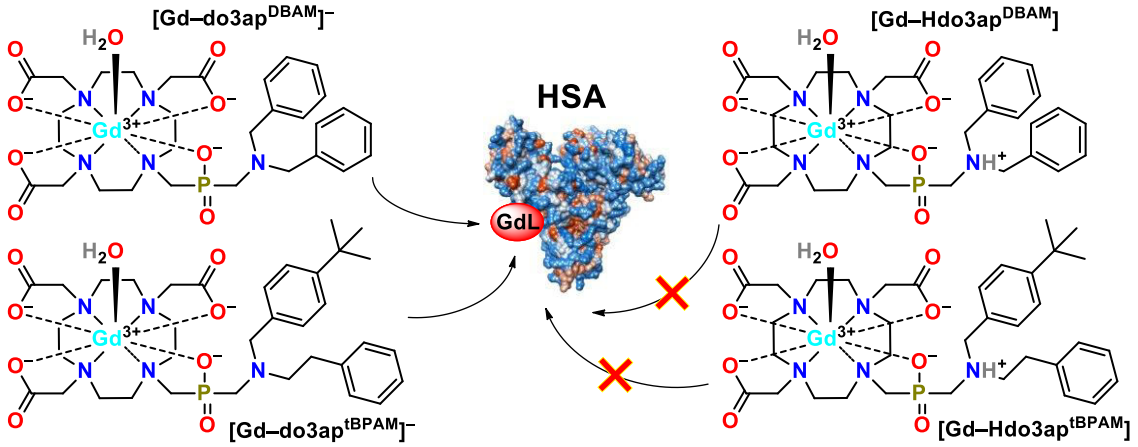

Figure A2

The Ln(III) complexes of the ligands were also investigated by single-crystal X-ray diffraction (17 structures). Results confirmed increase of Ln(III)–OH_2 bond length which is coupled with shorter Ln(III)–QN_4 distance with smaller Ln(III) ions. This large set of structures was compared with structures of Ln(III) complexes of the other DOTA-like ligands. Opening angles ω of Gd–DO3AP^R complexes are smaller than those of Gd–DOTA but still large enough to allow coordination of one water molecule. Hence, the "anhydrous" octa-coordinated transient state of Gd(III) ion during the water exchange is more accessible for the Gd–DO3AP^R complexes than for the Gd–DOTA complex and, thus, water exchange on Gd–DO3AP^R is faster.

The Ln(III) complexes of ligand with primary amino group, DO3AP^{AM} (Figure A3), are the simplest Ln–DO3AP^R whose properties are affected by the pendant amine (de)protonation. The properties of the Ln–DO3AP^{AM} complexes were compared with that of the Ln(III) complexes of the ligand DO3AP^{AcAM} (Figure A3) whose properties cannot be changed with pH. The TSA / SA isomers abundance of their Ln(III) complexes and determination of hydration number (Dy(III)-induced water ^{17}O chemical shift and Eu(III) luminescence) clearly showed presence of monoaqua Gd(III) species regardless of pH. Water residence times are not as extremely short (τ_M ~40 and ~32 ns for Gd–DO3AP^{AM} and Gd–DO3AP^{AcAM}, respectively; at 25 °C, pH ~7) as for the complexes discussed above but still significantly shorter than that for Gd–DOTA. It is likely caused by a more distant hydration break to Gd(III) within the Ln(III) series for Ln–DO3AP^{AM} / Ln–DO3AP^{AcAM}. Surprisingly, relaxivity of Gd–DO3AP^{AM} is not affected by pH and, thus, by protonation state of the amino group (pK_A ~8.3). Relaxivity is lower than expected – it can be caused by a low "effective hydration number q_{eff}" of ~0.8 (at pH ~7) determined by fitting of the measured data.

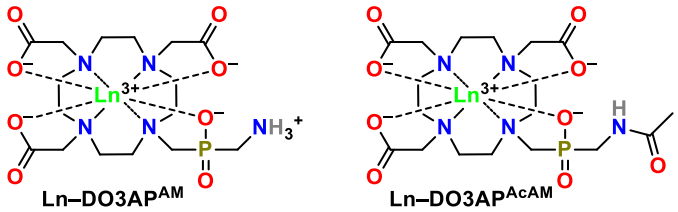

Figure A3

The Ln–DO3AP^{AM} complexes have protonable pendant amine in the proximity to phosphorus atom and, thus, ^{31}P NMR properties were dependent on pH. The coordinated paramagnetic metal ions induced short ^{31}P NMR relaxation times (down to small "ms" scale) as well as expansion of difference (up to tens of ppm) between ^{31}P NMR resonance frequencies of the (de)protonated forms of the complexes. The ^{31}P NMR chemical shifts of the complexes are shifted by tens-to-hundreds ppm away from those of endogenous phosphorus-containing compounds. However, the

pendant amino group pK_A ~8.3 is well above the *in vivo* pH range and the (T_2*/T_1) ratio of ^{31}P nucleus is the best, 0.4–0.7, for complexes with very short T_1 (1–7 ms). Thus, the research is a *proof-of-concept* study which confirmed that the protonable Ln–DO3AP^R complexes can be used as novel CAs for ^{31}P MRS imaging to describe pH *in vivo*; however, the basicity of the complexes has to be further tuned.

The last part of the Thesis introduces a ditopic DO3A–P–DO3A ligand (Figure A4) which has become available by the new Kabachnik–Fields reaction. The ligand structure allows preparation of thermodynamically stable and kinetically inert mono- and either homo- or heteronuclear dimetallic complexes (Figure A4). Metal ions in the dimetallic complexes are connected *via* bridging phosphinate group. It was confirmed in the solid state by single-crystal X-ray diffraction (six structures). The dimetallic complexes showed a complicated isomerism where the TSA / SA isomerism of the macrocyclic chelates is combined with chiral centre located on the phosphorus atom. Up to eight different diastereoisomers were observed in the solution but three-to-four diastereoisomers are the major isomers (overall sum > 85 %). The relaxometric evaluation of the Gd$_2$(III) complex revealed an unexpectedly short water residence time (τ_M ~7 ns at 25 °C) probably connected with the hydration break just behind Gd(III) in the Ln(III) series (determined by Eu(III) and Tb(III) luminescence). It leads to easily accessible octa-coordinated state in the Gd$_2$(III) complex. In the dinuclear complexes, the proximity of two paramagnetic ions connected *via* the phosphinate bridge seemingly does not significantly alter their electronic relaxation times. Hetero-dimetallic complexes GdM–(DO3A–P–DO3A) (Figure A4), where M is a trivalent metal ion (*e.g.* Sc(III), La(III), Bi(III)), were investigated to assess a possible relaxivity dependence of relaxivity on the total weight of molecules. However, the complexes showed no relaxivity dependence on molecular mass of the second coordinated ion and it was instead determined by the TSA / SA isomerism.

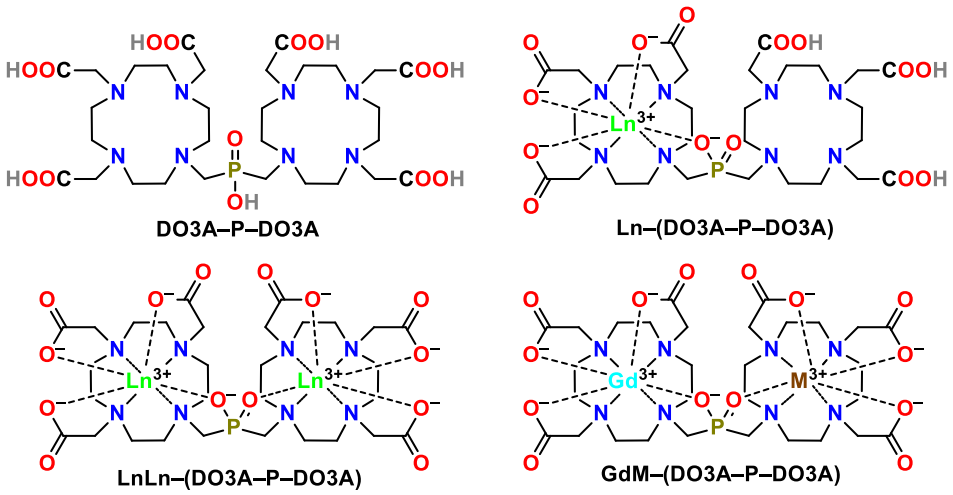

Figure A4

Abstrakt (česky)

Komplexy lanthanoidů(III) s deriváty DOTA jsou využívány pro zobrazování pomocí magnetické tomografie (MRI), magnetické rezonanční angiografie (MRA) nebo magnetické rezonanční spektroskopie (MRS). Tyto komplexy jsou také používány v nukleární medicíně (PET a SPECT) a pro zobrazování pomocí optických metod (luminiscence).

Je známo, že relaxometrické vlastnosti komplexů Gd(III) s deriváty DOTA obsahujících jednu fosfinovou skupinu jako pendantní rameno, Gd–DO3AP^{R}, mohou být blízké optimálním (např. rezidenční čas koordinované molekuly vody, τ_M, může dosáhnout optimální hodnoty ~10 ns). Relaxometrické parametry lze dále ladit pomocí substituentu na atomu fosforu. Je také známo, že tyto komplexy mají vysokou termodynamickou stabilitu a jsou kineticky inertní. Hlavním cílem této práce je zjistit, jak protonizace aminoskupiny přítomné v substituentu na atomu fosforu bude ovlivňovat vlastnosti těchto komplexů. V této práci byly připraveny a charakterizovány deriváty DOTA s jedním fosfinátovým pendantním ramenem obsahujícím aminoskupinu a jejich komplexy. Tyto komplexy by mohly posloužit jako kontrastní látky pro molekulární zobrazování pomocí MRI nebo ^{31}P MRS.

První část této práce je věnována dvěma „fosfa-Mannichovým“ reakcím, které probíhají za mírných podmínek. Amino-*H*-fosfinové kyseliny (AHPA) byly syntetizovány s použitím přebytku patřičného aldehydu a ekvimolárních množství sekundárního aminu a kyseliny fosforné v kyselině octové jako rozpouštědle (Obrázek 1). Sekundární aminy s pK_A > ~8 poskytovaly příslušné AHPA s vysokou konverzí. Získané AHPA byly většinou čištěny jen pomocí silného kationtového iontoměniče a byly izolovány ve vysokých výtěžcích. Byla připravena malá knihovna α-aminoalkyl-*H*-fosfinových kyselin (~40 sloučenin). Pro méně nukleofilní aminy (pK_A < ~7) a polyaminy s ethylen-diaminovým fragmentem byla jako hlavní reakce pozorována reduktivní *N*-methylace, která je spojená s oxidací kyseliny fosforné. Byl navržen mechanismus reakce syntézy AHPA. Jako první reakce byla pozorována *N*-hydroxymethylace sekundárního aminu následovaná esterifikaci této hydroxy skupiny octovou kyselinou. Poté pravděpodobně dochází k trans-esterifikaci s H_3PO_2 a vzniklý ester H_3PO_2 se přesmykuje na konečný produkt s P–C vazbou, AHPA.

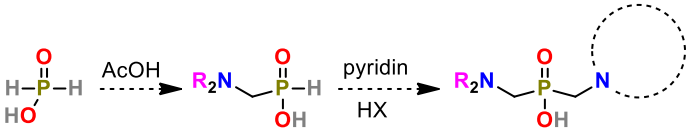

Obrázek 1

Deriváty cyklenu s fosfo(i)nátovými pendantními rameny byly připraveny novou variantou „Kabachnik–Fields“ reakce, ve které reaguje derivát cyklenu, alkyl ester *H*-fosfinové kyseliny nebo H–P(O)(OEt)$_2$, a CH_2O v bezvodém pyridinu jako rozpouštědle (Obrázek 1). Reakce musí být katalyzována silnou kyselinou (např. HBr) a pak probíhá s téměř kvantitativní konverzí. Reakce umožnila přípravu několika modelových látek. Byl navržen její reakční mechanismus, kdy nejprve vzniká aminal, >N–CH_2–N<, který se silnou kyselinou rychle rozkládá na iminiovou sůl, $(>N{=}CH_2)^+$ Cl^-. Tato sůl reaguje s P–H vazbou esteru fosforové kyseliny. Reaktivním intermediátem je pravděpodobně tautomer s trojmocným atomem fosforu.

Komplexy Ln(III) a makrocyklických ligandů typu DO3AP^R, které obsahují hydrofobní aminomethylovou skupinu vázanou na atom fosforu, byly zkoumány jako kontrastní látky (CAs) pro MRA. Jejichž vlastnosti jsou ovlivněny (de)protonací této aminové skupiny (Obrázek 2). Na základě zastoupení izomerů TSA / SA bylo zjištěno, že Gd(III) komplexy koordinují jednu molekulu vody nezávisle na pH. Tyto komplexy mají vysoké zastoupení izomeru TSA (~50–70 %), které se mění s protonaci pendantních aminoskupin majících pK_A 5–7. Komplexy Gd(III) s deprotonovanou aminoskupinou (tj. při pH > 7–8) mají velice krátký rezidenční čas vázané molekuly vody (τ_M až ~5 ns při 25 °C), což se dá vysvětlit snadnou tvorbou okta-koordinovaného komplexu v přechodovém stavu. V přítomnosti lidského sérového albuminu (HSA) se relaxivita těchto komplexů podstatně zvyšuje (5–10-krát; nejvyšší pozorována relaxivita byla r_{1p} ~55 mM^{-1} s^{-1} při 20 MHz, 37 °C a pH 7,4) díky vzniku supramolekulárního aduktu komplex–HSA. Rozsah této interakce se mění s pH a komplexy s protonovanou pendantní aminoskupinou mají o 1–2 řády nižší afinitu k HSA než komplexy deprotonované. Relaxivita protonovaných a deprotonovaných komplexů, jsou-li teoreticky plně navázány na HSA, je překvapivě takřka identická. Koncept navázání / uvolňování molekul na / z jejich aduktů s HSA v závislosti na jejich protonaci je novou a zajímavou možností, jak měnit farmakokinetiku léků.

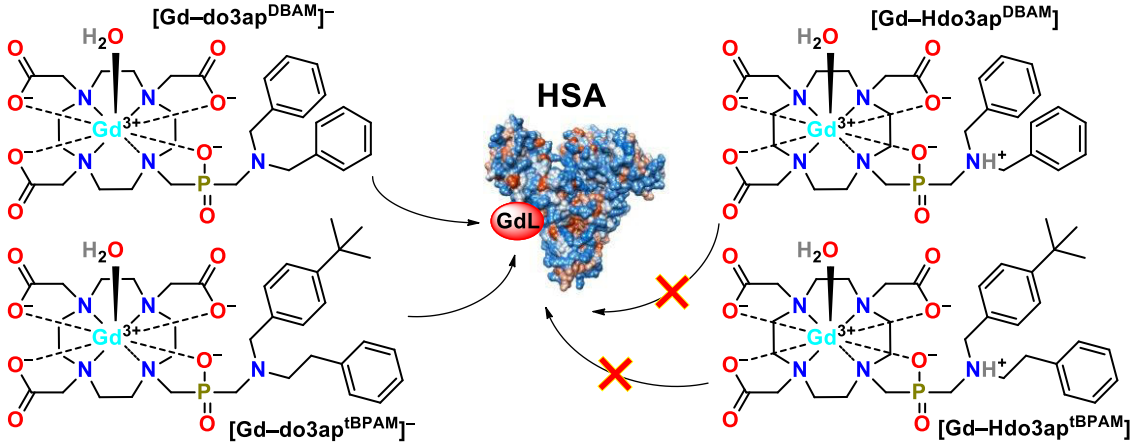

Obrázek 2

Monokrystaly komplexů Ln(III) s těmito ligandy byly také zkoumány pomocí rentgenové difrakce (17 struktur). Výsledky potvrdily prodlužování vazebné vzdálenosti Ln(III)–OH_2 pro menší ionty Ln(III) a to, že se současně zkracuje vzdálenost Ln(III)–QN_4. Tyto struktury byly porovnány se strukturami komplexů derivátů DOTA. „Otevírací úhel“ ω v komplexech Gd–DO3AP^{R} je menší než stejný úhel v Gd–DOTA, ale přitom stále umožňuje koordinaci jedné molekuly vody. „Bezvodý“ okta-koordinovaný přechodový komplex Gd(III) objevující se při výměně koordinované molekuly vody je tedy snáze dostupný pro komplexy Gd–DO3AP^{R} a výměna vody je tímto urychlena.

Komplexy Ln(III) a ligandu s primární aminoskupinou, DO3AP^{AM} (Obrázek 3) jsou nejjednodušší komplexy typu Ln–DO3AP^{R}, jejichž vlastnosti mohou záviset na protonaci aminové skupiny. Chování těchto komplexů bylo srovnáno s chováním komplexů DO3AP^{AcAM} (Obrázek 3), jejichž vlastnosti nemohou být závislé na protonaci aminové skupiny. Zastoupení izomerů SA / TSA v lanthanoidové sérii a sledování hydratace (změna chemického posunu ^{17}O vody indukovaná Dy(III) a luminiscence Eu(III)) jasně ukázalo, že komplex Gd(III) je monohydratován nezávisle na pH. Residenční čas koordinované molekuly vody (τ_M ~40 / ~32 ns pro Gd–DO3AP^{AM} / / Gd–DO3AP^{AcAM}; pro 25 °C, pH ~7) není tak krátký jako u komplexů uvedených výše, ale stále je podstatně kratší než u Gd–DOTA. Je to pravděpodobně způsobeno tím, že voda se nekoordinuje až dále v lanthanoidové řadě. Relaxivita Gd–DO3AP^{AM} v roztocích o různém pH se překvapivě nemění, ačkoli se změní protonace aminoskupiny s pK_A ~8,2. Relaxivita je nižší než očekávaná, což může být způsobeno nižším „efektivním hydratačním číslem q_{eff}“ ~0,8 (pH ~7), které bylo nalezeno při zpracování naměřených dat.

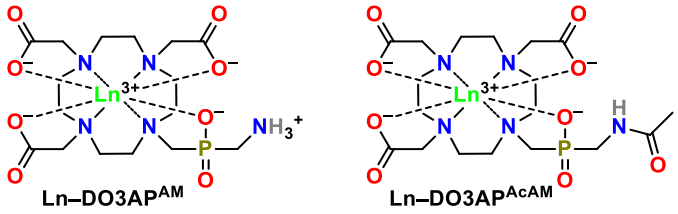

Obrázek 3

V komplexech Ln–DO3AP^{AM} je protonovatelná aminoskupina blízko atomu fosforu, což znamená, že NMR vlastnosti jádra ^{31}P budou záviset na pH. Koordinovaný paramagnetický kation způsobuje jak zkrácení relaxačních časů jádra ^{31}P (až do oblasti „ms“), tak zvětšení rozdílů chemických posunů ^{31}P pro různě protonované komplexy (až desítky ppm). Chemické posuny ^{31}P jsou desítky až stovky ppm jinde, než chemické posuny endogenních fosforových sloučenin. Hodnota pK_A ~8,2 pro aminoskupinu v komplexech je bohužel výše než je obvyklé

fyziologické pH a navíc byl nejlepší poměr T_2^*/T_1 pro jádro ^{31}P (0,4–0,7) nalezen v komplexech s velmi krátkým relaxačním časem T_1 (1–7 ms). Toto vede k tomu, že tato data mohou být pouze pokládána za výzkum dokazující, že protonovatelné komplexy typu Ln–DO3AP^R mohou být pokládány za nové kontrastní látky pro ^{31}P MRS pro zobrazování změn pH tkání *in vivo*. Je ale potřeba najít komplexy s vhodnější bazicitou.

Poslední část této práce se věnuje ditopickému ligandu DO3A–P–DO3A (Obrázek 4), který je dostupný teprve díky nové variantě reakce „Kabachnik–Fields“. Struktura ligandu umožňuje přípravu termodynamicky stabilních a kineticky inertních mono- a dimetalických komplexů, které lze získat, jak homo-, tak jako heteronukleární (Obrázek 4). Ionty kovů v dimetalických komplexech jsou spojeny přes fosfinátovou skupinu. Tato struktura byla potvrzena v pevném stavu pomocí rentgenové difrakce na monokrystalech (6 struktur). Tyto dinukleární komplexy se vyznačují složitou izomerií, kdy se izomerie SA / TSA makrocyklického ligandu kombinuje s chirálním fosforovým atomem. V roztoku bylo pozorováno nejméně osm rozdílných diastereoizomerů, z nichž ale jen tři až čtyři jsou výrazně zastoupeny (v součtu > 85 %). Zpracování relaxometrických dat pro dinukleární komplex Gd$_2$(III) ukázalo neobvykle krátký rezidenční čas koordinované molekuly vody (τ_M ~7 ns při 25 °C), což je pravděpodobně způsobeno blízkostí hydratačního zlomu v lanthanoidové sérii hned za Gd(III) (zjištěno pomocí luminiscencí komplexů Eu(III) a Tb(III)). Blízkost dvou paramagnetických iontů kovů, které jsou v dinukleárních komplexech spojené přes fosfinátový můstek, významně nemění jejich elektronové relaxační časy. Hetero-dimetalické komplexy typu GdM–(DO3A–P–DO3A) (Obrázek 4), kde M je trojmocný kovový kation (např. Sc(III), La(III), Bi(III)) byly zkoumány proto, aby se ověřila možná závislost relaxivity na celkové molekulové hmotnosti komplexu. Ukázalo se, že relaxivita komplexů nezávisí na molekulové hmotnosti, ale je spíše řízena izomerií SA / TSA.

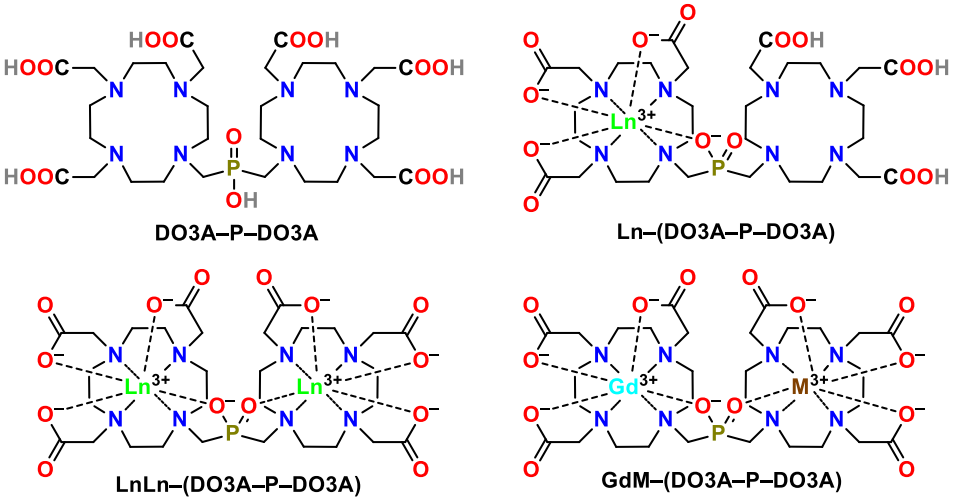

Obrázek 4

Introduction

1 . Aminophosphorus acids

1.1. General introduction

Natural amino acid analogues are an interesting group of compounds which show potent biological effects. Apart from amino carboxylates, aminoalkyl-phosphorus acids (Figure 1) possess unique properties. Tetrahedral phosphorus acids (phosphonic and phosphinic acids, PONs and PINs, respectively) and their derivatives containing α-amino group resemble the common amino acids (Figure 1). They are the compounds mimicking tetrahedral "transition state" of carboxyl group in enzyme active sites during *e.g.* peptide bond hydrolysis. The α-aminoalkyl-phoshonic and α-aminoalkylphosphinic acids have been investigated as highly potent peptidomimicking compounds for a long time.[1]

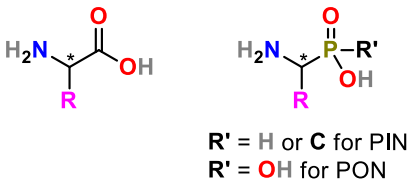

Figure 1 – Structures of α-amino carboxylic acid (left), α-aminoalkyl-phosphonic and α-aminoalkyl-phosphinic acids (right)

Phosphorus-containing organic substances are commonly found in living organism. Generally known derivatives of phosphoric acid are involved in bioenergetics of living cells (*e.g.* ATP and phosphocreatine, Figure 2) or in forming backbone of RNA and DNA. The 2-phosphoenolpyruvate (PEP, Figure 2) is essential molecule in glucose metabolism. In these compounds, phosphorus atom is attached to *O* or *N* atoms. However, compounds with a C–P bond possess some exceptional properties. Focusing only on medicinal applications, these organic phosphorus derivatives have advantage of hydrolytic stability of P–C bond, their great biocompatibity, and effective mimicking the natural amino acids. They have been utilized as potent antibiotics, antimalarics, antihypertensives, or other drugs.[2]

[1] (a) Collinsova, M.; Jiracek, J. Phosphinic acid compounds in biochemistry, biology and medicine. *Curr. Med. Chem.*, 7, **2000**, 629–647. (b) Didi, M. A.; Villemin, D. Phosphonic & aminophosphonic acids synthesis & applications. *Éditions Universitaires Européennes*, **2018**. (c) Kafarski, P. Phosphonates: their natural occurence and physiological role. *IntechOpen*, **2019**, DOI: 10.5772/intechopen.87155.

[2] (a) Abdou, M. M.; O'Neill, P. M.; Amigues, E.; Matziari, M. Phosphinic acids: current status and potential for drug discovery. *Drug Discov. Today*, 24, **2019**, 916–928. (b) Ragulin, V. V. Phosphonic aminocarboxylic acids. *Russ. J. Gen. Chem.*, 88, **2018**, 160–187. (c) Orsini, F.; Sello, G.; Sisti, M. aminophosphonic acids and derivatives. Synthesis and biological applications. *Curr. Med. Chem.*, 17, **2010**, 264–289.

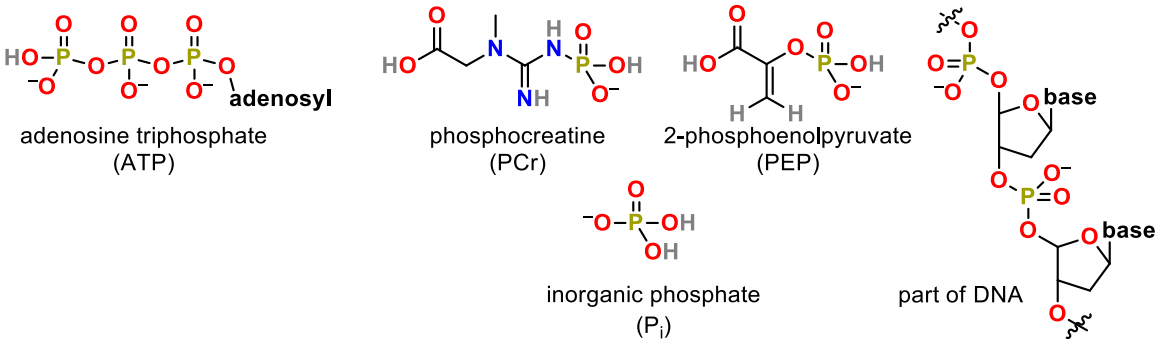

Figure 2 – Examples of phosphoric acid derivatives commonly found in living system

However, P–C bond formation is thermodynamically unfavourable. Lower living organisms (*e.g.* bacteria, archaea, fungi) use enzymes, *e.g.* PEP mutases. The P–C bonds are formed in an isomerisation reaction catalyzed by PEP (Figure 3).[3] To the best of author's knowledge, there is no natural synthetic pathway in human body leading to phosphorus compounds with P–C bond.[4]

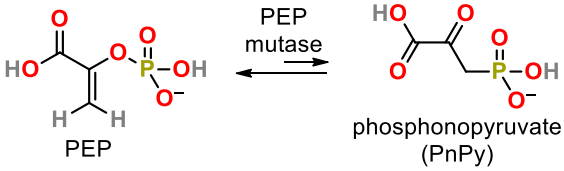

Figure 3 – An enzymatic reaction responsible for formation of P–C bond-containing compounds *in vivo*

The first observation of P–C-containing molecule in living organism dates back to 1959.[5] The 2-AEP (2-aminoethylphosphonic acid, Figure 4) is the most abundantly found compound with P–C bond in nature (especially in marine life forms). Later, many endogenous PONs have been discovered and man-made amino acid analogues prepared. The most important small-molecule PONs discovered in living organism include broad-spectrum antibiotic Fosfomycin (sold under trade name Monurol®; it is a "the last resort" drug effective against antibiotic-resistant bacteria)[6] and the potent antibacterial and antimalarial drug FR-900098 effective even on the drug-resistant strains.[7]

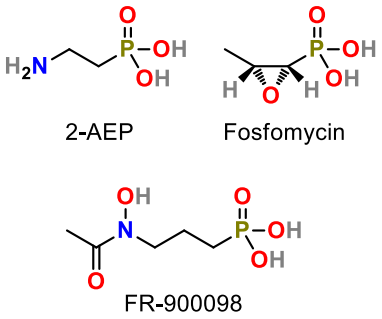

Figure 4 – The examples of P–C compounds found in nature

[3] Seidel, H. M.; Freeman, S.; Seto, H.; Knowles, J. R. Phosphonate biosynthesis: isolation of the enzyme responsible for the formation of a carbon-phosphorus bond. *Nature*, 335, **1988**, 457–458.

[4] Metcalf, W. W.; van der Donk, W. A. Biosynthesis of phosphonic and phosphinic acid natural products. *Annu. Rev. Biochem.*, 78, **2009**, 65–94.

[5] Horiguchi, M.; Kandatsu, M. Isolation of 2-aminoethane phosphonic acid from rumen protozoa. *Nature*, 184, **1959**, 901–902.

[6] Dijkmans, A. C.; Zacarias, N. V. O.; Burggraaf, J. *et al*. Fosfomycin: pharmacological, clinical and future perspectives. *Antibiotics*, 6, **2017**, 24.

[7] Edwards, R. L.; Brothers, R. C.; Wang, X. *et al*. MEPicides: potent antimalarial prodrugs targeting isoprenoid biosynthesis. *Sci. Rep.*, 7, **2017**, 8400.

Aside from the natural phosphonates, man-made PONs (*e.g.* those in Figure 5) contributed to the many industrial, agricultural, and medical breakthroughs.[8] The most known (and used) are undoubtedly the herbicide glyphosate,[9] amino-bis-phosphonate-containing osteoporosis drugs (*e.g.* alendronate),[10] and the antivirals (*e.g.* tenofovir).[11] Some excellent reviews,[1c,2a,12] thorough papers and books have been recently published on chemistry of the P–C bond.

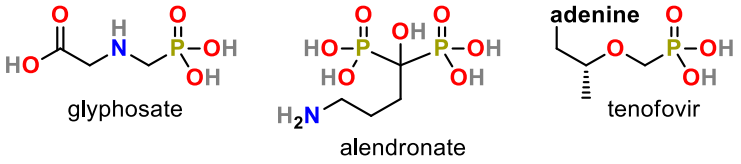

Figure 5 – Well-known and widely used xenogenic PONs

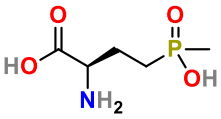

Figure 6 – The most known biogenic PIN, phosphinothricin

Apart from PONs, natural PINs compounds with C–P–C or C–P–H fragments are very rarely found in living organisms. The most known biogenic PINs are phosphinothricin-containing oligopeptides (Figure 6). These compounds are used as efficient herbicides in agriculture and also possess strong antimicrobial activity.

Moreover, synthetic PINs are progressively employed in pharmacy as drugs and they have been investigated in more detail only relatively recently. Several PINs have been suggested for treatment of malicious diseases like Alzheimer, hepatitis, influenza, HIV, malaria, and cancer, or a simple inflammation and parasitic infections.[2a]

Overall, amino derivatives of PONs and PINs play an important role in our lives. They are potent inhibitors of many biological processes due to their resemblance to the biogenic amino acids. Scope of their utilization may be expanded to agriculture, hydrometallurgy, industry, and diagnostic medicine.

---

[8] (a) Demkowicz, S.; Rachon, J.; Dasko, M.; Kozak, W. Selected organophosphorus compounds with biological activity. Applications in medicine. *RSC Adv.*, 9, **2016**, 7101–7112. (b) Acton, Q. A. Organophosphorus compounds – advances in research and application: 2013 Edition. *ScholarlyEditions*™, Atlanta, Georgia, **2013**. ISBN: 978-1-481-69071-3.

[9] Duke, S. O.; Powles, S. B. Glyphosate: a once-in-a-century herbicide. *Pest Management Sci.*, 64, **2008**, 319–325.

[10] Russell, R. G. G.; Watts, N. B.; Ebetino, F. H.; Rogers, M. J. Mechanism of action of bisphosphonates: similarities and differences and their potential influence on clinical efficacy. *Osteoporos. Int.*, 19, **2008**, 733–759.

[11] Lyseng-Williamson, K. A.; Reynolds, N. A.; Plosker, G. L. Tenofovir disoproxil fumarate: a review of its use in the management of HIV infection. *Drugs*, 65, **2005**, 413–432.

[12] Pallitsch, K.; Kalina, T.; Stankovic, T. Synthetic phosphonic acids as potent tools to study phosphonate enzymology. *Synlett*, 30, **2019**, 770–776.

1.2. Methods for synthesis of P–C bonds

1.2.1. Synthesis of phosphonic acids

Understanding the principles of P–C bond formation is crucial for preparation of versatile phosphorus-containing compounds. Synthetic approaches of phosphonic acids had been studied for a long time and the chemistry is rather well-explored.[13] The most frequent approaches employ precursors / intermediates with the trivalent phosphorus atom (*i.e.* P(III)). Generally, phosphorus compounds are presumed to be present in their P(III) tautomeric state which ultimately reacts with other reagents.

Trialkyl phosphites are commonly utilized as starting materials in nucleophilic substitutions with alkyl- or arylhalides, or in attacks on susceptible double bonds (*e.g.* double bond in alkenes or in carbonyl compounds) to form phosphonates (the reactions are summarized in Figure 7). Reaction of the phosphites with alkylhalides (*i.e.* Michaelis–Arbuzov reaction)[14] is well-known and commonly used.[15] Arylhalides (used *e.g.* in Hirao coupling) do not react in Michaelis–Arbuzov reaction and application of catalysts (*e.g.* Pd(II) or Pd(0) compounds) is necessary. The reaction has been extended with many variations in the last years.[16] More functional groups, which can be later used for a further derivatization, can be introduced into the molecule using a proper alkyl- or arylhalide.

Kabachnik–Fields reaction (known since 1952)[17] is among the most investigated P–C forming reactions. Here, dialkyl *H*-phosphite reacts with *in situ* generated C=N bond (*i.e.* with imine) to produce useful dialkyl α-aminoalkylphosphonates. This reaction type has been investigated under various conditions and with many catalysts.[2c] The imine components may be prepared separately beforehand and used in the "Kabachnik–Fields-like" reaction; this modification is called Pudovik reaction.[18] This

---

[13] Sevrain, C. M.; Berchel, M.; Couthon, H.; Jaffres, P.-A. Phosphonic acid: preparation and applications. *Beilstein J. Org. Chem.*, 13, **2017**, 2186–2213.

[14] (a) Michaelis, A.; Kaehne, R. Ueber das verhalten der jodalkyle gegen die sogen. Phosphorigsäureester oder *O*-phosphine. *Chem. Ber.*, 31, **1898**, 1048–1055. (b) Arbuzov, A. E. On the structure of phosphonic acid and its derivatives: Isomerization and transition of bonds from trivalent to pentavalent phosphorus. *J. Russ. Phys. Chem. Soc.*, 38, **1906**, 687–687.

[15] Babu, B. H.; Prasad, G. S.; Raju, C. N.; Raoe, M. V. B. Synthesis of phosphonates via Michaelis–Arbuzov reaction. *Curr. Org. Synth.*, 14, **2017**, 883–903.

[16] Henyecz, R.; Keglevich, G. P–C couplings by the Hirao reaction: novel developments. In Keglevich, G. (Ed.), *Organophosphorus chemistry*, de Gruyter, **2018**, pp. 158–178.

[17] (a) Kabachnik, M. I. Medved, T. Y. New synthesis of aminophosphonic acids. *Dokl. Akad. Nauk SSSR*, 83, **1952**, 689–692. (b) Fields, E. K. The synthesis of esters of substituted amino phosphonic acids. *J. Am. Chem. Soc.*, 74, **1952**, 1528–1531.

[18] Pudovik, A. N.; Arbuzov, B. A. Addition of dialkyl phosphites to unsaturated ketones, nitriles and esters. *Dokl. Akad. Nauk SSSR*, 73, **1950**, 327–330.

approach can be employed in the enantioselective procedures.[19] Next, α-hydroxy-phosphonates are formed in Abramov reaction, *i.e.* when Kabachnik–Fields reaction conditions are used, but without primary / secondary amine. Recently, its asymmetric synthesis variants have been greatly explored.[20] The activated C=C bonds (*e.g.* in acrylates) undergo phospha-Michael addition (initially reviewed by Pudovik in 1948)[21] with dialkyl phosphites (*i.e. H*-phosphonates) to produce substituted phosphonates. This approach is one of the most important P–C bond forming reactions; although, the asymmetric variants are not commonly found.[22]

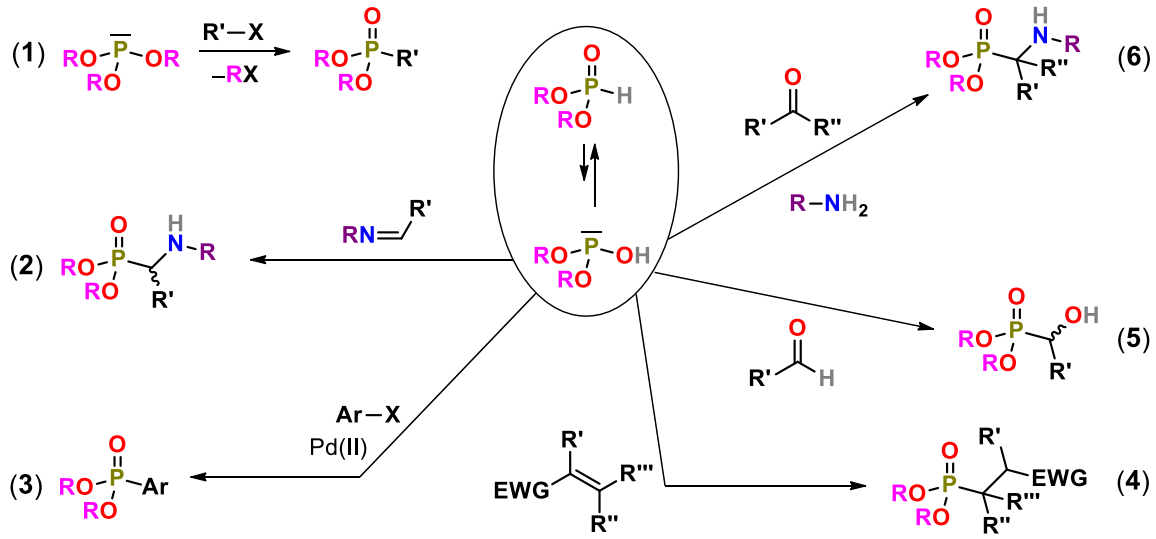

Figure 7 – Use of trialkyl phosphites in Michaelis–Arbuzov (**1**) and dialkyl *H*-phosphites in Pudovik (**2**), Hirao (**3**), phospha-Michael (**4**), Abramov (**5**), and Kabachnik–Fields (**6**) reactions; EWG means electron-withdrawing group

Phosphonic acids are commonly obtained after hydrolysis of alkyl phosphonates by boiling with conc. HCl. These harsh conditions may be overcome by using McKenna method[23] – trans-esterification with trimethylsilylbromide (TMSBr) and a subsequent alcoholysis of the formed trimethylsilyl esters. Interestingly, alkaline hydrolysis of phosphonate dialkyl esters selectively affords the corresponding phosphonate monoesters.

---

[19] Ma, J. A. Catalytic asymmetric synthesis of α- and β-aminophosphonic acid derivatives. *Chem. Soc. Rev.*, 35, **2006**, 630–636.

[20] Guin, J.; Wang, Q.; van Gemmeren, M.; List, B. The catalytic asymmetric Abramov reaction. *Angew. Chem. Int. Ed.*, 53, **2014**, 1–5.

[21] Pudovik, A. N. Addition of dilalkyl phosphites to unsaturated compounds. A new method of synthesis of β-ketophosphoric and unsaturated α-hydroxyphosphonic esters. *Dokl. Akad. Nauk SSSR*, 73, **1950**, 499–502.

[22] Enders, D.; Saint-Dizier, A.; Lannou, M.-I.; Lenzen, A. The phospha-Michael addition in organic synthesis. *Eur. J. Org. Chem.*, **2006**, 29–49.

[23] McKenna, C. E.; Higa, M. T.; Cheung, N. H.; McKenna, M.-C. The facile dealkylation of phosphonic acid dialkylesters by bromotrimethylsilane. *Tetrahedron Lett.*, 18, **1977**, 155–158.

All aforementioned syntheses in Figure 7 are performed under anhydrous conditions and generate phosphonate diesters. On the other hand, Moedritzer–Irani reaction[24] utilizes H_3PO_3 which reacts with *in situ* generated imine (formed from a primary / secondary amine and an aldehyde, mostly formaldehyde) in aqueous HCl as a solvent and the corresponding α-aminoalkylphosphonic acids are formed. However, many by-products are formed in the reaction and the reaction mixture purification is mostly narrowed only to crystallizations.

1.2.2. Synthesis of H-phosphinic acids

Diverse preparations of phosphonic acids (PONs) are well-known. However, syntheses of *H*-phosphinic acids (PINs) are rather underdeveloped compared to those for PONs. The main issues arise from reactivity of their P–H bond and hydrolytical instability of their esters which obstruct their purification and isolation. The synthetic strategies closely resemble those for PON but purification procedures are often more complicated due to a formation of many by-products.

A lot of precursors for synthesis of PINs can be found in literature[25] and some of them are discussed below. To prepare H–P(O)(OH)(R) compounds in the simplest way, substitution of only one P–H bond in hypophosphorous acid, H_3PO_2, can be used; however, the reaction is difficult to perform cleanly. Commonly, the acid is first transformed to a P(III) reagent under anhydrous conditions. The P(III) / P(V) equilibrium is also partially shifted to the P(III) state in esters of H_3PO_2; however, the esters are very unstable.[26] The most utilized approach was suggested by Boyd and Regan.[27] Here, anhydrous hypophosphorous acid is silylated by hexamethyldisilazane (HMDS) or TMSCl / R_3N system to form pyrophoric bis(trimethylsilyl)phosphite (H–P(OTMS)$_2$, Figure 8); therefore, it is mostly prepared only *in situ*. This reagent is reactive towards many electrophiles as alkylhalides, aldehydes, or Michael acceptors. The main drawback, except for instability of the compound, is its excessive reactivity and bis-substituted products are commonly formed (*i.e.* symmetrical phosphinic acids with C–P–C fragment). Hence, an excess of the phosphite (and so H_3PO_2) has to be used which complicates further purification of the reaction mixtures.

---

[24] Moedritzer, K.; Irani, R. R. The direct synthesis of α-aminomethylphosphonic acids. Mannich-type reactions with orthophosphorous acid. *J. Org. Chem.*, 31, **1966**, 1603–1607.

[25] Montchamp, J.-L. Phosphinate chemistry in the 21st Century: a viable alternative to the use of phosphorus trichloride in organophosphorus synthesis. *Acc. Chem. Res.*, 47, **2014**, 77–87.

[26] Montchamp, J.-L. Challenges and solutions in phosphinate chemistry. *Pure Appl. Chem.*, 91, **2019**, 113–120.

[27] Boyd, E. A.; Corless, M.; James, K.; Regan, A. C. A versatile route to substituted phosphinic acids. *Tetrahedron Lett.*, 31, **1990**, 2933–2936.

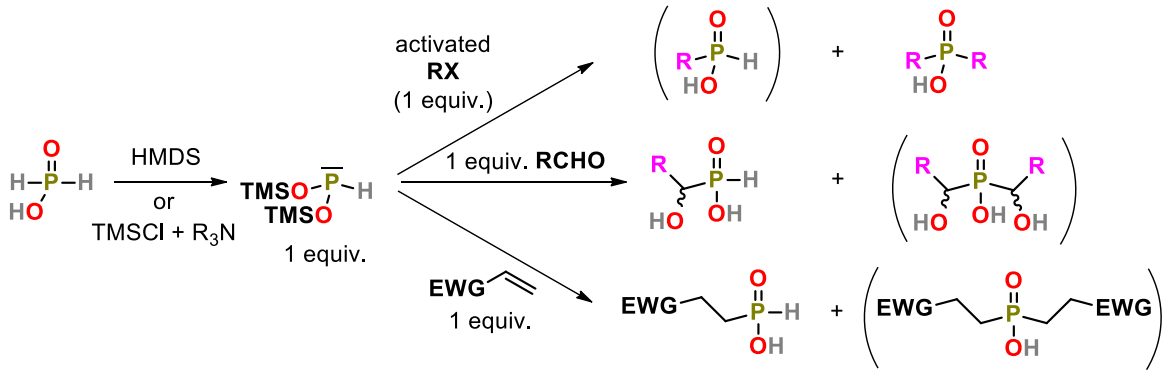

Figure 8 – Preparation and reactivity of bis(trimethylsilyl)phosphite, minor products are in parentheses; EWG means electron-withdrawing group

Other approaches employ ester formation (Figure 9–(**1**)), utilize "Ciba–Geigy reagents" (Figure 9–(**2**)), use borane-stabilized P(III) reagent (Figure 9–(**3**)), radical addition (Figure 9–(**4**)), or palladium cross-coupling reactions (Figure 9–(**5**)).[28] The approaches are summarized in Figure 9.

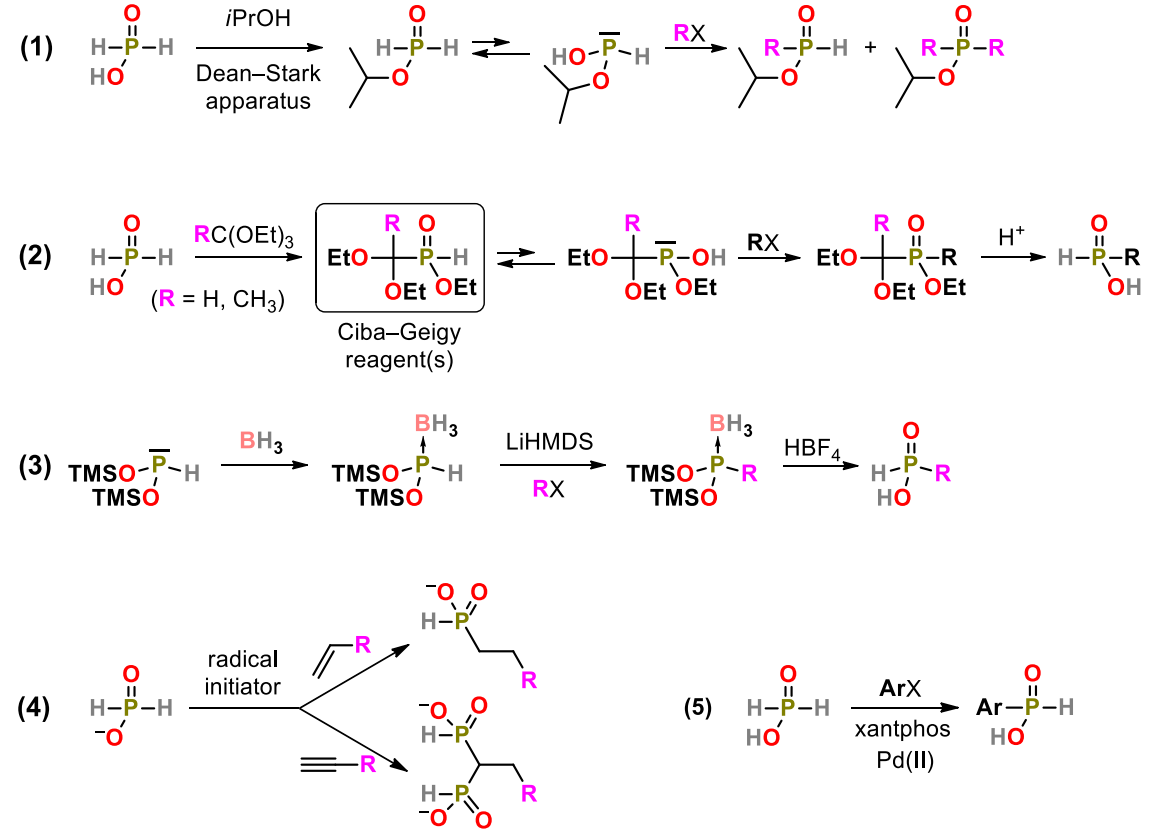

Figure 9 – Commonly used methods for synthesis of *H*-phosphinic acids

[28] Montchamp, J.-L. Recent advances in phosphorus–carbon bond formation: synthesis of *H*-phosphinic acid derivatives from hypophosphorous compounds. *J. Organomet. Chem.*, 690, **2005**, 2388–2406.

Syntheses of phosphonic and phosphinic acids and the formation of P–C bond commonly proceed through P(III) intermediates which are often not stable / isolable under the ambient conditions. To shift the tautomer equilibrium towards P(III) state, H_3PO_2 / H_3PO_3 can be dissolved in the aqueous strong acid or can be converted to esters / phosphites (*e.g.* silyl) in anhydrous media. Only major approach originating from P(V) state is the radical addition to multiple C–C bond. Conditions for the syntheses may be too harsh and, thus, are not "always" usable for additional function groups present in the precursor. New synthetic approaches are being pursued and investigated to broaden the range of usable starting materials and being not too demanding for user synthetic skills (*e.g.* use of inert atmosphere, strictly anhydrous conditions, *etc.*).

1.3. Methods for synthesis of C–P–C bonds

The *H*-phosphinic acids contain one P–H bond which can be further modified. The first common approach is use of aqueous strong mineral acid which protonates the *H*-phosphinic acid and, thus, the P(III) state is slightly favoured.[29] These conditions are used in the "Moedritzer–Irani-like" reaction to form *α*-aminoalkyl-phosphinic acids (Figure 10). Utilization of conc. (12 M) or diluted 1:1 (6 M) aq. HCl with the moderate / strong heating is the most prevalent strategy. Although other special additives can be used (such as TFA), conditions may be too harsh for many functional groups (*i.e.* amides, esters, carbonates, acetals, nitriles, *etc.*) which would decompose under these conditions. Therefore, only relatively uncomplicated starting reagents can be used. This approach is commonly used to synthesize macrocycles with phosphinic acid pendant arm bearing simple *P*-substituents.[30]

Even though *α*-hydroxyalkylation of phosphinic acids is the unwanted side reaction in the Moedritzer-Irani reaction, *α*-hydroxyalkylphosphinic acids have, similarly to *α*-amino-alkylphosphinic acids, a various medicinal utilization with the broad biological activities.[2a] The *α*-hydroxyphosphinic acids have potent biological effects and are prepared from the corresponding *H*-phosphinic acid by heating with

[29] Troev, K. D. Reactivity of P–H Group of Phosphorus Based Compounds. Chapter 1.2.3 Tautomerization of *H*-phosphinic acid. 1st Edition, *Academic Press Elsevier*, San Diego, CA, **2018**, pp. 10–11.

[30] (a) David, T.; Hlinova, V.; Kubicek, V. *et al*. Improved conjugation, 64-Cu radiolabeling, *in vivo* stability, and imaging using nonprotected bifunctional ligands: bis(phosphinate) cyclam (BPC) chelators. *J. Med. Chem*., 61, **2018**, 8774–8796. (b) Mate, G.; Simecek, J.; Pniok, M. *et al*. The influence of the combination of carboxylate and phosphinate pendant arms in 1,4,7-triazacyclononane-based chelators on their ^{68}Ga labelling properties. *Molecules*, 20, **2015**, 13112–13126. (c) Prochazkova, S.; Kubicek, V.; Bohmova, Z., *et al*. DOTA analogues with a phosphinate-iminodiacetate pendant arm: modification of the complex formation rate with a strongly chelating pendant. *Dalton Trans.*, 46, **2017**, 10484–10497.

an aldehyde in aqueous HCl or from alkyl *H*-phosphinates under basic (*e.g.* in the presence of tertiary amine) anhydrous conditions (Figure 10).

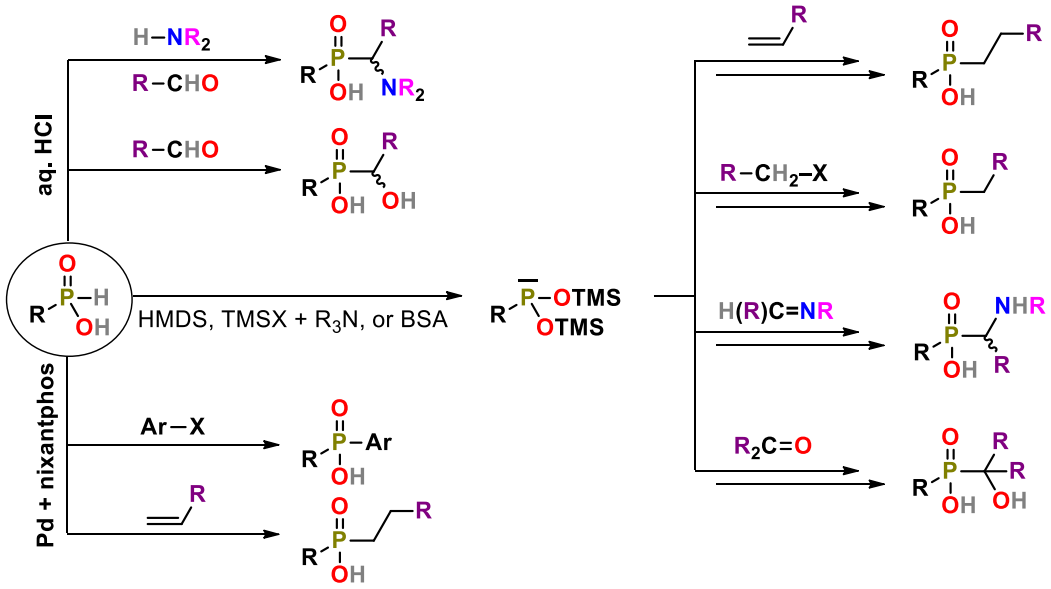

Figure 10 – Methods for preparation C–P–C compounds from *H*-phosphinic acids

Alteration of Kabachnik–Fields reaction utilizes silylation (Figure 10) which is probably the most common approach to synthesize unsymmetrical phosphinic acids from the P–H precursors. The method is carried out under anhydrous conditions and in the presence of silylation reagents – HMDS, TMSCl / R_3N, or BSA (BSA is *N*,*O*-bis(trimethylsilyl)acetamide). The silylated reagent reacts with double bond in C=C, C=N, and C=O to form (after hydrolysis) alkyl-, *α*-amino-, and *α*-hydroxy-phosphinates, respectively, and it also reacts with alkyl- / arylhalogenides.[31] The palladium coupling reactions also work well for the further derivatization of P–H compounds as it was demonstrated on preparation of several PINs from alkenes (Figure 10) and alkynes.[32]

All syntheses need either acid-resistant precursors or water-free, and sometimes oxygen-free, conditions due to use of sensitive reagents. Resulting mixtures often require a complicated purification due to formation of various by-products. For synthesis of the N–C–P–C fragment, no simple and general method has been proposed yet.

[31] Keglevich, G.; Kiss, N. Z.; Musci, Z. Synthesis of phosphinic acid derivatives; traditional versus up-to-date synthetic procedures. *Chem. Sci. J.*, 5, **2014**, 10000088.

[32] Petit, C.; Fecourt, F.; Montchamp, J.-L. Synthesis of disubstituted phosphinates *via* palladium-catalyzed hydrophosphinylation of *H*-phosphinic acids. *Adv. Synth. Catal.*, 353, **2011**, 1883–1888.

2 . Molecular imaging and T_1-MRI contrast agents

2.1. Molecular imaging techniques

Molecular imaging (MI) is defined as the non-invasive visualization, characterization and measurement of biological processes[33] and it is a necessary step towards "personalized medicine". It involves nuclear magnetic resonance methods (MRI and MRS), radiodiagnostic methods (SPECT, PET), optical imaging, and ultrasound-based methods, and their combinations (Figure 11).

Modality	Advantages	Disadvantages
PET	High sensitivity Highly quantitative Temporal monitoring possible Many translational agents under development	Radiation Cyclotron on site for short-lived agents Spatial resolution relatively low
SPECT	Widely available Many probes	Lower spatial resolution and less quantitative than PET Some radiation
Optical imaging	High spatial resolution possible Good sensitivity Quick and inexpensive	Limited detection depth Limited clinical use
MRS	Sensitive Native molecules, no contrast needed	Limited region examined
MRI	High resolution	Lower temporal resolution Sensitivity lower
Ultrasound with contrast	Portable No radiation Low cost High frequency with microbubbles provides good spatial resolution Real-time temporal monitoring	Microbubbles research only Sensitivity lower Quantitative ability low

Figure 11 – Advantages and disadvantages of functional and molecular imaging modalities, adapted from[33a]

PET and SPECT rely on their high sensitivity but they have somewhat low resolution.[33b] They require use of a radioactive isotope. The time-limited utilization and price / availability of the radioisotope are counter-balanced with nano-to-picomolar sensitivity.

Optical methods use "red" light (~650–720 nm) which has good tissue permeability. Although the depth of detection is very limited (few mm), method is inexpensive, and has a high spatial resolution and a great sensitivity.[34]

The last mentioned MI method, the ultrasound imaging, is very underdeveloped and the current research is focused on the stabilized microbubbles only (*e.g.* in liposomes or polymers).

[33] (a) Long, N.; Wing-Tak, W. The Chemistry of Molecular Imaging. 1st Edition, *Wiley*, Hoboken, NJ, **2015**. (b) Pysz, M. A.; Gambhir, S. S.; Willmann, J. K. Molecular imaging: current status and emerging strategies. *Clin. Radiol.*, 65, **2010**, 500–516.

[34] Qin, C.; Zhu, S.; Tian, J. New optical molecular imaging systems. *Curr. Pharm. Biotechnol.*, 11, **2010**, 620–627.

2.2. Magnetic resonance imaging (MRI)

Magnetic resonance imaging (MRI) has been constantly proving to be a powerful non-invasive diagnostic method.[35] Tens of millions examinations are performed annually.[36] The MRI is one of basic techniques and it shows small anatomic details with a great spatial resolution (≤ 1 mm^3). Nowadays, MRI does not only depict anatomy but also adds additional parameter(s) into the acquired MRI image(s) such as changes in pH, temperature, *etc.*

Standard MRI can acquire images affected only by a slight variation of water relaxometric properties in different tissues.[38] To improve the image, contrast agents (CAs) are applied. They alter NMR relaxation times of water protons in their proximity. The main advantage is undoubtedly CAs targeting to a particular tissue as *e.g.* cancerous tissue (Figure 12). Moreover, MRI image contrast can be sensitive towards pH of local environment, temperature, specific ion concentration, or substrate presence, if a proper CA is used.[39] Even intracellular processes and enzymatic reactions can be monitored with CAs.[40] Underlying irreplaceable benefits, MRI has carved up to the top of a modern diagnostic medicine and, likely, it will not be displaced in a near future.

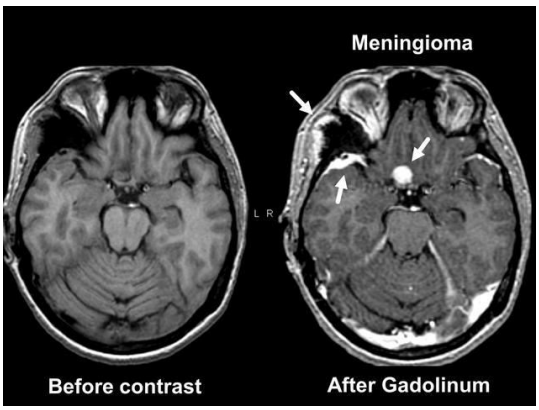

Figure 12 – Comparison of MR image before and after application of CA; reprinted from[37]

[35] Edelman, R. R. The history of MR imaging as seen through the pages of radiology. *Radiology*, 273, **2014**, S181–S200.

[36] https://ec.europa.eu/eurostat/statistics-explained/index.php?title=Healthcare_resource_statistics_-_technical_resources_and_medical_technology, [Online] Accessed 01-08-2019.

[37] https://si.wsj.net/public/resources/images/BN-VD534_YHEALT_8H_20170915163302.jpg, [Online] Accessed 01-08-2019.

[38] Bojorquez, J. Z.; Bricq, S.; Acquitter, C. *et al*. What are normal relaxation times of tissues at 3 T? *Magn. Reson. Imaging*, 35, **2017**, 69–80.

[39] Merbach, A. E.; Helm, L.; Toth, E. The Chemistry of Contrast Agents in Medical Magnetic Resonance Imaging. 2nd Edition, *Wiley*, Chichester, UK, **2013**.

[40] Hingorani, D. V.; Yoo, B.; Bernstein, A. S.; Pagel, M. D. Detecting enzyme activities with exogenous MRI contrast agents. *Chem. Eur. J.*, 20, **2014**, 9840–9850.

2.3. Gd(III)-based MRI contrast agents

"Classical" MRI measurement may use only an optimized acquisition pulse sequence and, thus, some essential small nuances in the code may alter the resultant anatomical MRI image. However, a "targeted" imaging (*i.e.* highlighting of selected area) is impossible with only the optimized MRI sequence. Presence of T_1-alternating MRI CAs reduces mainly relaxation time T_1 of water protons (*i.e.* bulk water) and it is easily recognized by MRI. From the physico-chemical point of view, relaxation time T_1 (together with T_2) is shortened by the presence of a paramagnetic ion. The largest magnetic momentum is observed in Ln(III) ions and some ions of *d*-elements. In addition, some of the crucial parameters for useful contrast agents are electron relaxation times (T_{ie}, i = 1 or 2) of the ion.[41] Unpaired electron spins in high-spin Mn(II) and Fe(III), and in Gd(III) ions are symmetrically distributed in their valence shell and their electron relaxation time T_{1e} is longer by several orders of magnitude when compared with other Ln(III) ions and the first-row *d*-element ions (Table 1).[42] Gd(III) ion has seven unpaired electrons in *f*-orbitals, the longest observed electron relaxation time T_{1e} and, thus, it is the most suitable as a relaxation agents for MRI. However, it is not possible to use "free" Gd(III) aqua ion due to its high toxicity ($LD_{50}(GdCl_3)$ ~0.35 mmol/kg in mouse, intravenous) and, thus, other safer methods of Gd(III) ion applications have been investigated.[43]

Metal ion	Electron configuration	Unpaired electrons	T_{1e} / s^{-1}
Cr(III)	d^3	3	10^9–10^{10}
Mn(II)	d^5	5 [a]	10^8–10^{10} [a]
Fe(III)	d^5	5 (HS)[a] or 1 (LS)[b]	10^9–10^{10} [a] or 10^{11}–10^{13} [b]
Co(II)	d^7	3 (HS)[a] or 1 (LS)[b]	10^{11}–10^{13} [a] or 10^9–10^{11} [b]
Ni(II)	d^8	2	10^{10}
Cu(II)	d^9	1	10^9
Ln(III)	$f^{1–13}$	1–6	10^{12}–10^{14}
Gd(III)	f^7	7	**10^8–10^9**

[a]HS = high-spin complex. [b]LS = low-spin complex.

Table 1 – Electron relaxation times T_{1e} of some metal ions in their complexes

[41] Kowalewski, J.; Kruk, D.; Parigi, G. NMR relaxation in solution of paramagnetic complexes: recent theoretical progress for S ≥ 1. In Eldik, R. Van; Bertini, I. (Eds.) *Adv. Inorg. Chem*., 57, **2005**, pp. 42–104.

[42] Bertini, I.; Luchinat, C.; Parigi, G.; Ravera, E. NMR of Paramagnetic Molecules. 2nd Edition, *Elsevier*, Amsterdam, NL, **2017**, pp. 83–84.

[43] Rogosnitzky, M.; Branch, S. Gadolinium-based contrast agent toxicity: a review of known and proposed mechanism. *Biometals*, 29, **2016**, 365–376.

MRI has a great spatial resolution in clinical setting (in mm^3) but a very low sensitivity. To acquire a reasonable contrast-enhanced MRI image of average human patient, roughly ~1.3 g of Gd(III) (calculated from the advised dose of 0.1 mmol/kg)[45] is used per examination. Use of unstable Gd(III) chelates which release free aqua Gd(III) ion *in vivo* was associated with medical problems, *e.g.* with the nephrogenic systemic fibrosis (NFS, Figure 13).[46] This disease involves fibrosis of skin, joints and any other organ. Hence, release of free aqua Gd(III) *in vivo* is undesired and must be avoided.

Figure 13 – Patients with NFS disease, adapted from[44]

2.3.1. *Stability of Gd(III) complexes*

To benefit from the water proton relaxation properties of Gd(III) ion, the thermodynamically stable and kinetically inert complexes have to be used. They must contain at least one water molecule(s) coordinated to the central ion. Toxicity of these compounds is decreased down to LD_{50} ~10 mmol/kg (vs. LD_{50} ~0.35 mmol/kg for $GdCl_3$ (intravenous, mouse))[48] and the CAs are considered as non-toxic. The chemical nature of Gd(III) ion requires nitrogen and charged oxygen donor atoms in the ligands. Stability of the complexes is improved by the use of chelating polydentate ligands. Thus, polyamino-polycarboxylates are the most suitable ligands. The first suitable ligand was DTPA (Figure 14, $\log K_{GdL}$ 22.5)[49] and its Gd(III) complex was clinically approved in 1988 under the trade name Magnevist®.

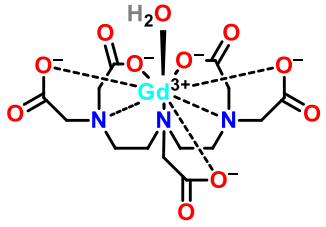

Figure 14 – Structure of Gd–DTPA[47]

---

[44] http://medicinespecifics.com/wp-content/uploads/2017/07/nephrogenic-systemic-fibrosis.jpg, [Online] Accessed 01-08-2019.

[45] https://www.radiology.wisc.edu/wp-content/uploads/2017/10/gadolinium-based-contrast-dosing-charts.pdf, [Online] Accessed 01-08-2019.

[46] Thomsen, H. S.; Morcos, S. K.; Almen, T. *et al*. Nephrogenic systemic fibrosis and gadolinium-based contrast media: updated ESUR contrast medium safety committee guideline. *Eur. Radiol.*, 23, **2013**, 307–318.

[47] Throughout this Thesis, the charges of the complexes in formulas were omitted for the sake of clarity.

[48] Idee, J.-M.; Port, M.; Raynal, I. *et al*. Clinical and biological consequences of transmetalation induced by contrast agents for magnetic resonance imaging: a review. *Fund. Clin. Pharm.*, 20, **2006**, 563–576.

[49] Anderegg, G.; Arnaud-Neu, F.; Delgado, R. *et al*. Critical evaluation of stability constants of metal complexes of complexones for biomedical and environmental applications. *Pure Appl. Chem.*, 77, **2005**, 1445–1495.

However, its kinetic inertness is not high enough which can cause release of the free aqua Gd(III) ion *in vivo*. Hence, its prolonged body circulation (*e.g.* in patients with renal failure) should be avoided. The Gd(III) complexes of DTPA derivatives are even more prone to the free aqua Gd(III) release. Currently, CAs based on DTPA derivatives have been withdrawn from the market.[50]

To increase stabilizing chelating effect, rigidified pre-organized ligands should be used. Thus, cyclen derivatives are the most suitable ones. The Gd(III) complex of the cyclen-based polyamino-polycarboxylate DOTA (logK_{GdL} 24.7, Figure 15)[51] is the "gold standard" among MRI CAs due to its stability *in vivo* and efficacy. Substitution of the acetates (bound to ring amines) with similar coordinating moieties (*e.g.* acetamides or methylphosphinates / methylphosphonates; see Figure 16) leads to ligands also suitable for the Gd(III) ion coordination. In those complexes, the Gd(III) ion forms only five-membered rings employing ring amines and ligand pendant arms. Presence of larger chelate cycles (*e.g.* six-membered) in the CAs leads to a lower stability of their complexes unless the ligands are additionally rigidified.[52]

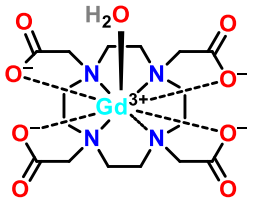

Figure 15 – Structure of Gd–DOTA

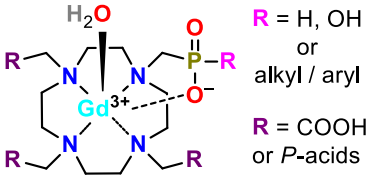

Figure 16 – Structures of cyclen-based complexes with a methylphosphinate or a methylphosphonate pendant arm(s)

In the terms of thermodynamic stability, Gd(III) ion forms stable complexes with any octadentate polyamino-polycarboxylates.[53] Mostly, one water molecule is bound in the ninth coordination site. Values of stability constant, logK_{GdL}, should be above ~18 to consider the complex as thermodynamically stable.[54]

[50] European Medicines Agency. PRAC confirms restrictions on the use of linear gadolinium agents. Document EMA/424715/2017, **2017**.

[51] Cacheris, W. P.; Nickle, S. K.; Sherry, A. D. Thermodynamic study of lanthanide complexes of 1,4,7-triazacyclononane-*N*,*N*′,*N*″-triacetic acid and 1,4,7,10-tetraazacyclododecane-*N*,*N*′,*N*″,*N*‴-tetraacetic acid. *Inorg. Chem.*, 26, **1987**, 958–960.

[52] Polasek, M.; Sedinova, M.; Kotek, J. *et al*. Pyridine-*N*-oxide analogues of DOTA and their gadolinium(III) complexes endowed with a fast water exchange on the square-antiprismatic isomer. *Inorg. Chem.*, 48, **2009**, 455–465.

[53] Clough, T. J.; Jiang, L.; Wong, K.-L.; Long, N. J. Ligand design strategies to increase stability of gadolinium-based magnetic resonance imaging contrast agents. *Nature Commun.*, 10, **2019**, 1420.

[54] Idee, J.-M.; Port, M.; Robic, C.; *et al*. Role of thermodynamic and kinetic parameters in gadolinium chelate stability. *J. Magn. Reson. Imaging*, 30, **2009**, 1249–1258.

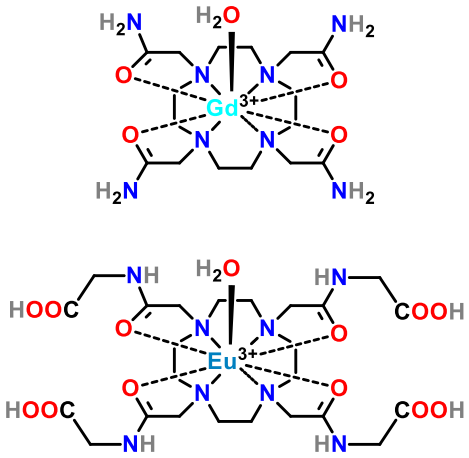

Figure 17 – Structure of Gd–DOTAM (up) and Eu–DOTA-(gly)$_4$ (down)

Kinetic inertness of the complexes is more important parameter. For instance, the stability of four complexes: Gd–DTPA (Figure 14), Gd–DOTA, Gd–DOTAM (tetraamide of DOTA, see Figure 17) and Eu–DOTA-(gly)$_4$ (all amides of DOTAM substituted with a glycine, Figure 17) were investigated in detail *in vitro* and *in vivo*. Testing proved the fastest acid-assisted decomplexation[55,56] of Gd–DTPA and slower of Gd–DOTA, and much slower decomplexation of Gd–DOTAM and Eu–DOTA-(gly)$_4$ (see Table 2), despite their rather low thermodynamic stability (*i.e.* low logK_{GdL}). Thus, kinetic inertness is the most decisive parameter for estimation of stability *in vivo*.

Parameter	Gd–DTPA	Gd–DOTA	Gd–DOTAM	Eu–DOTA-(gly)$_4$
logK_{GdL}	22.5	24.7	13.1	14.5
$\tau_{1/2}$ (pH 1, HCl, 25 °C)	9.6 min	9.2 h	68 h[a]	237 h

[a]in 2.5 M HNO_3, 25 °C[57]

Table 2 – Stability constants and inertness of selected Gd(III) complexes determined by decomplexation half-life $\tau_{1/2}$

The Gd(III) complexes of macrocyclic DOTA-like ligands are significantly more stable *in vivo* than complexes of linear DTPA-like ligands. The NSF has not been associated with any complexes of DOTA-like ligands till now.[46] Thus, the use of macrocyclic chelates in MRI CAs is advised.

2.4. Relaxometric parameters and ligand design

The efficacy of MRI CAs is characterized by relaxivity, r_1, which is defined as a reciprocal value of water protons relaxation time T_1 (*i.e.* relaxation R_1) divided by concentration of Gd(III) ion (Equation 1) present in the solution. Hence, relaxivity units are mM^{-1} s^{-1}. Relaxivity r_1 (and relaxation R_1) itself have a diamagnetic (r_{1d},

[55] Baranyai, Z; Brucher, E.; Ivanyi, T. *et al*. Complexation properties of H$_4$dotagl. Equilibrium, kinetic and relaxation behavior of the lanthanide(III) complexes. *Helv. Chim. Acta*, 88, **2005**, 604–617.

[56] Brucher, E. Kinetic stabilities of gadolinium(III) chelates used as MRI contrast agents. *Top. Curr. Chem.*, 221, **2002**, 103–122.

[57] Aime, S.; Barge, A.; Bruce, J. I. *et al*. NMR, relaxometric, and structural studies of the hydration and exchange dynamics of cationic lanthanide complexes of macrocyclic tetraamide ligands. *J. Am. Chem. Soc.*, 121, **1999**, 5762–5771.

physico-chemical properties of pure water) and a paramagnetic (r_{1p}, caused by presence of Gd(III) ion) contributions (Equation 1).

$$\frac{1}{T_1 c_{Gd}} = \frac{R_1}{c_{Gd}} = r_1 = r_{1d} + r_{1p} \qquad \text{Eq. 1}$$

In 1955–1961, Solomon, Bloembergen, and Morgan (SBM) postulated semi-empirical SBM theory which was simplified for $^8S_{7/2}$ state, *i.e.* for Gd(III) ion.[58] Main adjustable relaxometric parameters which arose from SBM theory are presented in Table 3. The following paragraphs analyze each parameter more in the detail from the ligand design point of view.

Parameter	Description
q	A number of water molecules directly coordinated to central metal ion
τ_M	Residence time of the coordinated water molecule ($\tau_M = 1/k_{ex}$)
k_{ex}	Exchange rate of coordinated water molecule ($k_{ex} = 1/\tau_M$)
τ_R	Rotational correlation time
r_{Gd-H}	Distance of coordinated water proton from central metal ion
T_{ie}	Electron relaxation times (i = 1, 2) of the central metal ion
Δ^2	The mean squared fluctuation of the zero-field splitting
τ_v	Correlation time for the modulation of the zero-field splitting

Table 3 – The most important parameters contributing to paramagnetic relaxivity r_{1p}

2.4.1. *Hydration number* q

Gd(III) ion commonly coordinates 8–9 donor atoms. To have sufficiently "thermodynamically stable CA", maximum of one or two coordination site(s) may be left for binding water molecule(s). Typical example is thermodynamically stable Gd–DOTA with q = 1 (Figure 15). If one pendant arm of the DOTA-like ligand was removed, corresponding Gd(III) complex would have q = 2. However, relaxivity

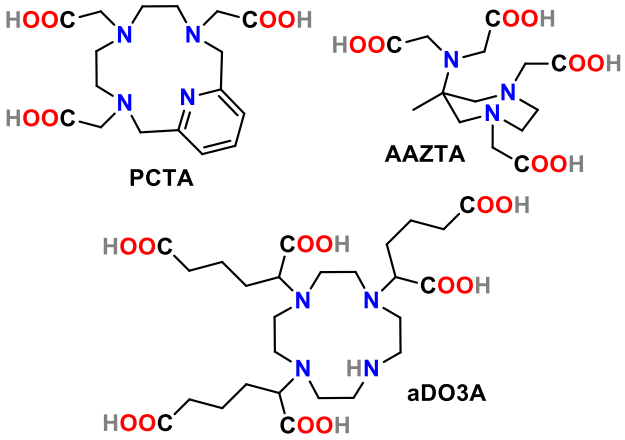

Figure 18 – Structures of PCTA, AAZTA and aDO3A

[58] (a) Bloembergen, N.; Purcell, E. M.; Pound, R. V. *Phys. Rev.*, 73, **1948**, 679–712. (b) Solomon, I. *Phys. rev.*, 99, **1955**, 559–565. (c) Solomon, I.; Bloembergen, N. *J. Chem. Phys.*, 25, **1956**, 261–266. (d) Bloembergen, N. *J. Chem. Phys.*, 27, **1957**, 572–573. (e) Bloembergen, N.; Morgan, L. O. *J. Chem. Phys.*, 34, **1961**, 842–850.

of CA with q = 2 is mostly decreased *in vivo* due to replacement of the water molecules by endogenous ligands as *e.g.* amino acids, proteins and / or inorganic anions (mainly CO_3^{2-} and HPO_4^{2-}) present in blood.[59] Therefore, complexes with a "non-geminal" binding sites on Gd(III) were suggested. However, decreased denticity of the ligands leads to a lower kinetic inertness. Complexes of heptadentate ligands with a reasonably high complex stability are *e.g.* Gd–AAZTA,[60] Gd–aDO3A[61] and Gd–PCTA[62] (ligands in Figure 18). The Gd(III) complex of a PCTA derivative has entered clinical studies.[63]

2.4.2. Water exchange rate k_{ex} *and water residence time* τ_M

Exchange rate of coordinated water molecule k_{ex} is a reciprocal value of its residence time τ_M ($k_{ex} = \tau_M^{-1}$). In Gd(III)-based MRI CAs, coordinated water molecule is exchanged with the bulk water mostly by dissociative mechanism. Thus, the coordination number changes between 9 and 8.[64] This mechanism is preferred in complexes with easily accessible Gd(III) octa-coordinated state, *i.e.* with bulky ligands.[65] If hydration break (*i.e.* change of q = 1 to 0) within the Ln(III) series in complexes is in proximity to Gd(III) ion, water residence time is also shortened. Moreover, the charge of CA was also proven to modify the exchange rate of water. Negatively charged CAs often exchange coordinated water molecule faster than neutral or positively charged MRI CAs.[66] The water residence time τ_M is optimally ~10–50 ns for currently used magnetic fields in diagnostic medicine.

---

[59] Helm, L. Optimization of gadolinium-based MRI contrast agents for high magnetic-field applications. *Future Med. Chem.*, 2, **2010**, 385–396.

[60] (a) Schuhle, D. T.; Caravan, P. Metal-based MRI Contrast Agents. Comprehensive Inorganic Chemistry II, 2nd Edition, *Elsevier*, Amsterdam, NL, **2013**. (b) Aime, S.; Calabi, L.; Cavallotti, C. *et al*. [Gd–AAZTA]$^-$: a new structural entry for an improved generation of MRI contrast agents. *Inorg. Chem.*, 43, **2004**, 7588–7590.

[61] Messeri, D.; Lowe, M. P.; Parker, D.; Botta, M. A stable, high relaxivity, diaqua gadolinium complex that suppresses anion and protein binding. *Chem. Commun.*, **2001**, 2742–2743.

[62] Aime, S.; Botta, M.; Geninatti, C. S. *et al*. Synthesis and NMR studies of three pyridine-containing triaza macrocyclic triacetate ligands and their complexes with lanthanide ions. *Inorg. Chem.*, 36, **1997**, 2992–3000.

[63] Hao, J.; Bourrinet, P.; Desche, P. Assessment of pharmacokinetic, pharmacodynamic profile, and tolerance of Gadopiclenol, a new high relaxivity GBCA, in healthy subjects and patients with brain lesions (phase I/IIa study). *Invest. Radiol.*, 54, **2019**, 396–402.

[64] Merbach, A. E.; Helm, L.; Toth, E. The Chemistry of Contrast Agents in Medical Magnetic Resonance Imaging. Chapter 2.2.3.3 Water exchange on monomer Gd(III) complexes. 2nd Edition, *Wiley*, Chichester, UK, **2013**, pp. 39–56.

[65] (a) Helm, L.; Merbach, A. E. Inorganic and bioinorganic solvent exchange mechanism. *Chem. Rev.*, 105, **2005**, 1923–1960. (b) Jaszberenyi, Z.; Sour, A.; Toth, E. *et al*. Fine-tuning water exchange on Gd^{III} poly(amino carboxylates) by modulation of steric crowding. *Dalton Trans.*, **2005**, 2713–2719.

[66] Caravan, P.; Esteban-Gomez, D.; Rodriguez-Rodriguez, A.; Platas-Iglesias, C. Water exchange in lanthanide complexes for MRI applications. Lessons learned over the last 25 years. *Dalton Trans.*, 48, **2019**, 11161–11180.

2.4.3. *Rotation correlation time* τ_R

Rotation correlation time τ_R characterizes the reorientational time of the whole CA (or better, the Gd–H_{water} vector). Excessive mobility (*i.e.* short τ_R) of the Gd(III) centre lowers relaxivity. Small molecules can diffuse and "reorientate" slower in the more viscous medium but this approach is not utilizable *in vivo*. The easiest way to increase τ_R is to increase a molecular volume (*i.e.* simplified as a "weight") of the CA. For instance, Vistarem® (Gadomelitol, Figure 19) is a Gd(III)-based CA with molecular weight of ~6.5 kDa and its relaxivity is increased six-to-sevenfold (27 mM^{-1} s^{-1} in 4% (w/w) HSA at 1.5 T, 37 °C) in comparison with Gd–DOTA (3.5 mM^{-1} s^{-1}, measured at the same conditions)[67] making it one of the best commercially available options to achieve a high relaxivity.

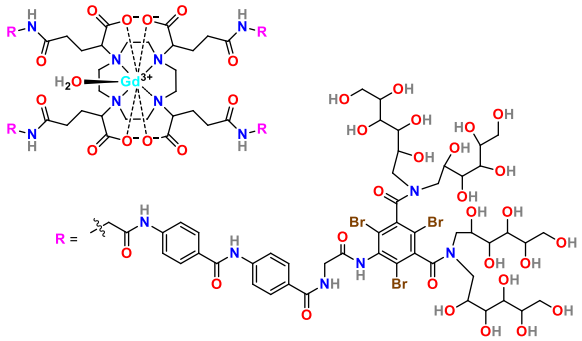

Figure 19 – Structure of Vistarem®

Another approach is to attach Gd(III) chelate covalently to a macromolecule. Gd(III) complexes attached to various polymers, as *e.g.* PAMAM dendrimers or *β*-cyclodextrins, have been studied and, in all cases, the relaxivity is increased severalfold.[68] However, the effect of Gd(III) ion anchoring is suppressed if the "local" motion of Gd(III) chelate attached to a macromolecule is fast (*i.e.* the Gd(III) chelate local τ_R dominates over the global τ_R of whole conjugate).[69] Relaxivity of these conjugates is always increased due to a higher number of Gd(III) ions per one molecule of the conjugates. The main problem with these macromolecules remains their problematic elimination from the body. "Small" compounds up to ~20 kDa are easily and preferentially filtered off by kidneys, and molecules up to ~60 kDa can be

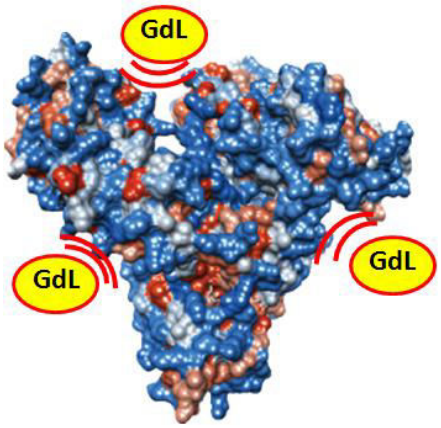

Figure 20 – A non-covalent interaction of the Gd-based CA with biomacromolecule (*e.g.* HSA)

[67] Elst, L. V.; Raynal, I.; Port, M. *et al. In vitro* relaxometric and luminescence characterization of P792 (Gadomelitol, Vistarem®), an efficient and rapid clearance blood contrast agent. *Eur. J. Inorg. Chem.*, **2005**, 1142–1148.

[68] Zhou, Z.; Lu Z.-R. Gadolinium-based contrast agents for magnetic resonance cancer imaging. *WIREs Nanomed. Nanobiotechnol.*, 5, **2013**, 1–18.

[69] Caravan, P.; Farrar, C. T.; Frullano, L.; Uppal, R. Influence of molecular parameters and increasing magnetic field strength on relaxivity of gadolinium- and manganese-based T_1 contrast agents. *Contrast Media Mol. Imaging*, 4, **2009**, 89–100.

still eliminated through kidneys.[70] Moreover, bulky and lipophilic CAs are absorbed by liver and are excreted with bile through small intestine.[71]

Gd(III)-based chelate can be also anchored non-covalently. The most commonly used approach is non-covalent interaction with biomacromolecules *in vivo*.[72] The most common target is human serum albumin (HSA, Figure 20). More information about CA–HSA interaction is given in the Chapter 2.6.

2.4.4. *Second-sphere hydration in MRI CAs*

Overall relaxivity can be divided into three contributions (Figure 21): (*i*) that of water molecule(s) in the first coordination sphere (inner-sphere, IS), (*ii*) that of water in the second-sphere (SS), and (*iii*) the bulk water molecules from the outer-sphere (OS). Amount, position and the local motion of these water molecules can significantly alter overall relaxivity. The Gd–DOTP (Figure 22) does not coordinate any water molecule directly to Gd(III) ion but its relaxivity is comparable to that of Gd–DOTA (Figure 15). One of the explanations is a rich SS hydration in which water molecules are tightly bound by the phosphonate groups. The SS water distance from Gd(III) is approx. ~3.5 Å,[74] thus, it is short enough to enhance SS water proton relaxation in presence of Gd(III) ion. Phosphorus acid analogues of DOTA complexes (*e.g.* Gd–DO3AP^{R}) are well-known to have a rich SS hydration which significantly contributes (by up to ~20 %, see Chapter 3.2.1) to their overall relaxivity.

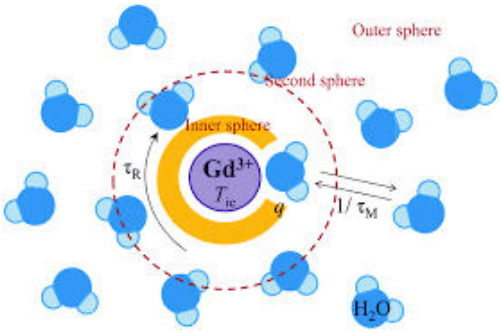

Figure 21 – A scheme of inner-sphere, second-sphere and outer-sphere hydration; reprinted from[73]

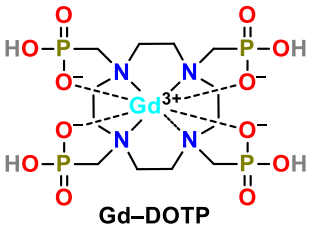

Figure 22 – Structure of Gd–DOTP

[70] Christensen, E. I.; Birn, H.; Storm, T.; Weyer, K.; Nielsen, R. Endocytic receptors in the renal proximal tubule. *Physiology*, 27, **2012**, 223–236.

[71] Bumb, A.; Brechbiel, M. W.; Choyke, P. Macromolecular and dendrimer based magnetic resonance contrast agents. *Acta Radiol.*, 51, **2010**, 751–767.

[72] (a) Caravan, P. Protein-targeted gadolinium-based magnetic resonance imaging (MRI) contrast agents: design and mechanism of action. *Acc. Chem. Res.*, 42, **2009**, 851–862. (b) Wahsner, J.; Gale, E. M.; Rodriguez-Rodriguez, A.; Caravan, P. Chemistry of MRI contrast agents: current challanges and new frontiers. *Chem. Rev.*, 119, **2019**, 957–1057.

[73] Debroye, E.; Parac-Vogt, T. N. Towards polymetallic lanthanide complexes as dual contrast agents for magnetic resonance and optical imaging. *Chem. Soc. Rev.*, 43, **2014**, 8178–8192.

[74] Borel, A.; Helm, L.; Merbach, A. E. Molecular dynamics simulations of MRI-relevant Gd(III) chelates: direct access to outer-sphere relaxivity. *Chem. Eur. J.*, 7, **2001**, 600–610.

2.4.5. *Other relaxometric parameters*

Relaxivity r_1 is a function of more parameters than those mentioned in Table 3. SBM theory equations also involve the proton Larmor frequency and, thus, relaxivity and "ideal" values of the relaxometric parameters are dependent on magnetic field. For MRI scanners operating at 0.5 T (20 MHz), relaxivity can achieve values up to ~100 mM^{-1} s^{-1} by the using CA with τ_M ~10 ns (k_{ex} ~10^8 s^{-1}) and τ_R ~50 ns. With increasing magnetic field, maximal achievable relaxivity drops with corresponding change of "optimal" values for τ_M and τ_R. However, optimal values are always in range of "ns" for both, τ_M and τ_R.[69]

Other parameters in Table 3 are hard to optimize by ligand design. The distance r_{Gd-H} significantly alters the overall relaxivity (*i.e.* the equation term $(r_{Gd-H})^{-6}$). If the distance was shortened by only 0.1 Å, relaxivity would increase by 20 %, and, by 0.2 Å, it would lead to 50 % increase which arises according to the SBM equations.[75]

Parameters T_{1e}, τ_v and Δ^2 are interlinked and their intentional alteration is rather difficult. Important parameter affecting their values is overall symmetry of the complexes as higher symmetry of crystal field extends T_{1e}.[76] Moreover, an introduction of another paramagnetic centre close to the coordinated Gd(III) alters T_{1e}.[77]

2.4.6. *State of the art*

Generally, octadentate ligands based on cyclen are preferred for Gd(III) ion coordination to afford thermodynamically stable and kinetically inert MRI CAs with q = 1. Currently used stable MRI CAs exchange IS water molecule slowly and the molecules are too mobile and, thus, their observed relaxivity is small compared to theoretically predicted value. The closest to the "ideal state" is the water exchange in complexes of DO3AP^R ligands. These complexes also benefit from the second-sphere hydration and complex mobility may be greatly affected by a further immobilization. Hence, DO3AP^R ligands have been studied and parameters of their Gd(III) complexes tuned up in "a controlled manner".

---

[75] Merbach, A. E.; Helm, L.; Toth, E. The Chemistry of Contrast Agents in Medical Magnetic Resonance Imaging. Chapter 2.2.2 Gd–H distance. 2nd Edition, *Wiley*, Chichester, UK, **2013**, pp. 37–39.

[76] Borel, A.; Bean, J. F.; Clarkson, R. B. *et al*. Towards the rational design of MRI contrast agents: electron spin relaxation is largely unaffected by the coordination geometry of gadolinium(III)-DOTA-type complexes. *Chem. Eur. J.*, 14, **2008**, 2658–2667.

[77] Nicolle, G. M.; Yerly, F.; Imbert, D. *et al*. Towards binuclear polyaminocarboxylate MRI contrast agents? Spectroscopic and MD study of the peculiar aqueous behavior of the Ln(III) chelates of OHEC (Ln = Eu, Gd, and Tb): implications for relaxivity. *Chem. Eur. J.*, 9, **2003**, 5453–5467.

2.5. Responsive MRI CAs

Complexes whose relaxometric properties are affected by the physiological conditions are called responsive, "activable" or "smart" MRI CAs.[78] Their responsiveness may be triggered by a specific metal ion in solution (*i.e.* by ion flux), an enzyme activity, pH, "redox" state of tissue (*i.e.* change in a chemical potential) or temperature.[79] However, the major impact and importance of development of these CAs are countered by a lack of quantification of the target biomarker. Relaxivity is always dependent on the concentration of the CA and, thus, a separation of two contributions: (*i*) the biomarker response and (*ii*) the concentration of the CA to overall relaxivity is often unsuccessful. Therefore, some ratiometric methods have been developed (*e.g.* R_2/R_1 measurement, successive injection of two CAs, or a multimodal approach).[80]

2.5.1. pH-sensitive MRI CAs

One of the most important properties, which are desirable to follow *in vivo*, is pH. It is well-known that pH lower than physiological one signalizes ongoing pathological processes as cancer, infections, stroke or kidney disease.[81] The pH change can differ significantly (up to ~0.5).[82] To determine pH, MRI relies on a change of relaxometric properties caused by different pH of tissues. The most common approach is utilization of CAs whose properties are sensitive to pH. It can be reached, for instance, by utilization of

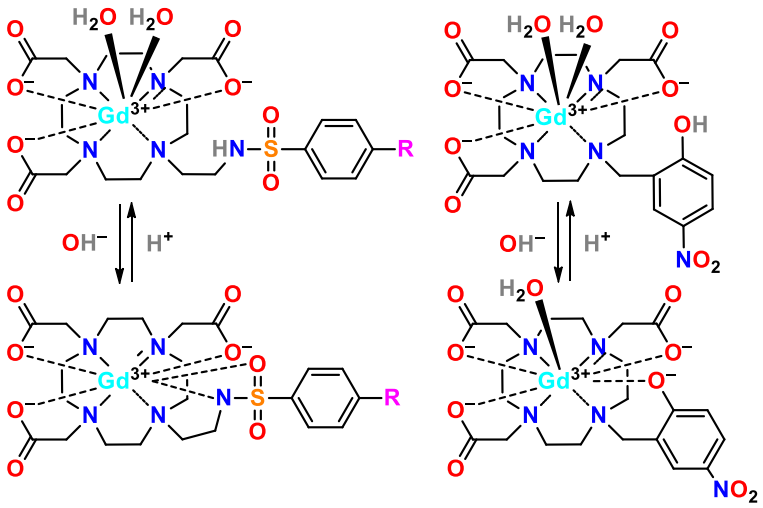

Figure 23 – Two pH-responsive MRI CAs with weakly binding pendant arm

[78] Li, H.; Meade, T. J. Molecular magnetic resonance imaging with Gd(III)-based contrast agents: challenges and key advances. *J. Am. Chem. Soc.*, 141, **2019**, 17025–17041.
[79] Hingorani, D. V.; Bernstein, A. S.; Pagel, M. D. A review of responsive MRI contrast agents: 2005–2014. Contrast media. *Contrast Media Mol. Imaging*, 10, **2015**, 245–265.
[80] Aime, S.; Fedeli, F.; Sanino, A.; Terreno, E. A R_2/R_1 Ratiometric procedure for a concentration-independent, pH-responsive, Gd(III)-based MRI agent. *J. Am. Chem. Soc.*, 128, **2006**, 11326–11327.
[81] Zollner, J. P.; Hattingen, E.; Singer, O. C.; Pilatus, U. Changes of pH and energy state in subacute human ischemia assessed by multinuclear magnetic resonance spectroscopy. *Stroke*, 46, **2015**, 441–446.
[82] Griffiths, J. R. Are cancer cells acidic? *Br. J. Cancer*, 64, **1991**, 425–427.

chelates where one pendant group is weakly bound, *e.g.* in Gd–DO3A-SA[83] with the pendant sulfonylamide group or Gd–NP-DO3A[84] with the *p*-nitrophenol pendant group (Figure 23). In these CAs, two water molecules are bound after protonation and decoordination of the pendant arm in solution with lower pH (Figure 23).

An interesting approach to determine pH is utilization of CAs with protonable group(s) (*e.g.* phosphonate groups in Gd–DOTA-4AMP, Figure 24). A gradual (de)protonation of the complexes may significantly contribute to the overall relaxivity due to the prototropic exchange with bulk water.[85a] In the case of phosphonate groups, ^{31}P MRS and the change of τ_M (connected *e.g.* with the overall charge of the CA) may be also successfully employed (see in Chapter 2.8.1).

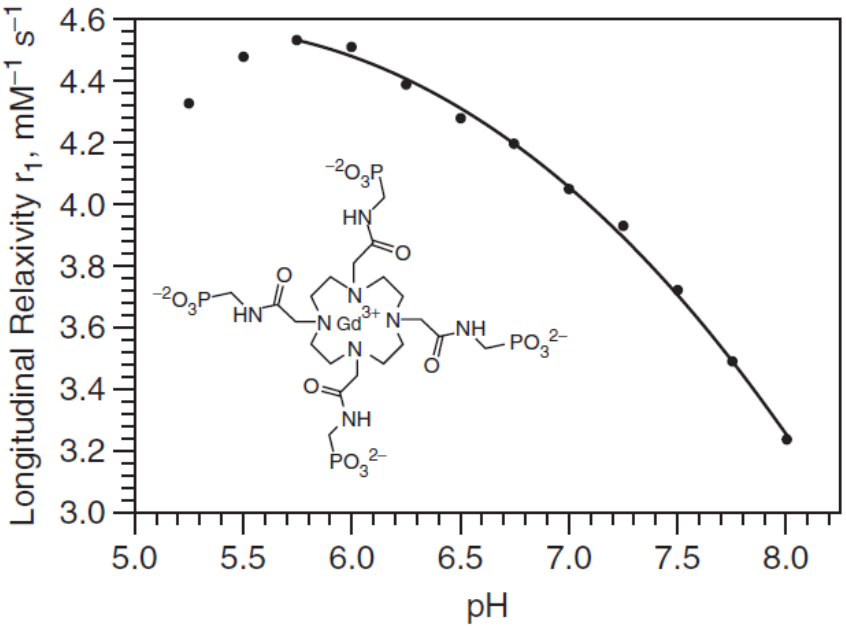

Figure 24 – Gd–DOTA-4AMP structure and its relaxivity dependence on pH; reprinted from[85b]

[83] Lowe, M.; Parker, D.; Reany, O. *et al*. pH-dependent modulation of relaxivity and luminescence in macrocyclic gadolinium and europium complexes based on reversible intramolecular sulfonamide ligation. *J. Am. Chem. Soc.*, 123, **2001**, 7601–7609.

[84] Woods, M.; Kiefer, G. E.; Bott, S. *et al*. Synthesis, relaxometric and photophysical properties of a new pH-responsive MRI contrast agent: the effect of other ligating groups on dissociation of a *p*-nitrophenolic pendant arm. *J. Am. Chem. Soc.*, 126, **2004**, 9248–9256.

[85] (a) Zhang, S.; Wu, K. C.; Sherry, A. D. A novel pH-sensitive MRI contrast agent. *Angew. Chem. Int. Ed.*, 38, **1999**, 3192–3194; (b) Merbach, A. E.; Helm, L.; Toth, E. The Chemistry of Contrast Agents in Medical Magnetic Resonance Imaging. Chapter 8.2 Probes responsive to physiological parameters. 2nd Edition, *Wiley*, Chichester, UK, **2013**, pp. 358.

2.6. Magnetic resonance angiography (MRA)

Non-specific MRI CAs circulate in blood pool for a very short time. They also leak into the interstitial space and some may enter the cells.[87] In addition, they are rather quickly filtered off by the kidneys or eliminated by the hepatobiliary system. To localize a CA purely in vessels, it has to interact with some blood pool component(s).

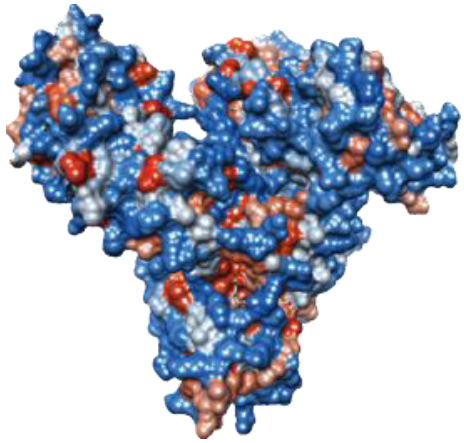

Figure 25 – Structure of human serum albumin (HSA)[86]

Human serum albumin (HSA, Figure 25) is the most abundant plasma protein (35–50 mg/L, 4.5% (w/w), 0.67 mM)[88] and, therefore, is commonly used for targeting. This biomacromolecule helps to maintain plasma pH and colloid osmotic pressure, and it is used as a carrier of fatty acids, hormones, billirubin, exogenous lipophilic molecules, *etc*. Thanks to the abundant charged amino acids on its surface, HSA is highly soluble and stable at pH 4–9 (some literature declares pH 4–8),[89] even at higher temperature (up to 60 °C for 10 h). Albumin is mostly localized in the vessels; however, it was also found trapped in tumors, inflammation sites or atherosclerotic plaque due to the presence of leaky capillaries.[90] For its unique properties, the HSA-binding strategies have been utilized in many diagnostic techniques such as MRI, nuclear medicine or optical imaging, and in therapy.

The heart-shaped molecule of HSA (M_r ~67 kDa) contains two major binding sites commonly called Sudlow's site I and II[91] in domain IIA and IIIA, respectively (Figure 26). The "sock-shaped" binding sites are decorated with many hydrophobic amino acid residues and with a few positively charged lysines and arginines.[92] Hence, these binding pockets have a huge affinity towards the neutral or negatively charged

---

[86] https://spinoff.nasa.gov/Spinoff2011/Images/hm-12_fmt.png, [Online] Accessed 01-08-2019.

[87] Aime, S.; Caravan, P. Biodistribution of gadolinium-based contrast agents, including gadolinium deposition. *J. Magn. Reson. Imaging*, 30, **2009**, 1259–1267.

[88] Cao, W.; Lu, X.; Cheng, Z. The advancement of human serum albumin-based molecular probes for molecular imaging. *Curr. Pharm. Des.*, 21, **2015**, 1908–1915.

[89] Peters, T., Jr. All about albumin: biochemistry, genetics and medical applications. *Academic Press Elsevier*, San Diego, CA, **1995**.

[90] Maeda, H.; Wu, J.; Sawa, T.; Matsumura, Y.; Hori, K. Tumor vascular permeability and the EPR effect in macromolecular therapeurics: a review. *J. Controlled Release*, 65, **2000**, 271–284.

[91] Sudlow, G.; Birkett, D. J.; Wade, D. N. The characterization of two specific drug binding sites on human serum albumin. *Mol. Pharmacol.*, 11, **1975**, 824–832.

[92] Yamasaki, K.; Chuang, V. T. G.; Maruyama, T.; Otagiri, M. Albumin-drug interaction and its clinical implication. *Biochim. Biophys. Acta*, 1830, **2013**, 5435–5443.

lipophilic substrates and those with "alkyl-like" (narrow, long and flexible) over "aryl-like" (bulky and rigid) groups.[93] Except these two major cavities, HSA contains many other binding sites which are highly specific for some molecules but rarely used as a target in drug design. Currently, many drugs utilize interactions with HSA in the blood pool to extend their circulation time and slow down their body clearance.[94]

From the chemical point of view, HSA might be used for the non-covalent interaction, as given above, or for a covalent coupling. A dominant strategy used for the covalent coupling with HSA is by a conjugation to its amino acid residues such as free thiol on Cys34 and the lysine amines (Figure 26). However, coupling is usually non-site-specific and an accurate quantification of the probe attachment is not available. The covalent coupling is often carried out *in vitro* and the decorated HSA is then injected into living body.

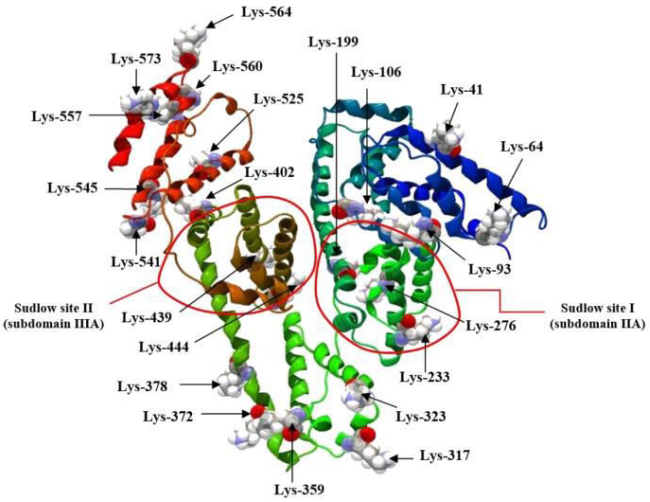

Figure 26 – HSA with highlighted lysine residues which may be used for covalent coupling; reprinted from[95]

2.6.1. Non-covalent binding

The main advantage of the non-covalent binding (to HSA) is reversibility of the interaction. Simple hydrophobic interaction is thermodynamically driven and excretion of drug is delayed. The fraction of drug not bound to HSA is (preferentially) filtered off by kidneys and, because of the dynamic equilibrium, a new fraction of drug dissociates from HSA–CA non-covalent conjugate. If the drug is MRI CA and it is bound to HSA, its relaxivity is increased due to a longer rotation correlation time τ_R. If the linker is too mobile, the relaxivity increase is not too significant.[72a]

---

[93] Henrotte, V.; Elst, L. V.; Laurent, S.; Muller, R. N. Comprehensive investigation of the non-covalent binding of MRI contrast agents with human serum albumin. *J. Biol. Inorg. Chem.*, 12, **2007**, 929–937.

[94] Sleep, D.; Cameron, J.; Evans, L. R. Albumin as a versatile platform for drug half-life extension. *Biochim. Biophys. Acta*, 1830, **2013**, 5526–5534.

[95] Szkudlarek, A.; Pentak, D.; Ploch, A. *et al*. *In vitro* investigation of the interaction of tolbutamide and losartan with human serum albumin in hyperglycemia state. *Molecules*, 22, **2017**, 2249.

Two clinically used CAs, which non-covalently interact with HSA, were Eovist® (or Primovist®) and MultiHance® (Figure 27). These DTPA derivatives possess ethoxybenzyl and benzyloxymethyl side groups, respectively, which interact with HSA *in vivo*. Relaxivity increase is only in few tens of percents as the binding interaction is not efficient and other relaxometric parameters are far from the optimal ones. Besides MRA, Eovist® is currently utilized for MRI imaging of liver as the CA is largely excreted through the hepatobiliary pathway.

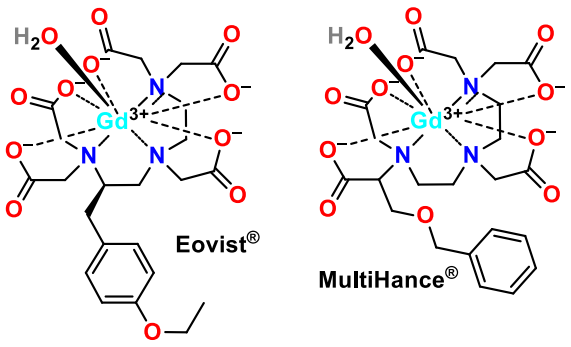

Figure 27 – Structures of MRI CAs Eovist® and Multihance® which non-covalently bind to HSA

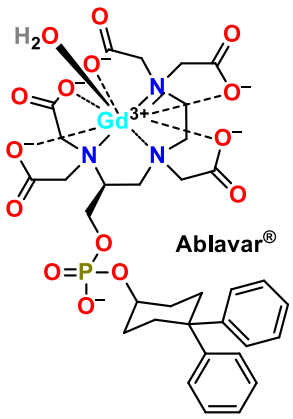

Figure 28 – Structure of MS–325 (Ablavar®)

Closer to the ideal angiographic CA is a molecule abbreviated as MS–325 (Figure 28), formerly known as Vasovist®, now sold (in U.S.) under trade name Ablavar® (generic name is Gadofosveset).[96] It was the first clinically approved MRI CA purely for MRA. Its diphenylcyclohexyl group strongly binds to Sudlow's site II in HSA and ~80–90 % of CA (concentration dependent) interacts with HSA in blood stream. When compared with non-bound form, the adduct has fivefold increase in relaxivity (measured *in vivo*; *in vitro*, there was tremendous ninefold increase, both measured at 20 MHz, 37 °C).[97] However, the interaction is so strong (K_{Aff} ~10^4 M^{-1}, 37 °C)[96] that the body clearance is too slow and it increases the risk of release of the toxic free Gd(III) ion from the kinetically labile DTPA chelate used in this CA. Nevertheless, CA was approved by U.S. FDA for MRA applications but it was never approved in Europe.[98] In addition, all three aforementioned MRA CAs are DTPA-based and, thus, they are currently almost completely withdrawn from the clinical use.[50]

[96] Caravan, P.; Cloutier, N. J.; Greenfield, M. T. *et al*. The interaction of MS-325 with human serum albumin and its effects on proton relaxation rates. *J. Am. Chem. Soc.*, 124, **2002**, 3152–3162.

[97] Goyen, M. Gadofosveset-enhanced magnetic resonance angiography. *Vasc. Health Risk Manag.*, 4, **2008**, 1–9.

[98] https://www.ema.europa.eu/en/medicines/human/EPAR/ablavar-previously-vasovist, [Online] Accessed 01-08-2019.

Hence, stable Gd(III) complexes of DOTA-like ligands with the lipophilic side group are sought for non-covalent binding to HSA. Negatively charged complexes are preferred due to the lysine- and arginine-rich decoration of the HSA cavities close to its surface.[93] Caravan *et al*. prepared a small library of MRA CAs and investigated water exchange rates.[99] Complexes possessed a side biphenyl-phosphate group which is known to interact with HSA efficiently (Figure 29). The fastest water exchange rate was found for complexes of ligands with one phosphonate and one phenolate pendant arms ("R" in Figure 29 is in Figure 30). Their τ_M was in a low "ns" scale (Figure 30). When that fast exchange rate (τ_M ~1 ns, 37 °C) had been coupled with the very long rotation correlation time τ_R upon formation of the albumin conjugate, it caused that the limiting factor of relaxivity (at 1.5 T) became electron relaxation time T_{1e}.

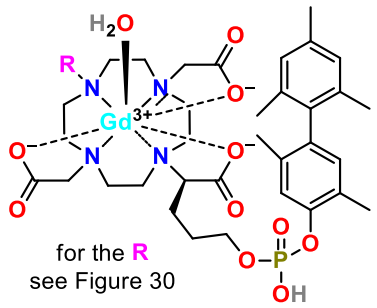

Figure 29 – Structure of biphenyl-phosphate derivatives of Gd–DOTA-like MRA CAs

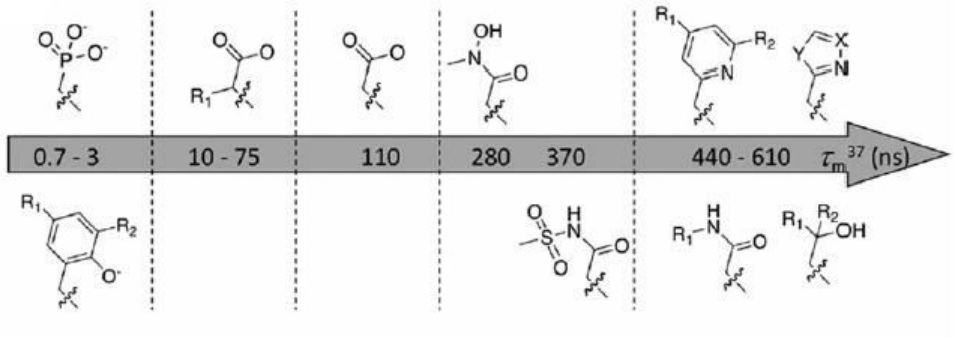

Figure 30 – Impact of an "R" group in MRA CAs from Figure 29 on their water residence time (at 37 °C); reprinted from[99a]

[99] (a) Caravan, P.; Zhang, Z. Structure–relaxivity relationships among targeted MRI contrast agents. *Eur. J. Inorg. Chem.*, **2012**, 1916–1923; (b) Dumas, S.; Jacques, V.; Sun, W.-C. *et al.* High relaxivity magnetic resonance imaging contrast agents part 1: impact of single donor atom substitution on relaxivity of serum albumin-bound gadolinium complexes. *Invest. Radiol.*, 45, **2010**, 600–612.

2.7. Polynuclear MRI probes

Magnetic fields of the most common MRI scanners currently used in human medicine are 1.5 and 3.0 T, and MRI scanners with "stronger fields" (above 3 T) are being tested. In these "stronger" magnetic fields, relaxation enhancement of MRI CAs is not so efficient and optimal relaxation parameters of MRI CAs are different: both τ_M and τ_R should be in a low "ns" scale. This optimal water residence time τ_M was observed for Gd–DO3AP^R complexes and, thus, they are good adepts for such applications. The optimal τ_R is achieved with relatively "small" molecules with max. ~8–10 Gd(III) ions per molecule over tens of Gd(III) ions, *e.g.* in dendrimers. In those structures, Gd(III) chelates have to be rigidly interconnected to slow down molecular tumbling of both, Gd(III) chelates and the whole structure (characterized by τ_R^{LOCAL} and τ_R^{GLOBAL}, respectively), otherwise "free tumbling" of Gd(III) chelate would greatly decrease efficiency of a possible relaxation enhancement of the whole structure. Moreover, Gd(III) complexes must be stable and must not release toxic free Gd(III) ion. Hence, the ideal chelators of Gd(III) ion are those based on macrocycles because of their Gd(III) complexes have optimized properties (*e.g.* for relaxometry, stability).

"Interconnection" of Gd(III) complexes has been investigated from early 1990s but the relaxation parameters were evaluated only for a few of them. The dimeric BO(DO3A)$_2$ complex (Figure 31) was one of the first to be studied.[100] The main aim was to slow down the molecular tumbling τ_R and, thus, to increase relaxivity by a covalent connection of two Gd(III) chelates in one molecule. The interconnection in the GdGd–BO(DO3A)$_2$ complex led to improved relaxometric parameters, mainly of τ_R which was increased almost threefold (to τ_R ~250 ps) in the comparison with Gd–DOTA (τ_R ~77 ps).[101] However, the linker was still too flexible and, in addition, the water residence time was too long (τ_M ~1 μs) which caused the relaxivity (20 MHz, 37 °C) increase to be only ~21 % when compared with Gd–DOTA (4.6 and 3.8 mM^{-1} s^{-1}, respectively).[100]

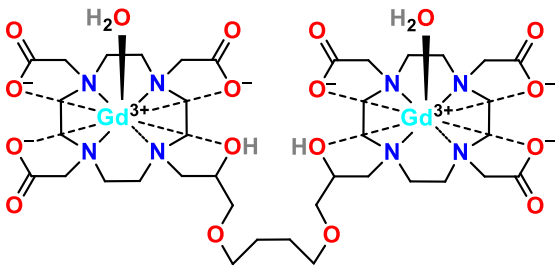

Figure 31 – Structure of dimetallic Gd(III) complex of the ligand BO(DO3A)$_2$

[100] Toth, E.; Vauthey, S.; Pubanz, D.; Merbach, A. E. Water exchange and rotational dynamics of the dimeric gadolinium(III) complex [BO{Gd(DO3A)(H$_2$O)}$_2$]: a variable-temperature and -pressure ^{17}O NMR study. *Inorg. Chem.*, 35, **1996**, 3375–3379.

[101] Powell, D. H.; Dhubhghaill, O. M. N.; Pubanz, D. *et al*. Structural and dynamic parameters obtained from ^{17}O NMR, EPR, and NMRD studies of monomeric and dimeric Gd^{3+} complexes of interest in magnetic resonance imaging: an integrated and theoretically self-consistent approach. *J. Am. Chem. Soc.*, 118, **1996**, 9333–9346.

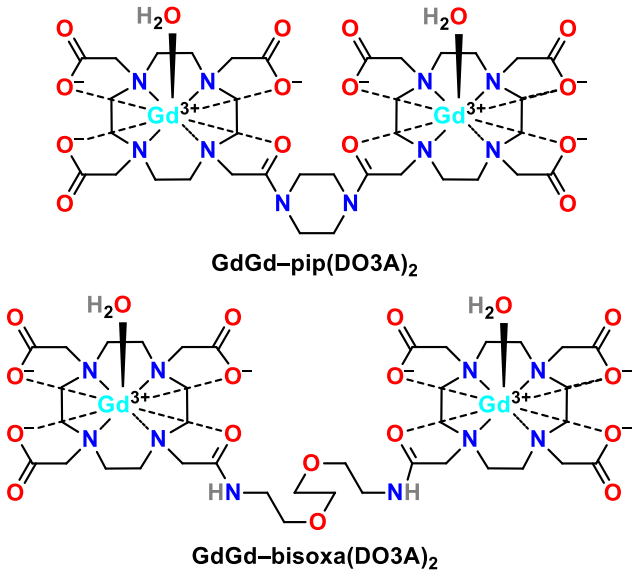

Figure 32 – Structures of two dimetallic Gd(III) complexes of dimeric DOTA-monoamide ligands with a rigid (up) and flexible (bottom) linker

Other early studies were done on the complexes of DOTA mono-amides, pip(DO3A)$_2$ and bisoxa(DO3A)$_2$ (Figure 32), with a bridging moiety between two units.[101] The IS water residence time in both complexes was longer (τ_M ~700 ns, as it is common in Gd–DOTA-monoamide complexes) than that in Gd–DOTA (τ_M ~244 ns) as well as τ_R (171 and 106 ps, respectively) in comparison with that in Gd–DOTA (τ_R ~77 ns). The flexibility of the bridge differs: GdGd–pip(DO3A)$_2$ has a rigid piperazine bridge whereas GdGd–bisoxa(DO3A)$_2$ has a flexible ethylene glycol chain. The relaxivities (20 MHz, 37 °C) of the dimeric complexes were 5.8 and 4.9 mM^{-1} s^{-1}, respectively, which are higher (by ~53 and ~29 %, respectively) than that for Gd–DOTA (3.8 mM^{-1} s^{-1}). Hence, connecting two Gd–DOTA-like complexes *via* the rigid bridge as present in GdGd–pip(DO3A)$_2$ causes a significant increase of relaxivity.

Another example of a conjugate with a semi-rigid linker is the dimeric Gd(III) complex of two DO3AP^{ABn} ligands connected mutually together *via* thiourea bridge (Figure 33).[102] Water residence time τ_M of the "dimer" is short (~53 ns) as expected for Gd–DO3AP^R complex (see Chapter 3.2.1), much shorter than that for Gd–DOTA (τ_M ~244 ns). Due to the presence of the semi-rigid linker, the molecular tumbling of the "dimer" was slowed and rotation correlation time τ_R was more than doubled (~183 ps) when compared with the monomeric unit (~88 ps for Gd–DO3AP^{ABn}) and Gd–DOTA (~77 ps). In addition, one SS water molecule per Gd–DO3AP^R unit (see Chapter 3.2.1) also contributes to overall relaxivity. Hence, "dimerization" of Gd(III) complex by the

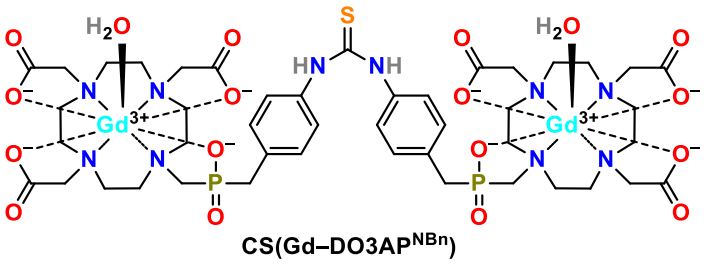

Figure 33 – Structure of the dimeric Gd(III) complex CS(Gd–DO3AP^{NBn})$_2$

[102] Rudovsky, J.; Botta, M.; Hermann, P. *et al*. Relaxometric and solution NMR structural studies on ditopic lanthanide(III) complexes of a phosphinate analogue of DOTA with a fast rate of water exchange. *Dalton Trans.*, **2006**, 2323–2333.

linker improved its relaxivity (20 MHz, 25 °C) by ~44 % (8.7 and 5.7 mM^{-1} s^{-1} for dimeric and monomeric complex, respectively) and even by ~85 % when compared with Gd–DOTA (4.7 mM^{-1} s^{-1}).[101]

If seven Gd–DO3AP^{ABn} complexes were conjugated to an even more rigid scaffold, *e.g.* to *β*-cyclodextrin (*β*-CD) *via* NCS coupling (Figure 34), the resultant conjugate had relaxometric parameters close to optimal ones.[103] The IS water residence time remained as short as that for monomeric unit and its value is nearly optimal (τ_M ~11 and 16 ns for the conjugate and monomer, respectively). The tumbling of the Gd(III) chelate was significantly slowed (τ_R^{LOCAL} ~290 ps and τ_R for monomeric unit is ~88 ps) and, moreover, combined with the rigidity of *β*-CD (τ_R^{GLOBAL} was fitted to lengthy ~2 ns). Both relaxometric parameters, τ_M and τ_R, were in a range of the optimal values suitable for MRI CA for the "higher" magnetic fields. Moreover, the Gd–DO3AP^{R} complexes also benefit from the tightly bound SS water molecules (see Chapter 3.2.1) and, thus, their relaxivity was additionally increased. Hence, the Gd–DO3AP^{ABn} conjugate with *β*-CD has one of the highest relaxivities per Gd(III) (r_{1p} ~20 and 14 mM^{-1} s^{-1} at 1.5 and 3.0 T, respectively) measured till now and this Gd(III) conjugate is suitable as MRI CA for "higher" magnetic fields.

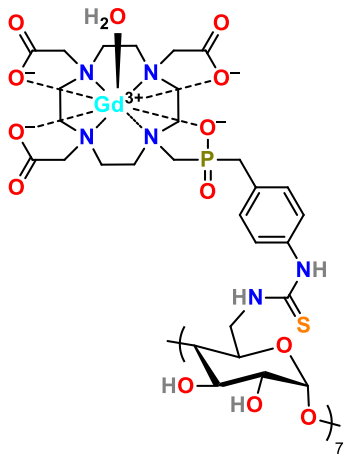

Figure 34 – Structure of *β*-CD decorated with Gd–DO3AP^{ABn}

[103] Kotkova, Z.; Helm, L.; Kotek, J.; *et al*. Gadolinium complexes of monophosphinic acid DOTA derivatives conjugated to cyclodextrins scaffolds: efficient MRI contrast agents for higher magnetic fields. *Dalton Trans.*, 41, **2012**, 13509–13519.

Relaxation parameters which are commonly tuned in a controlled manner involve q, τ_M and τ_R. Moreover, Gd(III) ion has a long electron relaxation time (T_{1e})[104] when compared with other metal ions. Thus, extension of relaxation time T_{1e} is an another way to increase relaxivity of Gd(III) complexes. One of the approaches to studying a change of relaxation time T_{1e} is to place two metal ions in a proximity to each other. For example, ligand OHEC (Figure 35)[75] forms dinuclear complexes with Ln(III) ions. The structure of its dinuclear complexes resembles two Ln–DOTA-like complexes connected inside of "a macro-macrocycle". The Ln(III) ions mutually interact through space as their distance in solution is ~6.6–6.8 Å which was confirmed also in the solid state by X-ray diffraction.[105] Such a short distance between metal ions alters their relaxation times T_{1e}. In the case of the homonuclear dimetallic Gd(III) complex, the EPR measurements confirmed that transverse electron relaxation time was extended by the factor of three (~4.5 × 10^9 s^{-1} at 0.34 T) in comparison with that for Gd–DOTA.[75] Hastened electron relaxation is not in favour of relaxivity increase mainly if water exchange rate of the complex is fast. However, this study proved that relaxivity of Gd(III) complexes can be also altered by changing the relaxation time T_{1e}, *e.g.* by placing two metal ions close to each other.

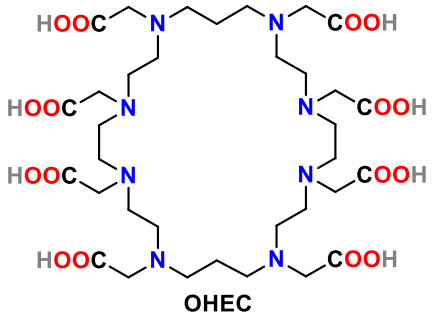

Figure 35 – Structure of the ligand OHEC

[104] T_{1e} is directly dependent on squared zero-field splitting parameter, Δ^2, and its correlation time of its modulation, τ_v (see above).

[105] (a) Schumann, H.; Bottger, U. A.; Weisshoff, H. *et al*. Structures of rare earth homodinuclear macrocyclic complexes with the polyamine polycarboxylic ligand 1,4,7,10,14,17,20,23-octaazacyclohexacosane-1,4,7,10,14,17,20,23-octaacetic acid (H_8OHEC) in the crystal and in solution. *Eur. J. Inorg. Chem.*, **1999**, 1735–1743. (b) Schumann, H.; Bottger, U. A.; Zietzke, K. *et al*. 1,4,7,10,13,16,19,22-octaazacyclotetracosane-1,4,7,10,13,16,19,22-octaacetic acid (H_8OTEC) and 1,4,7,10,14,17,20,23-octaazacyclohexacosane-1,4,7,10,14,17,20,23-octaacetic acid (H_8OHEC): synthesis and characterization of two large macrocyclic polyamine polycarboxylic ligands and some of their copper(II) and lanthanide(III) complexes. *Chem. Ber./Recueil*, 130, **1997**, 267–277.

2.8. Magnetic resonance spectroscopy (MRS)

Aside from the measuring proton water signal and visualizing it as a T_1-weighted MRI image, other compounds (and nuclei) present *in vivo* can be detected by MRI. MRI scanner may be used to acquire "normal" ^{1}H NMR data after a proper adjustment. If a result of the measurement is NMR spectrum instead of an image (Figure 36), the analytical method is called magnetic resonance spectroscopy (MRS).[108] However, a signal-to-noise ratio (SNR) is very low and the measurements are commonly limited to a small selected investigated area instead of the whole body scans.

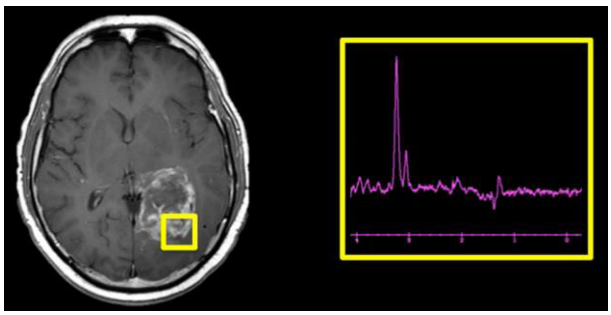

Figure 36 – Comparison of MRI image (left) and MRS spectrum (right) of the yellow area[106]

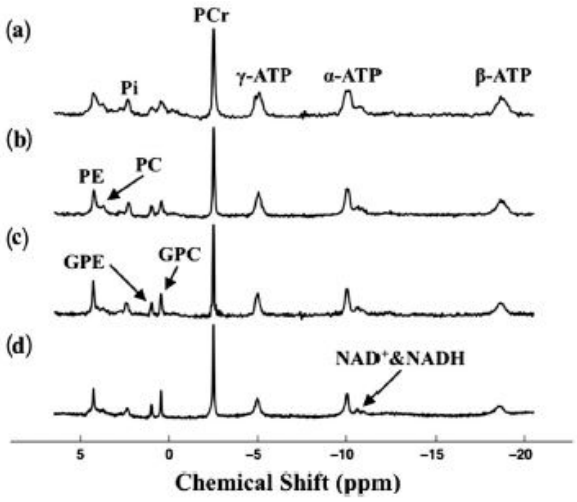

Figure 37 – ^{31}P MRS spectra of cat brain *in vivo* measured at (a) 4 T (NT 192), (b) 7 T (NT 128), (c) 9.4 T (NT 64), and (d) 16.4 T (NT 40); no line-broadening applied, NT = a number of scans; reprinted from[107]

Among all the body tissues, brain has been the most investigated and well-explored organ due to its rich chemical composition.[109] The main advantage of MRS is its non-invasiveness and it has been recognized as a valid diagnostic tool used mainly in neuroscience. The lack of good SNR is partially compensated by an applied magnetic field – "ultrahigh" (> 3 T) static magnetic fields are preferred as the SNR is sufficiently increased (Figure 37) and measuring times are shortened. However, diagnostic procedures still require tens of minutes of scanning time motionless which is hardly achieved, *e.g.* with the young or elderly patients.

---

[106] http://mriquestions.com/uploads/3/4/5/7/34572113/image-and-spectrum_orig.jpg, [Online] Accessed 01-08-2019.

[107] Lu, M.; Chen, W.; Zhu, X.-H. Field dependence study *in vivo* brain ^{31}P MRS up to 16.4 T. *NMR Biomed.*, 27, **2014**, 1135–1141.

[108] Alger, J. R. Magnetic resonance spectroscopy. In Squire, L. R. *Encyclopedia of Neuroscience*. 1st Ed., *Academic Press Elsevier*, San Diego, CA, **2009**, pp. 601–607.

[109] Morris, P. G. Magnetic resonance imaging and magnetic resonance spectroscopy of neurotransmitters in human brain. *Ann. Neurol.*, 13, **1999**, 330–336.

2.8.1. ^{31}P MRS

The ^{31}P MRS (utilized since 1970s) is based on the monoisotopic ^{31}P nucleus. Extracellular and intracellular fluids contain diverse phosphorus compounds and each has a unique resonance frequency. Because the monoisotopic ^{31}P has a reasonable sensitivity and nuclear spin ½, signals are narrow (with a small half-width and a long T_2), the compounds can be easily distinguished (Figure 38). Low-molecular-weighted water-soluble and mobile compounds are *e.g.* ATP and phosphocreatine (utilized in bioenergetics; their abnormal ratio is a marker of unhealthy pathological processes), inorganic phosphate, phospholipids (found in cell membrane), and sugar phosphates. All are present in an "mM" range of concentrations.

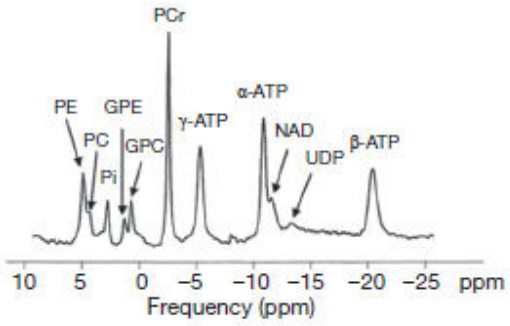

Figure 38 – A representative ^{31}P MRS spectrum of human brain; reprinted from[110]

Intensity ratio of the measured ^{31}P NMR signals gives information about the "local" metabolism. Any measured abnormalities point to the pathological processes being involved (*e.g.* cancer, genetic diseases, inadequate autoimmune response, inflammation, *etc.*).[111] However, diagnosis requires entire chemical shift range to be measured in the each evaluated voxel. The ^{31}P relaxation rates are very long (in range of few seconds). Many optimizations of the pulse sequences have been suggested (*e.g.* flexTPI[112] which allows acquirement of all ^{31}P metabolites successively within a single measurement) but still measurements performed on the motionless patient take an obnoxious time (up to ~30 min). Finally, a spatial resolution with 9.4 T reaches up to (15 mm^3)[112] which limits the potential clinical applications of ^{31}P MRS and its clinical impact is currently minimal. Hence, a significant method improvement is generally required.

More attractive utilization arises from ^{31}P NMR / MRS signal resonance frequency dependence on pH (*e.g.* caused by (de)protonation of group in the proximity to phosphorus atom). Inorganic phosphate is a suitable candidate for pH measurement *in vivo* but its concentration and the signal overlap with endogenous phosphorus-

---

[110] de Graaf, R. A. *In Vivo* NMR Spectroscopy: Principles and Techniques. 3rd Edition, *Wiley*, Hoboken, NJ, **2019**.

[111] Liu, Y.; Gu, Y.; Yu, X. Assessing tissue metabolism by phosphorus-31 magnetic resonance spectroscopy and imaging: a methodology review. *Quant. Imaging Med. Surg.*, 7, **2017**, 707–726.

[112] Lu, A.; Atkinson, I. C.; Zhou, X. J.; Thulborn, K. R. PCr/ATP ratio mapping of the human head by simultaneous imaging of multiple spectral peaks with interleaved excitations and flexible twisted projection imaging readout trajectories at 9.4 T. *Magn. Reson. Med.*, 69, **2013**, 538–544.

containing compounds spoil the measurements. Anyway, ^{31}P MRS has been successfully used to measure pH *in vivo* many times.[113]

Endogenous phosphorus compounds are present in low mM concentrations and their ^{31}P chemical shifts are similar to each other. Thus, exogenous phosphorus-containing compounds have been introduced and investigated. The first and only requirement for the applied exogenous compounds is absolute non-toxicity (*i.e.* no undesired interaction with biological processes *in vivo*) combined with an easy elimination from the patient organism (preferentially, in urine). In 1994, this was accomplished by 3-aminopropylphosphonic acid (3-APP, Figure 39)[114] with pK_A of the phosphonate group ~6.7. By using 3-APP, it was verified that the extracellular fluid around the cancerous tissue is slightly acidic (6.3–7.0) due to lactic acid excreted by the more energy-demanding cancerous cells.[82] Except cancer, many diseases and pathological processes change "local" pH and, thus, it is desired to localize these areas and diagnose patient in the early stages to improve subsequent treatment. Currently, efficient novel extracellular pH probes are clinically desired.

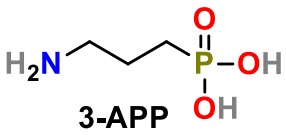

Figure 39 – Structure of 3-aminopropyl-phosphonic acid

3 . Complexes of DOTA and DOTA-like ligands

3.1. Stability and solution structure of Ln–DOTA

The "gold standard" among MRI CAs, Gd–DOTA (Figure 15), possesses high thermodynamic stability (logK_{GdL} ~24.7), kinetic inertness (no observable transmetalation for several weeks at physiological pH; acid-assisted decomplexation $\tau_{1/2}$(pH = 2) is ~3930 h)[115] and one inner-sphere water molecule coordinated to Gd(III) ion. It is used in clinics as one of the safest MRI CA under trade name Dotarem®. Its structure consists of four five-membered "glycine-like" and four "ethylene-diamine-like" chelates (Figure 40). The central Ln(III) ion is coordinated by four amine nitrogen atoms (forming N_4-plane) and by four pendant carboxylate oxygen atoms (forming O_4-plane,

[113] Rata, M.; Giles, S. L.; de Souza, N. M. *et al*. Comparison of three reference methods for the measurement of intracellular pH using ^{31}P MRS in healthy volunteers and patients with lymphoma. *NMR Biomed.*, 27, **2014**, 158–162.

[114] Gillies, R. J.; Liu, Z.; Bhujwalla, Z. M. ^{31}P-MRS measurements of extracellular pH of tumors using 3-aminopropylphosphonate. *Am. J. Physiol.*, 267, **1994**, 195–203.

[115] Pulukkody, K. P.; Norman, T. J.; Parker, D. *et al*. Synthesis of charged and uncharged complexes of gadolinium and yttrium with cyclic polyazaphosphinic acid ligands for *in vivo* applications. *J. Chem. Soc. Perkin Trans. 2*, **1993**, 605–620.

Figure 40). The DOTA coordination polyhedron in its Gd(III) complex allows the ninth coordination site to be occupied by a water molecule above the O_4-plane.

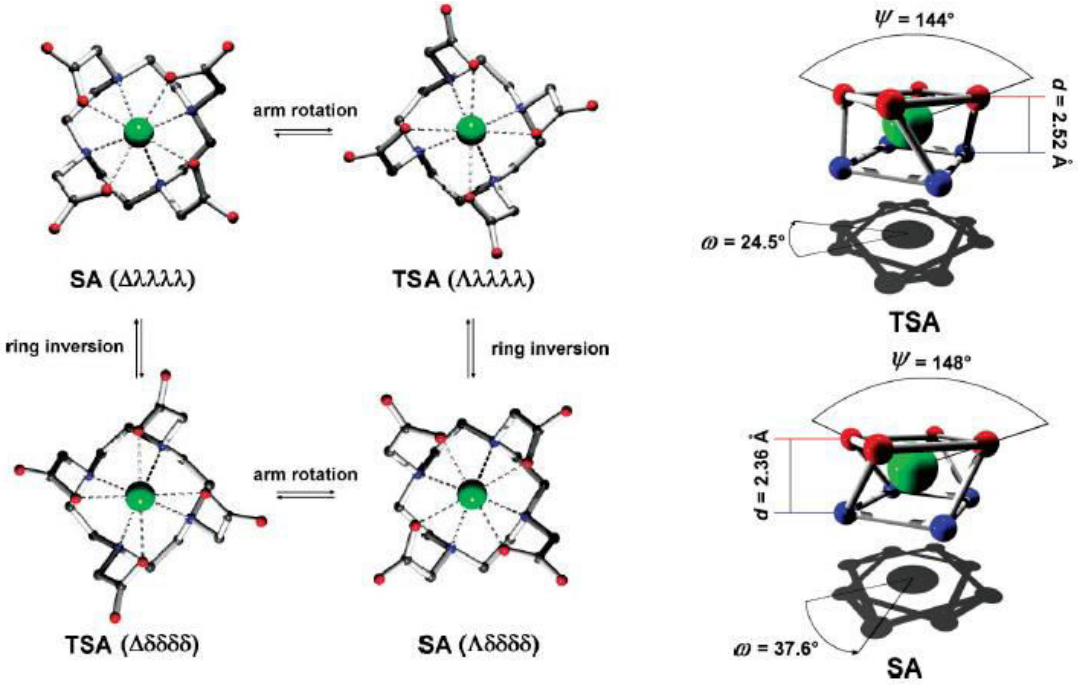

Figure 40 – Isomerism of Ln–DOTA as a consequence of macrocycle ethylene and the pendant arms orientation; coordinated water molecule is omitted; herein, SA and TSA isomers are represented by Pr–DOTA and Ce–DOTA, respectively; reprinted from[116]

In solution, Ln(III) (including Gd(III)) complexes of DOTA are present in two diastereomeric pairs of enantiomers (Figure 40).[117] Conformation of the cyclen chelate rings (λ / δ) generates one kind of isomerism whereas a formal rotation of the pendant arm (Λ / Δ) causes the second one. From the theoretical computations and the practical observance, only one type of the ethylene conformation (all four λ or δ) and the pendant arm orientation (all four Λ or Δ) are thermodynamically favourable. Hence, complexes with $\Lambda\delta\delta\delta\delta$ and $\Delta\lambda\lambda\lambda\lambda$ conformations are enantiomers known as square antiprismatic diastereoisomer (SA or SAP) and, *vice-versa*, enantiomeric pairs of $\Delta\delta\delta\delta\delta$ and $\Lambda\lambda\lambda\lambda\lambda$ conformations are known as twisted square antiprismatic diastereoisomer (TSA or TSAP).[118]

---

[116] Hermann, P.; Kotek, J.; Kubicek, V.; Lukes, I. Gadolinium(III) complexes as MRI contrast agents: ligand design and properties of the complexes. *Dalton Trans.*, **2008**, 3027–3047.

[117] (a) Desreux, J. F. Nuclear magnetic resonance spectroscopy of lanthanide complexes with a tetraacetic tetraaza macrocycle. Unusual conformation properties. *Inorg. Chem.*, 19, **1980**, 1319–1324. (b) Aime, S.; Botta, M.; Ermondi, G. NMR study of solution structures and dynamics of lanthanide(III) complexes of DOTA. *Inorg. Chem.*, 31, **1992**, 4291–4299.

[118] Benetollo, F.; Bombieri, G.; Calabi, L.; Aime, S.; Botta, M. Structural variations across the lanthanide series of macrocyclic DOTA complexes: insights into the design of contrast agents for magnetic resonance imaging. *Inorg. Chem.*, 42, **2003**, 148–157.

The SA and TSA isomers of complexes of the DOTA-like ligands have a different geometry of "the coordination cavity". In the SA isomer, the O_4-plane is closer to the N_4-plane, thus, allowing coordinated water to be closer to central metal ion in comparison with the TSA isomer. The O_4–N_4-planes distance is shorter by ~0.16 Å in SA isomer.[116] This also causes shortening of the Gd–OH_2 bond length. For MRI CA design, SA isomers may contribute more to the overall relaxivity due to shorter Gd–H_2O distance but tend to exchange IS water more slowly because of its "stronger" binding.

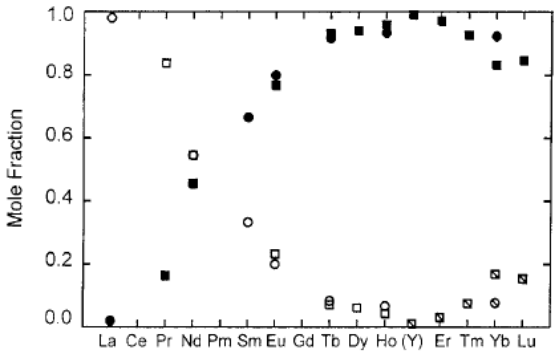

Figure 41 – TSA (empty) and SA (filled) isomers abundance of Ln–DOTA complexes; reprinted from[119]

Introducing Ln(III) ions larger than Gd(III) ion increases abundance of the TSA isomer over SA isomer as the TSA arrangement is more adapted for the large ions. Smaller Ln(III) ions prefer SA arrangement but, for Ln(III) commonly around Ho(III), a change in the Ln(III) hydration number arises and, thus, the coordination number drops from 9 to 8. Concomitantly, the TSA isomers are preferred again but now with no metal-ion-bound water molecule (*i.e.* the TSA' isomers). In Figure 41, abundance of isomers of Ln–DOTA complexes is shown.

3.1.1. *Design of DOTA derivatives for MRI CAs*

The Gd–DOTA is a non-specific MRI CA and, thus, it is not able to specifically interact with different tissues. To introduce any modification and retain the desired properties (*e.g.* stability) of Gd–DOTA, a targeting moiety should be attached *via* the ligand backbone (Figure 42). However, compounds with modified cyclen ring are synthetically hardly accessible. Another commonly used approach is derivatization of one of the pendant acetates (Figure 42). Syntheses and purifications of these compounds are generally much easier than that of aforementioned compounds and the beneficial properties of Gd–DOTA are retained but these complexes lack optimal relaxometric properties, *e.g.* they do not have optimal water residence time (their τ_M ~50–100 ns).[66]

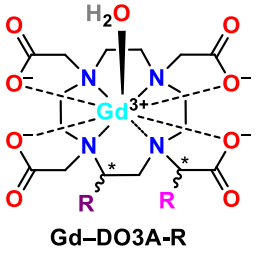

Figure 42 – Structure of Gd–DOTA decorated on the cyclen backbone and on the pendant arm

[119] Aime, S.; Botta, M.; Fasano, M. *et al*. Conformational and coordination equilibria on DOTA complexes of lanthanide metal ions in aqueous solution studied by ^{1}H-NMR spectroscopy. *Inorg. Chem.*, 36, **1997**, 2059–2068.

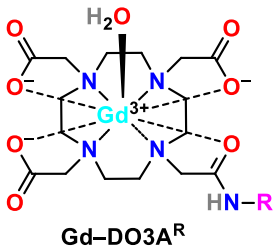

Figure 43 – Structure of Gd–DO3A-monoamide

However, the oldest and the most commonly used approach is substitution of one pendant acetate for its functional amide (Figure 43). In these CAs, non-charged carbonyl oxygen is coordinated instead of charged carboxylate one. It results in sufficient complex stability. However and the most importantly, the water residence time is greatly prolonged, by one order of magnitude, to τ_M ~0.3–1.5 μs.[66,120] Thus, they are not perfectly suitable for MRI applications and wholly inappropriate for the "higher" magnetic fields.

3.2. DOTA derivatives with phosphorus acid pendant arm(s)

Analogously to "glycine-like" coordination of Gd(III) in Gd–DOTA, "aminomethylphosphonic" and "aminomethylphosphinic" acids can form the five-membered chelating ring. Therefore, Gd(III) complexes of phosphorus acid analogues of DOTA, Gd–DOTP and Gd–DOTP^{H}, have been widely investigated (Figure 44).

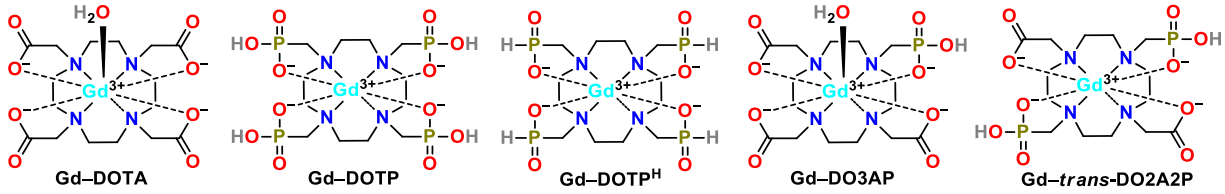

Figure 44 – Examples of Gd(III) complexes of DOTA and its analogues with phosphorus acid pendant arm(s)

Charged oxygen donor atoms of phosphonates / phosphinates are harder donors than the those of carboxylates and, thus, they prefer hard acids (*i.e.* Ln(III) ions). Phosphonates significantly increase basicity of the *α*-amino group (due to strong electron-donating effect of the fully deprotonated PO_3^{2-} group). Generally, complexes stability

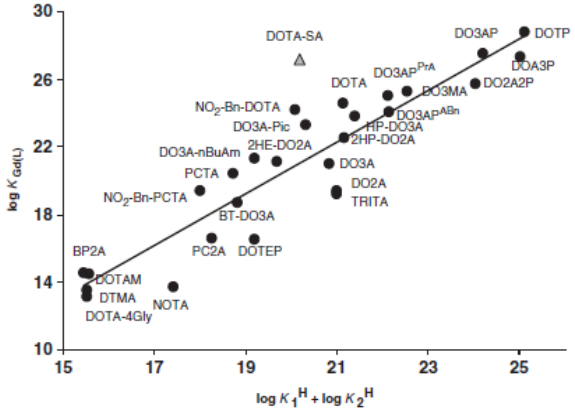

Figure 45 – Plot of thermodynamical stability constants of Gd–L complexes vs. sum of two most basic protonation constant of the macrocycle; reprinted from[121]

[120] Buddhima, N. S.-M.; Allen, M. J. Strategies for optimizing water-exchange rates of lanthanide-based contrast agents for magnetic resonance imaging. *Molecules*, 18, **2013**, 9352–9381.

[121] Merbach, A. E.; Helm, L.; Toth, E. The Chemistry of Contrast Agents in Medical Magnetic Resonance Imaging. Chapter 4.3.3 Stability of complexes of macrocyclic ligands. 2nd Edition, *Wiley*, Chichister, UK, **2013**, pp. 176.

correlates with basicity (expressed in logK_A) of the ligands. For instance, sum of the first two protonation constants of macrocyclic ligands (corresponding to protonation of the macrocyclic amines) is in a linear correlation with thermodynamic stability of their complexes (Figure 45). It shows the complexes of ligands with phosphorus acid pendant arm(s) possess a high stability.

Moreover, phosphorus atom is larger than carbon atom and P–C bond is longer than the C(O)–C bond and, thus, the coordinated phosphonate / phosphinate oxygen atoms tend to be more distant from the N_4-plane than the carboxylate ones. It leads to a higher abundance of TSA isomers in their complexes. Relaxometric parameters of Gd–DO3AP (Figure 46) are nearly optimal (short τ_M and q = 1, Table 4). Fast water exchange is caused by bulkiness of the pendant phosphonate / phosphinate. Similar values of the parameters have been observed for complexes of monophosphinic acid analogues of DOTA, DO3AP^R (Figure 48). However, introduction of additional phosphorus acid groups (*e.g.* in *trans*-DO2A2P or DOTP) leads to removal of the IS water molecule in the Gd(III) complexes.

Parameter	Gd–DOTA[101]	Gd–DO3AP[122]	Gd–*trans*-DO2A2P[123]	Gd–DOTP[124]
$^{20}r_{1p}$ / mM^{-1} s^{-1}	4.7 (25 °C) 3.8 (37 °C)	– 4.6 (37 °C)	3.6 (25 °C)[a] –	– 3.5 (37 °C)[a]
q	1	1	0	0
q^{ss}	0	1	N.D.	≈3.3
τ_M / ns	244	14	–	–
TSA or TSA‘ abundance / %	15	50	100	100

[a]No inner-sphere water molecule (q = 0). Relaxation is caused mainly by the second-sphere hydration.

Table 4 – Comparison of some relaxometric parameters of Gd(III) complexes with parameters of Gd(III) complexes of DOTA and DOTA-like ligands; at 20 MHz, pH ~7, 25 °C, if not stated otherwise; N.D. means “not determined”.

[122] Rudovsky, J.; Cigler, P.; Kotek, J. Lanthanide(III) complexes of a mono(methylphosphonate) analogue of H$_4$dota: The influence of protonation of the phosphonate moiety in the TSAP/SAP isomer ratio and the water exchange rate. *Chem. Eur. J.*, 11, **2005**, 2373–2384.

[123] Kalman, F. K.; Baranyai, Z.; Toth, I. *et al*. Synthesis, potentiometric, kinetic, and NMR studies of 1,4,7,10-tetraazacyclododecane-1,7-bis(acetic acid)-4,10-bis(methylenephosphonic acid) (DO2A2P) and its complexes with Ca(II), Cu(II), Zn(II) and lanthanide(III) ions. *Inorg. Chem.*, 47, **2008**, 3851–3862.

[124] Kotkova, Z.; Pereira, G. A.; Djanashvili, K. *et al*. Lanthanide(III) complexes of phosphorus acid analogues of H$_4$DOTA as model compounds for the evaluation of the second-sphere hydration. *Eur. J. Inorg. Chem.*, **2009**, 119–136.

3.2.1. *Gd–DO3AP^{R} complexes*

As presence of IS water molecule is crucial for the MRI CAs, DO3AP^{R} ligands (Figure 46) are suitable as DOTA analogues for Gd(III) ion coordination. The Gd–DO3AP^{R} properties can be further tuned by pendant phosphinic acid substituent, "^{R}".

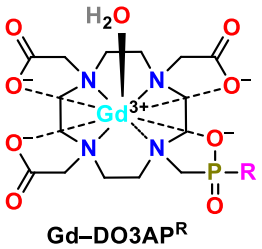

Figure 46 – Structure of Gd–DO3AP^{R} complexes

Many DO3AP^{R} derivatives and their complexes have been prepared and studied but only a few of them were thoroughly evaluated from relaxometric point of view. The presence of the bulky phosphinate group induces prevalence of TSA isomers over SA ones. Hydration break in Ln(III) series is similar to that of Ln–DOTA, *i.e.* around Dy(III)–Ho(III). In their Gd(III) complexes, one SS water molecule is expected, which increases relaxivity by up to ~20 % (Table 5). Moreover, it was observed that all Gd–DO3AP^{R} complexes have a short τ_M and its value is close to the optimal value. Table 5 summarizes relaxation parameters for some Gd–DO3AP^{R} complexes (Figure 47).

Parameter	Gd–DOTA[101]	Gd–DOTP^{H} [124]	Gd–DO3AP^{OEt} [125]	Gd–DO3AP^{ABn} [126]	Gd–DO3AP^{BP} [127]
$^{20}r_{1p}$ at 37 °C / mM^{-1} s^{-1}	3.8	2.2	3.5	4.2	5.3
q	1	0	1	1	1
τ_M / ns	244	–	50	16	198
τ_R / ps	77	86	84	88	134
q^{SS}	0	≈1.3	1	1	≈1.8
τ_M^{SS} / ps	–	–	50	1	56
$A/\hbar^{a}$ / 10^6 rad s^{-1}	–3.7	–	–3.3	–2.89	–3.24
TSA abundance / %	15	100	35	50	35

[a]The hyperfine coupling constant $A/\hbar$ indirectly evaluates a number of bound water molecules to Gd(III). Values of $A/\hbar$ equal to approx. (–3.0)–(–3.7) × 10^6 rad s^{-1} point to q = 1 for the complex.

Table 5 – Relaxation data for Gd–DOTA, Gd–DOTP^{H}, and selected derivatives of Gd–DO3AP^{R} (see Figure 47); measured at pH ~7 and 25 °C, if not stated otherwise

[125] Lebduskova, P.; Hermann, P.; Helm, L. *et al*. Gadolinium(III) complexes of mono- and diethyl esters of monophosphinic acid analogue of DOTA as potential MRI contrast agents: solution and relaxometric studies. *Dalton Trans.*, **2007**, 493–501.

[126] Rudovsky, J.; Kotek, J.; Hermann, P. *et al*. Synthesis of a bifunctional monophosphinic acid DOTA analogue ligand and its lanthanide(III) complexes. A gadolinium(III) complex endowed with an optimal water exchange rate for MRI applications. *Org. Biomol. Chem.*, 3, **2005**, 112–117.

[127] Vitha, T.; Kubicek, V.; Kotek, J. *et al*. Gd(III) complex of a monophosphinate-bis(phosphonate) DOTA analogue with a high relaxivity; lanthanide(III) complexes for imaging and radiotherapy calcified tissues. *Dalton Trans.*, **2009**, 3204–3214.

The phosphorus atom allows further derivatization of the pendant phosphinic acid group. For instance, geminal bis(phosphonate) of DO3AP^{BP} serves as Ca^{2+} sensitive probe and its complexes have a high affinity to calcified tissues and bones.[127] Aminobenzyl group of DO3AP^{ABn} (Figure 47) is a suitable candidate for a NCS-based couplings. The Gd–DO3AP^{ABn} conjugates with *β*-cyclodextrin (Figure 34) have one of the highest relaxivity per Gd(III) ion (~21 mM^{-1} s^{-1}) ever achieved for MRI CA smaller than ~10 kDa.[103] Likewise, DO3AP with *P*-propionic acid (abbreviated as DO3AP^{CE} or DO3AP^{PrA}, Figure 47) can also be used for coupling reactions.[128] In the conjugates, fast water exchange rate of Gd–DO3AP^{R} is retained and, thus, the ligands are suitable Gd(III) chelators for MRI applications.

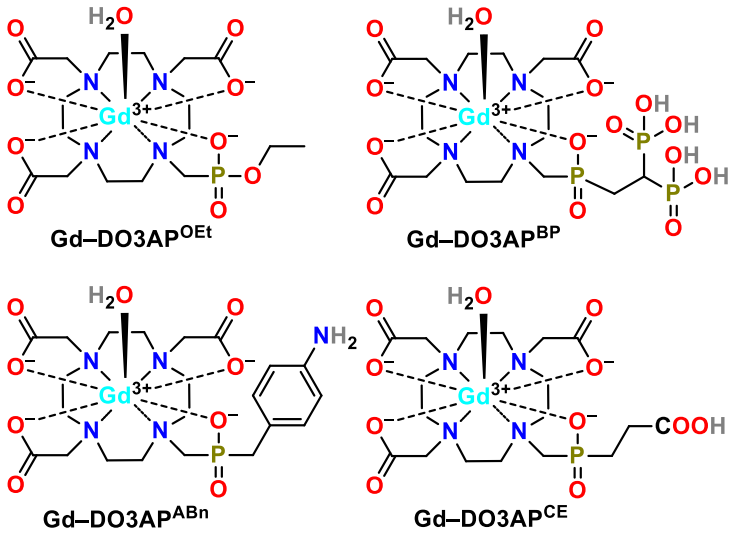

Figure 47 – Structures of several Gd–DO3AP^{R} complexes

3.2.2. *Future prospects*

Generally, DO3AP^{R} ligands are suitable for stable Gd(III) chelation with q = 1. Their Gd(III) complexes have almost optimal water residence time and a rich SS hydration sphere and, thus, they are perspective MRI CAs. However, other relaxation parameters (*e.g.* τ_R) can be tuned by attachment of a proper phosphinate substituent. Moreover, the presence of ^{31}P nuclei may be utilized in ^{31}P MRS which is beneficial for determination of tissue pH. In order to fulfil this demand, novel DO3AP^{R}-based CAs with protonable group and, thus, with pH-dependent properties were introduced in this Thesis and their relaxometric parameter properties were evaluated.

[128] Forsterova, M.; Petrik, M.; Laznickova, A. *et al*. Complexation and biodistribution study of ^{111}In and ^{90}Y complexes of bifunctional phosphinic acid analogs of H_4dota. *Appl. Radiat. Isot.*, 67, **2009**, 21–29.

Thesis Aims and Scope

In vivo stability is the most crucial property of exogenous MRI contrast agent. The Ln(III) complexes of linear polyamino-polycarboxylates are kinetically labile and CAs based on them were withdrawn from the market. To increase complex stability, complexes of macrocyclic ligands are preferred. MRI relaxometric parameters (*e.g.* water residence time τ_M and rotation correlation time τ_R) of Gd–DOTA are far from the optimal ones and, thus, new DOTA derivatives have been investigated.

Monophosphorus acid derivatives of DOTA, the DO3AP^R, have the most suitable properties as ligands for Gd(III)-based contrast agents. The Gd–DO3AP^R complexes have been shown to have high complexes stability and kinetic inertness, and MRI relaxometric parameters close to the optimal ones (*e.g.* fast water exchange rate). To further explore relaxometric behaviour of these complexes, effect of a protonation close to the phosphinate group will be investigated.

This Thesis aims are:

1) Optimization of synthesis of DOTA-like ligands with the phosphinic acid pendant arm(s) to get an access to new ligands;

2) Exploration of complexes of new DO3AP^R ligands with a protonable aminomethylphoshinate pendant arm and description of impact of its protonation state on the complex properties (in solution and the solid state);

3) Investigation of effect of the protonation on non-covalent hydrophobic interactions of the Gd(III) complexes with HSA.

In order to fulfil these tasks, several goals have to be accomplished. Planned DOTA-like derivatives with phosphinic acid pendant arm(s) are hardly accessible with current synthetic strategies. Hence, it is necessary to find suitable synthetic methods for preparation of compounds with the N–C–P–H moiety as well as for the reaction of aminomethyl-*H*-phosphinic acids with cyclen derivatives.

The second goal is investigation of properties of new Ln–DO3AP^R complexes which are altered with protonation of the pendant amino group. The Ln(III) complexes of DOTA (aminomethyl)phosphinic acid derivative, DO3AP^{AM}, are chosen as the model compounds with protonable pendant amine. The goal is to evaluate change in their properties (*e.g.* relaxometry, isomerism) with the pendant amine protonation. Moreover, the Ln–DO3AP^{AM} complexes are good candidates for ^{31}P MRS as currently used diagnostic techniques based on

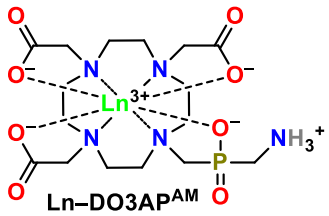

^{31}P MRS have many disadvantages (*e.g.* long measurement times, overlapping signals). The Ln(III) complexes of the DO3AP^{AM} ligand should have these ^{31}P relaxation properties improved and ^{31}P NMR properties of the Ln(III) complexes should be dependent on the protonation state of the pendant amine group.

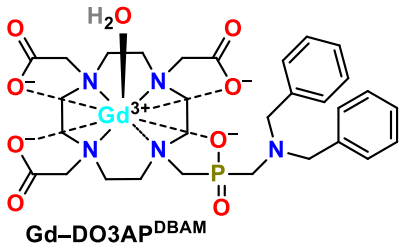

Gd–DO3AP^{DBAM}

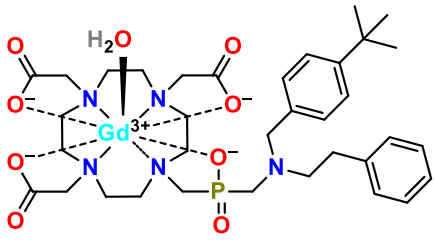

Gd–DO3AP^{tBPAM}

Gd(III)-based complexes with hydrophobic pendant group(s) are used in magnetic resonance angiography (MRA). The U.S. approved DTPA-based CA Ablavar® is used for MRA. However, stability of the complex is insufficient and release of toxic free Gd(III) aqua ion was observed in patient with renal disease as complex elimination from the patient body is too slow. As the main binding sites (I and II) of HSA have on their surface positively charged amino acids, the Gd(III)-based complex interaction with HSA should change with the protonation state of pendant amine of complex. Thus, the Gd–DO3AP^{DBAM} and Gd–DO3AP^{tBPAM}, which have hydrophobic *N*-alkyl substituents, should be stable (they are based on DO3AP^{R} ligand), they should have properties and binding to HSA dependent on protonation state of the pendant amine, and they should have faster elimination from patient body than Ablavar® because of lower pH in kidneys than in bloodstream.

Synthesis of a unique ditopic ligand, DO3A–P–DO3A, emerged from the new synthetic protocol and enhanced reactivity of alkyl hypophosphite. The ligand should form mono- and dimetallic (homo- and heteronuclear) complexes. The metal ions in the dimetallic complexes should have a rigid phosphinate bridge and, thus, tumbling of the complexes should be fully coupled. It should result in a high relaxivity of the homonuclear dimetallic Gd$_2$(III) complex. The heteronuclear dimetallic complexes, GdM–(DO3A–P–DO3A), may serve as model compounds whose relaxivity should depend on the second coordinated ion (*i.e.* on its molecular mass).

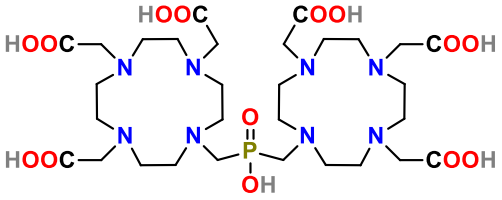

DO3A–P–DO3A

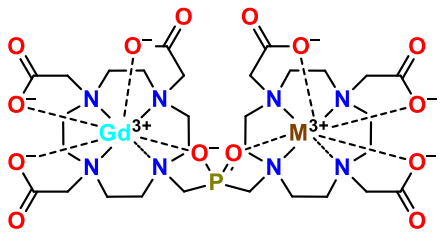

GdM–(DO3A–P–DO3A)

4. Synthesis of amino-*H*-phosphinic acids and their macrocyclic derivatives

The synthetic strategies for synthesis of amino-*H*-phosphinic acids (AHPAs) were thoroughly described in Chapter 1.2.2. The current approaches utilize unstable hypophosphorous acid esters, pyrophoric phosphites, H–P(OR)$_2$, or thermally unstable anhydrous H_3PO_2. In addition, purification of esterified intermediates is often difficult due to instability of *H*-phosphinate esters and presence of a number of by-products.[26] Thus, new straightforward synthetic strategies leading to AHPAs are desired. These acids are necessary synthetic precursors for the DO3AP^R compounds with an aminomethyl pendant arm. More detailed information is given in the published paper[129] reprinted in Appendix A.

4.1. "Phospha-Mannich" reaction in acetic acid as a solvent

The simplest phosphorus precursor, aqueous H_3PO_2, has been successfully utilized in syntheses of *H*-phosphinic acids only in the "Moedritzer–Irani-like" (M–I) reactions. In the standard protocol, formation of AHPA from amine, aldehyde and H_3PO_2 requires acidic aqueous conditions, such as in commonly used excess of H_3PO_2 or conc. or diluted (1:1) aq. HCl. However, reactions are often not clean and many by-products are formed (Figure 48).

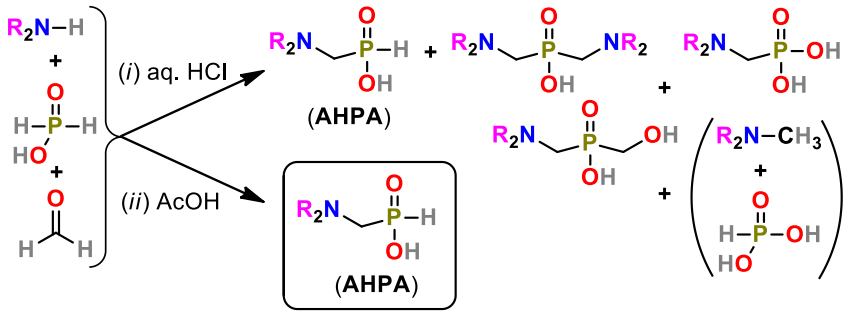

Figure 48 – Reaction scheme of the "Moedritzer–Irani-like" reaction performed: (*i*) in aq. HCl with formation of by-products, (*ii*) in AcOH without any by-products

The novel synthetic approach presented here involves use of acetic acid as a solvent under mild conditions (40 °C, 1–2 d). Reaction of 50% aq. H_3PO_2, paraform-aldehyde and nucleophilic secondary amine (in molar ratio 1.1:2:1, respectively) smoothly and cleanly led to the corresponding AHPAs in high conversions and yields. Purification

[129] Urbanovsky, P.; Kotek, J.; Cisarova, I.; Hermann, P. Selective and clean synthesis of aminoalkyl-*H*-phosphinic acids from hypophosphorous acid by phospha-Mannich reaction. *RSC Adv.*, 10, **2020**, 21329–21349.

often consisted of only ion exchange chromatography on a strong cation exchanger where AHPAs were mostly retained and eluted off with 10% aq. pyridine (see Appendix A).

As the "standard" M–I reaction is carried out in water and in the presence of a HCl, effects of water content and a HCl were investigated. The reaction rate gradually decreased with increasing water content (from hours to days). Strictly anhydrous conditions (*i.e.* use of anhydrous H_3PO_2) led to a minor increase in formation of some by-products (*e.g.* C–P–C compounds). Hence, a small amount of water (*i.e.* introduced as 50% aq. H_3PO_2) was beneficial. If hydrochloride of the starting amine was used, conversion to AHPA was greatly decreased and by-products were observed. An addition of 10 equiv. of conc. aq. HCl[130] stopped the reaction and reaction at elevated temperature led to a large amount of by-products.

Other *H*-phosphorus acids were also tested. Under the used conditions, H_3PO_3 reacted slowly, so longer reaction time and increased temperature were needed. Yields of the desired products were poor. In all cases, *N*-methylation of the starting amine connected with oxidation of H_3PO_3 to H_3PO_4 was observed as main reaction. Reactions of *H*-phosphinic acids were similar as *P*-oxidation was nearly always significant. However, reactions outcomes were likely dependent on the nuclephilicity of *H*-phosphinic acid – "electron-rich" RPO_2H_2 (R = alkyl) gave better results than "electron-poor" ones (*e.g.* R = aryl; for more information, see Appendix A).

The reaction (Figure 49) outcome for several aldehydes (different **R**, **R** = Bn) was investigated. The optimal conditions were found to be AcOH, 60–80 °C, 1–2 d; amine, H_3PO_2, and aldehyde in molar ratio 1:1.1:2, respectively. "Higher aldehydes" were less reactive than formaldehyde as it is common in "phospha-Mannich" reactions (*e.g.* K–F, M–I). Only acetaldehyde gave a good conversion and yield.

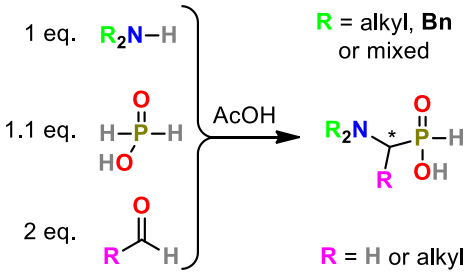

Figure 49 – The reaction for synthesis of AHPAs

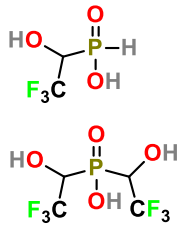

Figure 50 – The fluorinated phosphinic acids

Reaction of *n*-butanal or phenylacetaldehyde led to lowered yields of the product. Aromatic benzaldehyde, sterically hindered pivaldehyde (*i.e.* trimethyl-acetaldehyde) or acetone did not give any isolable product.

Unexpectedly, trifluoroacetaldehyde monohydrate (*i.e.* fluoral) reacted at the elevated temperature to form $CF_3CH(OH)PO_2H_2$ (Figure 50). If the reaction was done without amine, $[CF_3CH(OH)]_2PO_2H$ was formed and isolated (Figure 50). This *H*-phosphinic acid is an interesting compound combining

[130] Water content of the reaction mixture did not exceed 5 % (v/v) after addition of conc. aq. HCl (10 equiv.).

presence of reactive functional groups (hydroxyl, P–H) and fluorine atoms (*e.g.* for ^{19}F MRI, fluorinated drugs) with a high solubility.

Several secondary amines were employed in the model reaction (Figure 49; **R** = H, different **R**). The optimal conditions were found as AcOH, 40 °C, 1 d; amine, H_3PO_2, and formaldehyde in molar ratio 1:1.1:2, respectively. Starting secondary amines with alkyl, benzyl or mixed substituents gave almost quantitative conversions as well as isolated yields after the simple ion exchange purification. Similarly, simple cyclic amines (*e.g.* piperidine, morpholine) gave the AHPAs in high yields.

On the other hand, *N*-(2-hydroxyethyl)amines caused an enhanced bis-substitution of phosphorus atom, *i.e.* formation of the fragment N–C–P–C–N. Aromatic amines gave rich hardly separable mixtures. Heterocyclic amines (*e.g.* imidazole) and amides did not react at all. The less basic *N*-trifluoroalkylated amines promoted H_3PO_2 oxidation and the corresponding *N*-methyl amines were detected (see Appendix A). The amino acids, *N*-alkyl glycine derivatives and L-proline, showed slightly decreased conversion and isolated yields than those obtained with nucleophilic secondary amines. The phosphorus amino acids reacted differently: (*i*) AHPAs with a secondary *α*-amine (*i.e.* with the H(R)N–CH_2–**PO_2H_2** fragment, see Figure 51) gave rich mixtures, and (*ii*) *α*-aminomethylphosphonic acids (APAs, with the H(R)**N**–CH_2–**PO_3H_2** fragment) gave two isolable products, R_2**N**–CH_2–PO_2H_2 and (R_2**N**–CH_2)$_2$–PO_2H, which are mono- and bis-substituted products derived from H_3PO_2. This property of AHPAs and APAs is probably caused by lower pK_A of amine of AHPA than that of APA.[131] Moreover, two APAs, glyphosate and phosphonic acid analogue of IDA, gave the corresponding AHPAs (Figure 51) in high conversions and moderate isolated yields (58 and 69 %, respectively).

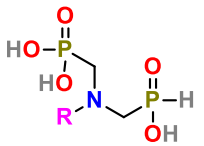

Figure 51 – AHPAs derived from APAs

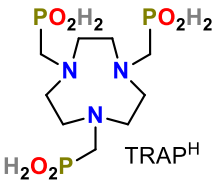

Figure 52 – Structure of $TRAP^H$

The secondary polyamines were also tested. The presence of the ethylene-diamine fragment (*i.e.* N–(CH_2)$_2$–N) causes a cyclic aminal formation (detected *in situ*). Conversion to the corresponding *N*,*N*′-bis(*H*-phosphinic acids) was suppressed and *N*-methylated *N*′-mono-*H*-phosphinic acids were isolated. Thus, almost all polyazamacrocycles did not form the corresponding AHPAs with exception of TACN (*i.e.* formation of $TRAP^H$,[132] Figure 52). Extended linker between

[131] Amino group of APA is more basic (~two orders of magnitude) than the same amino group of AHPA.[116]

[132] Simecek, J.; Schulz, M.; Notni, J. *et al*. Complexation of metal ions with TRAP (1,4,7-triazacyclononane phosphinic acid) ligands and 1,4,7-triazacyclononane-1,4,7-triacetic acid: phosphinate-containing ligands as unique chelators for trivalent gallium. *Inorg. Chem.*, 51, **2012**, 577–590.

secondary amines (utilization of N–$(CH_2)_3$–N and N–$(CH_2)_6$–N moieties instead of N–$(CH_2)_2$–N one) afforded only the expected bis-AHPAs which were isolated in almost quantitative yields (Figure 53). Furthermore, these *H*-phosphinic acids were oxidized[133] with Hg^{2+} ions to phosphonic acids and *N*-benzyl protecting groups were removed by hydrogenation (Figure 53). Both reactions were clean and high-yielding. The formed APAs are unique compounds which are not easily accessible by other way. The same results were obtained with corresponding polyalkylene-triamines.

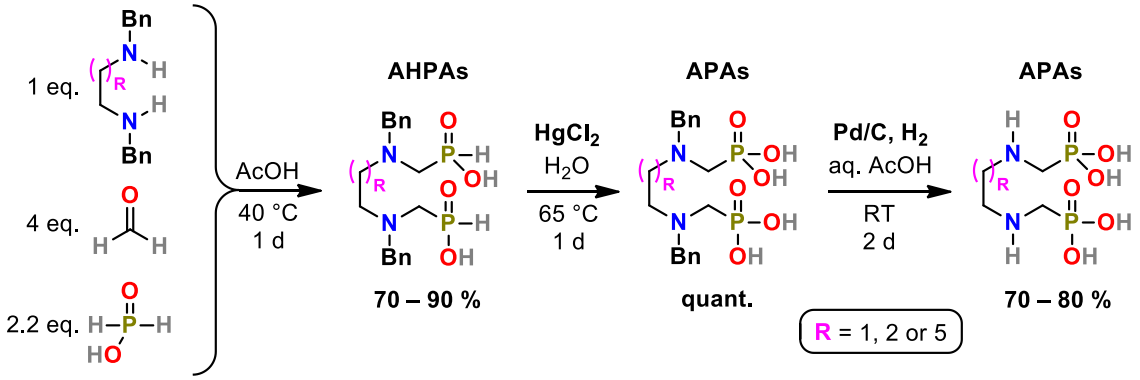

Figure 53 – Reaction of linear secondary polyamines, oxidation of the AHPAs and removal of *N*-benzyl group to get APAs with secondary amines

Under the used reaction conditions, reactivity of various secondary amines is different. Nucleophilicity / basicity (*i.e.* pK_A) of the amines seems to play an important role. Secondary amines with pK_A > ~8 reacted smoothly and only AHPAs were formed. However, secondary amines with pK_A < ~7 were *N*-methylated and simultaneously H_3PO_2 oxidized. In the case of the primary amine, the first reaction step gave mono-AHPA and the amine basicity / nucleophilicity is greatly decreased as *H*-phosphinic acid group is an electron-withdrawing group.[116] Therefore, only some electron-rich amines (*e.g.* adamantylamine, cyclohexylamine, *t*-butylamine) provided the corresponding bis-AHPAs in reasonable conversions and yields.

4.1.1. Reaction mechanism investigations

Reaction mechanism was investigated in AcOH-d_4 by ^1H and ^{31}P NMR. The compounds Me_2NH + paraformaldehyde, $(Me_2N{=}CH_2)^+$ Cl^-, and $(Me_2N)_2CH_2$ (the latter two compounds were both amine and formaldehyde sources) were used in the reactions. The reaction of Me_2NH with gradually increasing amount of paraformaldehyde gave a new set of signals which were assigned to two intermediates, Me_2NCH_2OR and $[Me_2N(CH_2OR)_2]^+$ (R = H or Ac, Figure 54). A quick addition of

[133] Motekaitis, R. J.; Murase, I.; Martell, A. E. New multidentate ligands. XIII. Ethylenediaminetetra(methylenephosphinic acid). *Inorg. Nucl. Chem. Lett.*, 7, **1971**, 1103–1107.

H_3PO_2 (as 50% aq. solution) in excess caused fast formation of two products: the major one was the desired AHPA, $Me_2NCH_2PO_2H_2$, and the minor one was the compound $[Me_2N(CH_2OR)(CH_2PO_2H_2)]^+$ (from $[Me_2N(CH_2OR)_2]^+$). The latter product hydrolysed to the final product, $Me_2NCH_2PO_2H_2$, after addition of water in excess.

Dissolution of $(Me_2N{=}CH_2)^+$ Cl^- in AcOH-d_4 led to a quite different ^{1}H NMR spectrum than reaction above. The $(Me_2N{=}CH_2)^+$ Cl^- partially reacted with AcOH-d_4 to a mixture of $[Me_2N(CH_2OR)_{1/2}]^{0/+}$ and "free" Me_2NH leading to equilibrium mixture. When anhydrous H_3PO_2 was quickly added to this mixture, $Me_2NCH_2PO_2H_2$ started to form but together with $(Me_2NCH_2)_2PO_2H$. Hence, the presence of the iminium species enhanced formation of C–P–C moiety. Addition of aqueous H_3PO_2 (*i.e.* the water addition) favours the mono-substitution as the water quickly reacted with the iminium species to Me_2NCH_2OR and, thus, the reaction followed the previous case.

The aminal, $(Me_2N)_2CH_2$, decomposed into Me_2NH, $(Me_2N{=}CH_2)^+$ and Me_2NCH_2OR after dissolution in AcOH-d_4. The addition of anhydrous H_3PO_2 caused a slow formation of $Me_2NCH_2PO_2H_2$ and $(Me_2NCH_2)_2PO_2H$, and the signal of $(Me_2N{=}CH_2)^+$ decreased. Addition of D_2O to this mixture caused an instant transformation of $(Me_2N{=}CH_2)^+$ into Me_2NCH_2OR, and formation of $(Me_2NCH_2)_2PO_2H$ significantly dropped. Hence, under the used conditions (*i.e.* use of wet AcOH), Me_2NCH_2OR and $[Me_2N(CH_2OR)_2]^+$ can be presumed as the main reaction intermediates.

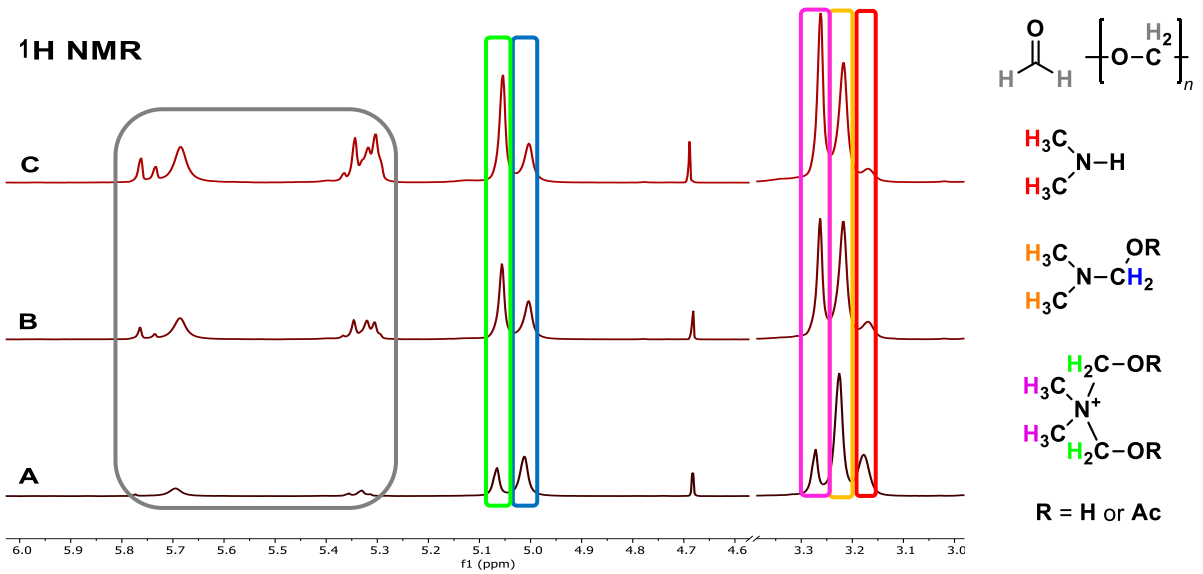

Figure 54 – ^{1}H NMR spectra (300 MHz) of the reaction of Bn_2NH and $(CH_2O)_n$ (in molar ratio 1:1 (**A**), 1:2 (**B**) and 1:3 (**C**)) with formation of two intermediates, Me_2NCH_2OR and $[Me_2N(CH_2OR)_2]^+$ (R = H or Ac); the colour codes are used as labelled

Based on the data, it is possible to speculate about reaction mechanism (Figure 55). Firstly, nucleophilic secondary amine reacts with formaldehyde to form R'_2NCH_2OR and $[R'_2N(CH_2OR)_2]^+$ (R = H or Ac). In AcOH, H_3PO_2 is presumed to be present in equilibrium of two forms, $H_2P^{V}(O)(OH)$ and $H–P^{III}(OH)_2$. In the next step, either of these two forms of H_3PO_2 reacts with R'_2NCH_2OR and / or $[R'_2N(CH_2OR)_2]^+$ to form intermediate species with N–C–O–P fragments. The final product, $R'_2NCH_2PO_2H_2$, is formed after instant re-arrangement of the intermediates (and after additional hydrolysis of $[R'_2N(CH_2PO_2H_2)(CH_2OR)]^+$). The small amount of water suppresses formation of the iminium species and, thus, the unwanted formation of the compounds with N–C–P–C–N fragment. The absence of strong acids prevents formation of P–CH_2–OH species.

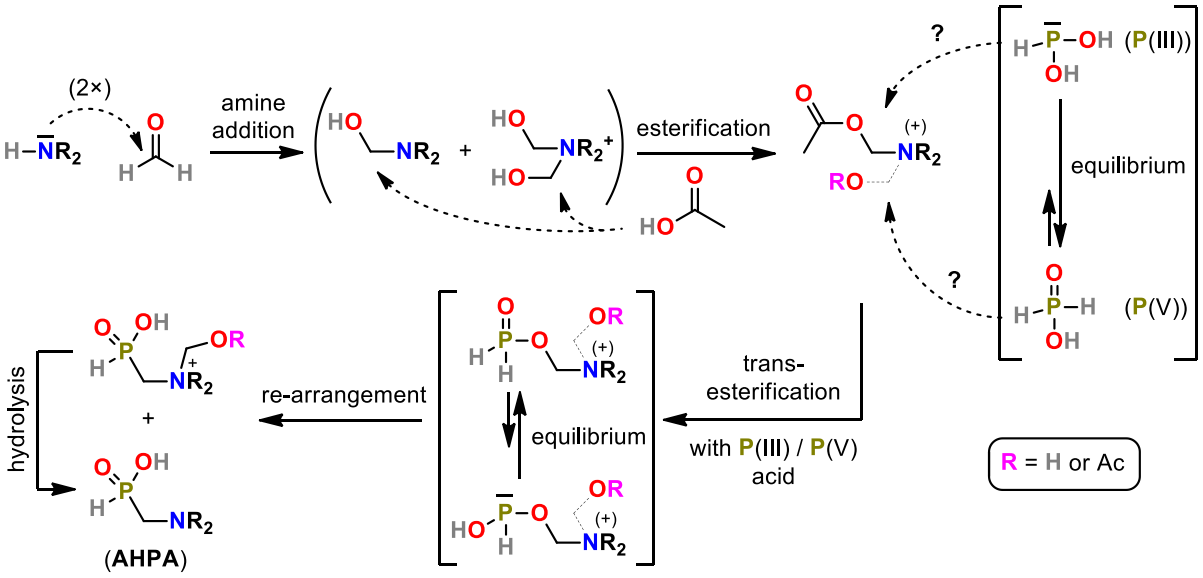

Figure 55 – Tentative reaction mechanism of "phospha-Mannich" reaction of secondary amine, formaldehyde and H_3PO_2 in AcOH

4.1.2. Summary

- AHPAs were cleanly formed in AcOH (40–60 °C, 1–2 d) from 50% aq. H_3PO_2, electron-rich and not sterically hindered aldehydes, and nucleophilic secondary amines (pK_A > ~8) in molar ratio 1.1:2:1, respectively. In most cases, purification consisted of only strong cation exchanger. Conversions and yields were high.
- Only basic primary amines produced bis-AHPAs but in moderate yields.
- Presence of the ethylene-diamine fragment (*i.e.* with N–C–C–N moiety) caused undesired reductive *N*-methylation coupled with *P*-oxidation.
- Three key intermediates were detected, R_2NCH_2OR, $[R_2N(CH_2OR)_2]^+$ and $[R_2N(CH_2PO_2H_2)(CH_2OR)]^+$ (R = H or Ac), by investigation of the reaction mechanism in AcOH-d_4. The tentative reaction mechanism was proposed.

4.2. Kabachnik–Fields reaction in pyridine as a solvent

AHPAs have protonable amino group and, thus, they are interesting precursors for ligands with pH-dependent properties. In the previous Chapter 4.1, AHPAs were efficiently synthesized in AcOH as a solvent and further reactions of AHPAs with other amines in AcOH (to form N–C–P–C–N fragment) were complicated. Thus, the "synthetic protocol" in AcOH could not be used to prepare the cyclen-based ligands. Commonly, PINs are being attached to a macrocycle (*e.g.* TACN, cyclen, cyclam)[30] under aqueous acidic conditions (*e.g.* in hot aq. HCl). However, this reaction has often moderate conversions mainly due to formation of many by-products (*e.g. P*-hydroxymethylation, *N*-methylation of amine coupled with *P*-oxidation; see Figure 56) and, thus, purifications of the reaction mixtures are complicated and the reactions have low yields. Hence, a new synthetic method was necessary to get straightforward access to the cyclen-based ligands which will be then used for metal ion coordination.

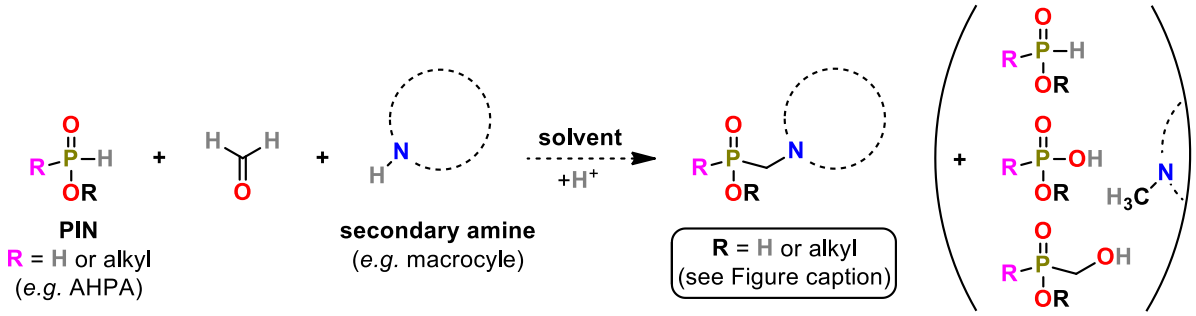

Figure 56 – A scheme of the "phospha-Mannich" reaction performed in aq. HCl (**R** = H, with by-products in parenthesis) or in pyridine (**R** = alkyl, without by-products in parenthesis)

The compounds with C–P–C fragment are commonly prepared by Kabachnik–Fields (K–F) reaction.[134] In this reaction of amine, aldehyde, and compound with P–H bond, the phosphorus reactants are esters of phosphorus acid (commonly, dialkyl *H*-phosphites / *H*-phosphonates and alkyl *H*-phosphinates), benzene or toluene are used as solvents and Lewis acids as catalysts. Alkyl esters of PINs are hardly accessible in a pure form and they are unstable and, thus, it is convenient to prepare them *in situ*. Because of a low solubility of PINs in solvents common for K–F reaction, other solvents were tested and pyridine gave the best reaction conversions (see Appendix B). Also, no by-products were observed in the presence of an acid catalyst (Figure 56). Hence, K–F reaction in pyridine was investigated in more detail. Pyridine has nucleophilic nitrogen atom and, thus, Lewis acids could not be used to catalyse the reaction. Therefore, Brønsted acids were tested as catalysts.

[134] Keglevich, G.; Balint, E. The Kabachnik–Fields reaction: mechanism and synthetic use. *Molecules*, 17, **2012**, 12821–12835.

The common phosphorus reagents in K–F reaction are dialkyl *H*-phosphites. Thus, the reaction of various dialkyl *H*-phosphites with Bn_2NH and paraformaldehyde (in molar ratio 1:1.1:2, respectively; pyridine, 40 °C; Figure 57) were investigated. In all cases, pyridinium hydrobromide (*i.e.* HBr as a Brønsted acid) had to be added as a catalyst otherwise conversions considerably decreased and the starting dialkyl *H*-phosphites decomposed faster. The $H–P(O)(OBn)_2$, $H–P(O)(OMe)_2$ and $H–P(O)(OPh)_2$ were not stable in pyridine and gradually decomposed. Only $H–P(O)(OiPr)_2$ and $H–P(O)(OEt)_2$ (*i.e.* DEP) gave the quantitative conversions. Hence, DEP was further used as a source of phosphonate group in K–F reaction in pyridine. The results are summarized in Appendix B.

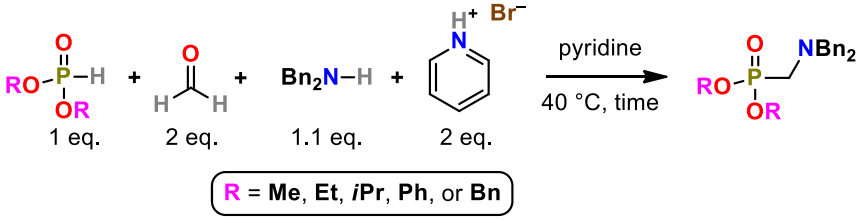

Figure 57 – Dialkyl *H*-phosphites in K–F reaction in pyridine

Then, different pyridine derivatives and their salts were tested as solvents and catalysts, respectively, with DEP, Bn_2NH, and paraformaldehyde in a model reaction. The best results were achieved with pyridine and py · HBr (2 equiv.). The 2-picoline with its hydrobromide (2 equiv.) and 2,6-lutidine with its hydrobromide (2 equiv.) significantly decelerated reaction rate up to two- and six-times, respectively (see Appendix B). Anyway, these reactions were clean and no by-products were observed.

Pyridine is a great solvent to dissolve various compounds which are hardly soluble in other anhydrous solvents used for K–F reaction (*e.g.* amino acids or phospho(i)nic acids in toluene). Hence, the optimized K–F reaction conditions in pyridine were successfully tested on preparation of several cyclen-based ligands. The DEP was used to prepare *cis*-*t*Bu_2DO2A2P^{OEt2}, *trans*-*t*Bu_2DO2A2P^{OEt2}, *Z*-DOA3P^{OEt2} and DOTP^{OEt2} from the appropriate precursors (see Appendix B). In all cases, conversions were not quantitative but still excellent (75–85 %) and the products were efficiently purified using only extractions and ion exchangers. After *P*-ester removal and alkylations with chloroacetic acid, the DOTA derivatives (Figure 58) were isolated in higher yields than those currently found in literature.

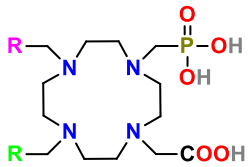

R	R	ligand
COOH	COOH	DO3AP
PO_3H_2	COOH	*cis*-DO2A2P
COOH	PO_3H_2	*trans*-DO2A2P
PO_3H_2	PO_3H_2	DOA3P

Figure 58 – Structure of cyclen-based ligands with phosphonic acid pendant arm(s)

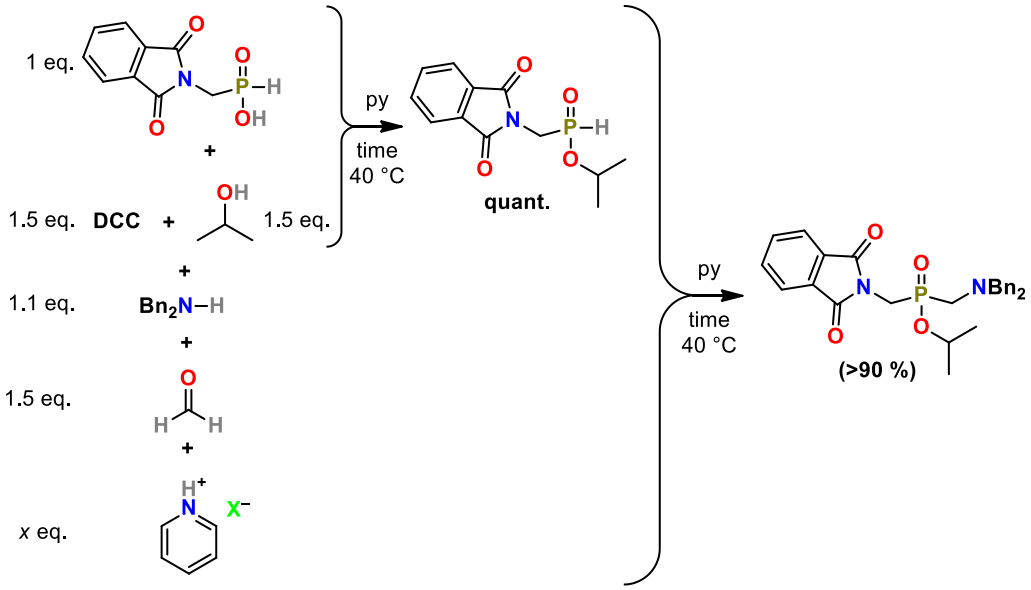

Figure 59 – The reaction with alkyl PIN carried out in a "one-pot"

The target ligands were obtained by utilization of esters of AHPAs. The esters of AHPA as well as esters of other phosphinic acids can be prepared from the acids by Steglich esterification (*i.e.* with use of DCC and alcohol)[135] *in situ*. These reagents did not interfere with K–F reaction in pyridine and both reactions were carried out in a "one-pot". To check the reaction conditions for AHPA esters, a model reaction of (phthalimido)methyl-*H*-phosphinic acid, Bn_2NH, paraformaldehyde, DCC, and *i*PrOH (in molar ratio 1:1.1:1.5:1.5:1.5, respectively; in pyridine, 40 °C; Figure 59) was investigated. Without a strong acid catalyst, conversion was ~70 % and several by-products were detected. Addition of strong acid in a form of py · HX or TFA improved reaction conversion significantly. The best results were obtained with 2–4 equiv. of the acids (see Appendix B). From practical point of view, HBr is the best acid as py · HBr is commercial as stable solid. Conversions with other strong acids in form of their pyridinium salts were similar but they have other undesired properties (*e.g.* py · HI is light-sensitive, py · HCl is hygroscopic, and py · TFA is not compatible with *t*Bu ester protective groups, for instance, in commonly used tBu_3DO3A · HBr). Weaker acids (*e.g.* AcOH, MsOH) gave insignificant conversions.

[135] Neises, B.; Steglich, W. Simple method for the esterification of carboxylic acids. *Angew. Chem. Int. Ed.*, 17, **1978**, 522–524.

These optimized conditions of the K–F reaction in pyridine were utilized to prepare several cyclen derivatives with aminophosphinates in ester form. In the DO3AP^{R} family, the synthetic protocol was successfully utilized to prepare several compounds (Figure 60, Appendix B) and the final ligands were prepared after removal of the protective group(s). The K–F reaction in pyridine is so versatile that even highly unstable $H_2P(O)(OEt)$ was used to "connect" two *t*Bu$_3$DO3A units in the almost quantitative conversion and the ditopic ligand "(DO3A)$_2$P" was isolated, after deprotection, in a high yield (see Chapter 7). To the best of Thesis author's knowledge, it is the most general and high-yielding reaction for synthesis of cyclen [136] derivatives with phosphonic / / phosphinic acid pendant arm(s).

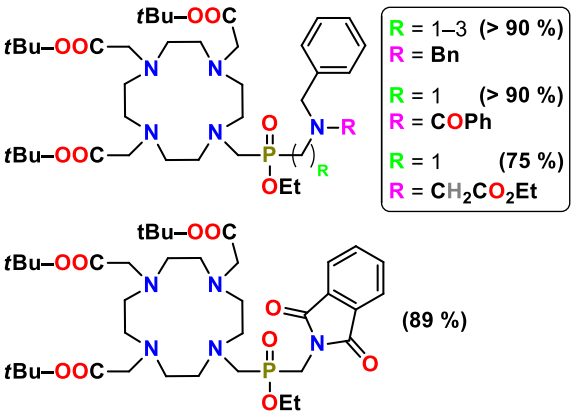

Figure 60 – Structures of ligands prepared by K–F reaction in pyridine

4.2.1. *Reaction mechanism investigations*

The K–F reaction mechanism was investigated in pyridine-d_5 (Figure 61). Mixture of Bn_2NH and paraformaldehyde (in molar ratio 1:1.5) under anhydrous conditions gradually (10 h, 40 °C) formed the corresponding aminal, $(Bn_2N)_2CH_2$, which is stable under given conditions (pyridine-d_5, 40 °C; further decomposition was very slow). After the addition of DEP, no instant reaction was observed. Only after a slow mono-dealkylation of DEP by pyridine (*i.e.* after formation of medium-strong acid, H–P(O)(O**H**)(OEt)), the formation of $Bn_2NCH_2PO_3Et_2$ was detected. Hence, the presence of acid is necessary. The similar results were obtained after using commercial aminal, $(Me_2N)_2CH_2$ (Appendix B), instead of Bn_2NH and $(CH_2O)_n$. In the next experiment, aminal $(Bn_2N)_2CH_2$ was generated *in situ* and the strong acid (pyridine deuterobromide or TFA, 2 equiv.) was added. The $(Bn_2N{=}CH_2)^+$ cation and Bn_2NH were formed in equimolar amounts quantitatively (Figure 61). After addition of DEP, a quick formation of the $Bn_2NCH_2PO_3Et_2$ (30 %, < 5 min at RT) was observed and reaction was completed in ~1 h at 40 °C. The addition of water decreased $(Bn_2N{=}CH_2)^+$ cation abundance and, thus, significantly decelerated $Bn_2NCH_2PO_3Et_2$ formation. The similar results as above were observed when $(Me_2N{=}CH_2)^+$ Cl^- was used directly (Appendix B). Hence, K–F reaction in pyridine follows the "generally accepted" mechanism of the reaction[134] in

[136] TACN- and cyclam-based amines are problematic due to fast formation of their formaldehyde aminals in the anhydrous conditions which are very stable and do not react further.

which the iminium species is the reactive intermediate and the presence of a strong acid is necessary to generate and stabilize it.

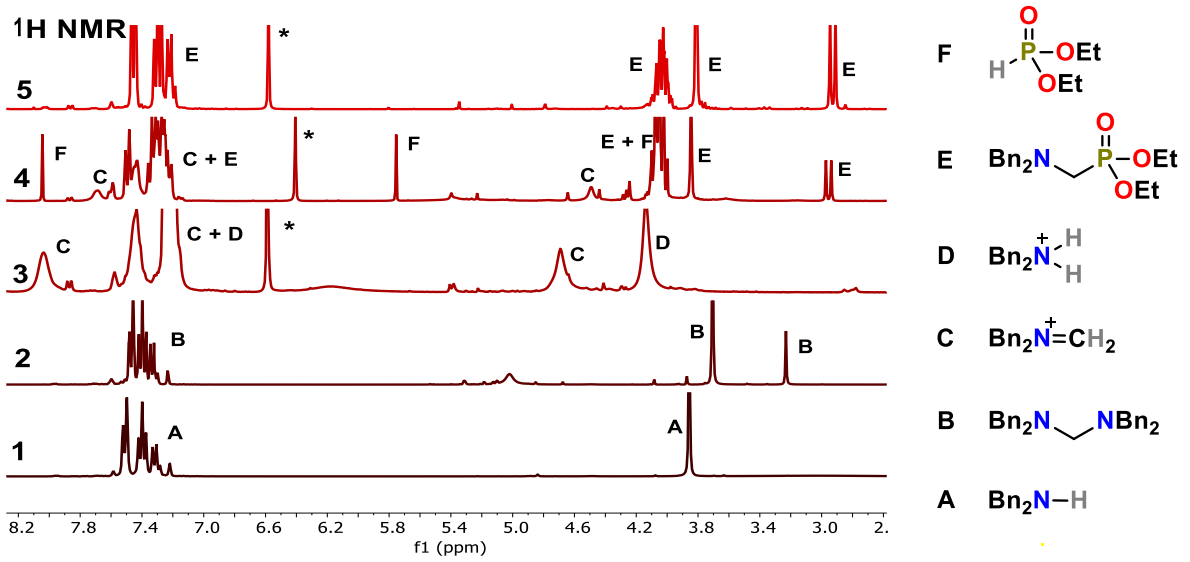

Figure 61 – The K–F reaction mechanism investigation in pyridine-d_5 (^{1}H NMR spectra, 300 MHz). Mixture of Bn_2NH and paraformaldehyde (in molar ratio 1:1.5, < 5 min, RT, spectrum **1**) was heated for 10 h at 40 °C (spectrum **2**). To this mixture, the py · DBr (2 equiv.) was added and mixture was heated for additional 7 h at 40 °C (spectrum **3**). Then, the DEP (1 equiv.) was added to this mixture (< 5 min, RT, spectrum **4**) and the mixture was heated at 40 °C for additional 1 h (spectrum **5**). *The signal was assigned to CH_2O.

4.2.2. Summary

- Pyridine is the optimal solvent for K–F reaction due to (*i*) cleanness of the reactions, (*ii*) very good solubility of the reactants, (*iii*) increased stability of the formed products, and (*iv*) a "buffering effect" for the necessary catalyst, a strong acid.
- Commercial pyridinium hydrobromide is a good source of the strong acid needed as a catalyst of the K–F reaction in pyridine.
- The dialkyl *H*-phosphites, AHPA esters, and even alkyl hypophosphite were used to prepare several cyclen-based ligands (sometimes not accessible by other procedures) with excellent conversions and high yields.
- The K–F reaction mechanism in pyridine follows the common mechanism of K–F reaction with iminium cation as a key intermediate.

5 . Interaction of protonable MRI CAs with HSA

The MRI CAs must be stable *in vivo* and, thus, the Gd(III) complexes must exhibit a high thermodynamic stability and kinetic inertness. They should also have relaxometric parameters with optimal values. It means that Gd(III) complex should optimally have one IS water molecule (q = 1), fast exchange of bound water molecule with the bulk ones (τ_M ~5–50 ns) and slow "local movement" of whole complex (τ_R in "ns" scale). To slow down the "molecular tumbling", (non-)covalent binding of the complexes with macromolecules is the most general approach. One of the most commonly used strategies is non-covalent interaction of the CA with plasma proteins, mainly with human serum albumin (HSA). In the past years, Ablavar®,[97] which interacts strongly with HSA, was used as CA for magnetic resonance angiography (MRA) but its stability against transchelatation is not optimal as it is a complex of DTPA derivative. The Ablavar® interaction with HSA is too strong to be efficiently filtered off from body. Hence, new approaches for MRA CAs are sought. Some of the most suitable ligands for Gd(III) coordination are those from DO3AP^R family as their Gd(III) complexes have properties close to the optimal ones (Chapter 3.2.1). Regarding the interaction strength of CA–HSA, some HSA cavities surfaces are covered by positively charge amino-acids (*e.g.* lysines, arginines)[93] and, thus, a positive charge near the binding group of CA should be introduced to weaken the interaction CA–HSA. Therefore, two complexes, Gd–DO3AP^{DBAM} [137] and Gd–DO3AP^{tBPAM} (Figure 62), were investigated as they should have relaxometric parameters approaching optimal values and be stable *in vivo*. Both complexes have a protonable pendant amine group and, thus, their properties (*e.g.* their interaction with HSA) should be pH-dependent.

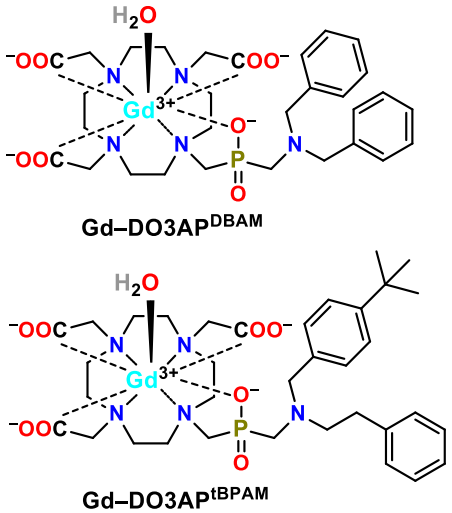

Figure 62 – Structures of the investigated MRA CAs, Gd–DO3AP^{DBAM} and Gd–DO3AP^{tBPAM}

Syntheses of both ligands (see Appendices C and D) were similar. The appropriate AHPAs were prepared by "phospha-Mannich" reaction in AcOH. The AHPAs were attached to the macrocycle precursor, *t*Bu$_3$DO3A · HBr, by the K–F reaction in pyridine. Protective groups were removed by common procedures (*t*-butyl groups

[137] Urbanovsky, P.; Kotek, J.; Carniato, F.; Botta, M.; Hermann, P. Lanthanide complexes of DO3AP–(dibenzylamino)methylphosphinate: effect of protonation of the dibenzylamino group on the water-exchange rate and the binding of human serum albumin. *Inorg. Chem.*, 58, **2019**, 5196–5210.

were eliminated in TFA and *P*-ethyl ester was hydrolyzed in aq. pyridine). The solid ligands were obtained in their *zwitterionic* form (isolated yields were ~70 %). Ln(III) complexes were prepared by a standard complex-forming procedure (see Appendix C) and were isolated as thick oils. Single-crystals of the ligand DO3AP^{DBAM} and its Ln(III) complexes were obtained by a careful diffusion of organic solvents into aqueous solutions of the compounds. Structures were determined by X-ray diffraction and the Ln(III) complexes evaluated in more detail (see Chapter 5.2).

The NMR titrations and potentiometry analysis of the ligands provided their protonation constants, logK_A's. The logK_A's of macrocyclic amines and acidic groups had expected values. The logK_A of the pendant amines were 6.8 and 7.4 for DO3AP^{DBAM} and DO3AP^{tBPAM}, respectively. Hence, their logK_A's are in a physiological pH range. Thermodynamic stability of Ln–DO3AP^{DBAM} complexes (determined by potentiometry) is comparable with that of Gd–DOTA.[56] The pK_A of the pendant amine of the Gd–DO3AP^{DBAM} complex dropped to ~5.9 and it was confirmed by the ^{31}P NMR titrations of few Ln–DO3AP^{DBAM} complexes (*e.g.* for Eu–DO3AP^{DBAM}, pK_A of the pendant amine was ~5.8 and ~6.3 for TSA and SA isomer, respectively). For Eu–DO3AP^{tBPAM}, pK_A of the pendant amino group was determined to be ~6.5 and ~6.7 for TSA and SA isomer, respectively (^{31}P NMR titration; see Appendix D). Thus, pK_A of the pendant amine of the Gd–DO3AP^{tBPAM} is closer to the physiological pH range than that of Gd–DO3AP^{DBAM}.

Hydration break in the Ln(III) series of Ln–DO3AP^{R} was estimated from isomers abundance across the Ln(III) series (^{31}P NMR). The breaks were estimated between Tb–Dy and Gd–Tb (Figure 63) for both protonated and deprotonated complex forms, respectively. The TSA isomer abundance of Gd–DO3AP^{DBAM} is ~45 % and ~75 %, and for Gd–DO3AP^{tBPAM} is ~50 and ~60 % for protonated and deprotonated complexes, respectively. The TSA abundance is three-to-five times higher than that for Gd–DOTA (~15 %).[101] The data predict that relaxometric behaviour of Gd–DO3AP^{DBAM} and Gd–DO3AP^{tBPAM} would be governed mainly by the TSA isomers.

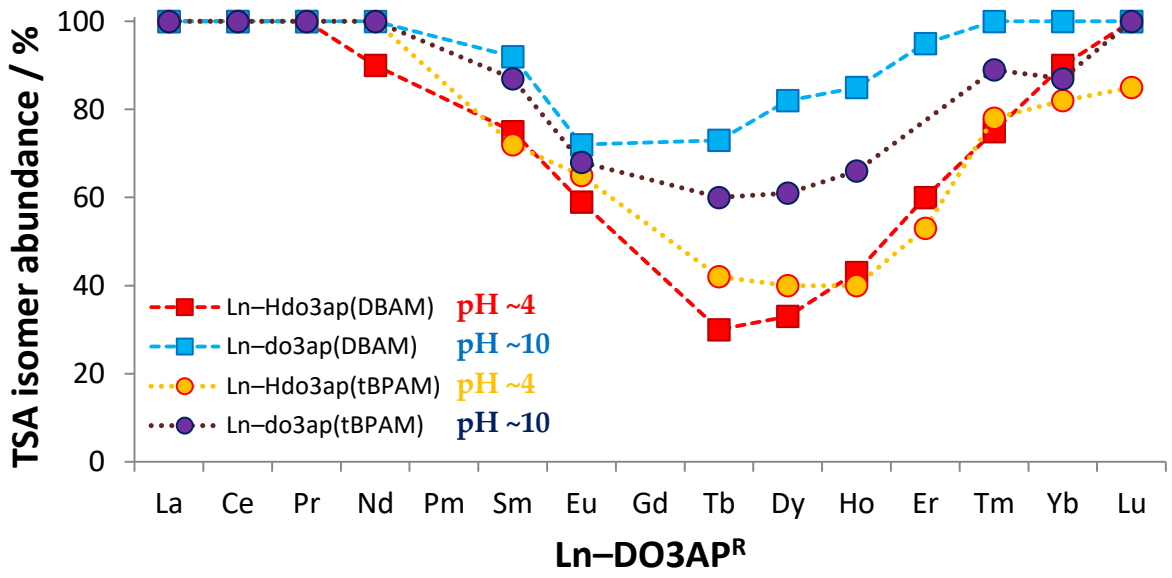

Figure 63 – TSA(') isomer abundance of the Ln–DO3AP^{DBAM} and Ln–DO3AP^{tBPAM} (^{31}P NMR)

The hydration break in the Ln(III) series of DO3AP^{DBAM} complexes was also evaluated by other methods (luminescence lifetime, variable-temperature (VT) high-resolution UV-VIS measurements of Eu–DO3AP^{DBAM}, and ^{17}O NMR Dy(III)-induced shift (DIS) measurement of Dy–DO3AP^{DBAM}). All measurements suggested that q = 1 should be expected in the Gd–DO3AP^{DBAM} complexes regardless of the pendant amine protonation.

5.1. Relaxation properties

The investigated Gd(III) complexes contain hydrophobic groups and, thus, formation of micelles was tested at pH 3.6 and 12.0 (relaxometry at 40 MHz). Micelles were formed only for deprotonated form of the Gd–DO3AP^{tBPAM} complex. Critical micelle concentration for Gd–DO3AP^{tBPAM} was ~5 mM (25 °C, Appendix D). Hence, all relaxometric measurements had to be carried out at concentrations of Gd–DO3AP^{tBPAM} well below ~5 mM. In the case of Gd–DO3AP^{DBAM}, no micelles were observed.

Relaxometric pH titration of Gd–DO3AP^{DBAM} in water (37 °C, 40 MHz) gave pK_A ~5.8 (Appendix C) which roughly matches the pendant amine pK_A of Eu–DO3AP^{DBAM} (see above). Similarly, dependence of Gd–DO3AP^{tBPAM} relaxivity on pH (30 °C, 40 MHz; Appendix D) gave pK_A ~6.9 which was similar to that of Eu–DO3AP^{tBPAM} (^{31}P NMR). The relaxivity change between the differently protonated species was ~10 % for both Gd(III) complexes. The relaxivity change with the pendant amine protonation is only dependent on local hydrogen bonding system, water exchange rates and SS hydration changes, and either parameter should not change relaxivity significantly.

Gd–DO3AP^{DBAM} ^{1}H NMRD profiles and VT ^{17}O NMR measurements were fitted according to SBM theory at two different pH (*i.e.* for species fully protonated or

deprotonated on the pendant arm). The fitting (see Table 6 and Appendix C) showed a greatly increased IS water exchange ($^{298}\tau_M$ = 15 and 5 ns for acidic and alkaline pH, respectively) comparing to Gd–DOTA and MS–325 (= Ablavar®). Such a short water residence time has been rarely observed before for compounds with q = 1. This is probably caused by a high abundance of TSA isomer of the Gd–DO3AP^{DBAM} complex, the proximity of hydration break to Gd(III) in the Ln(III) series, and presence of the hydrophobic moiety (*i.e. N*,*N*-dibenzyl group, see Chapter 5.2).

Parameter	[Gd(Hdo3ap^{DBAM})] (pH 4.0)	[Gd(do3ap^{DBAM})]$^-$ (pH 8.3)	[Gd(dota)]$^-$ [101]	[Gd(do3ap^{ABn})]$^-$ [126]	MS–325 [138]
$^{298}r_{1p}^{20}$ / mM^{-1} s^{-1}	6.3	5.5	4.7	6.7 (10 MHz)	5.6
$^{298}\tau_M$ / ns	14.9	5.0	244	16.2	195
$^{298}\tau_R$ / ps	102	92	77	88	142
$\Delta H^{\#}_M$ / kJ mol^{-1}	40.3	34.1	49.8	20.6	51.3
Δ^2 / 10^{19} s^{-1}	4.1	4.1	1.6	2.5	5.2
$^{298}\tau_v$ / ps	15	13	11	11.2	18.7
$A/\hbar$ / 10^6 rad s^{-1}	–3.3	–3.5	–3.7	–2.9	–4.1
$r_{Gd–H}$ / Å	3.1[a]	3.1[a]	3.15	3.1	3.1
q^{SS}	1[a]	1[a]	–	1	–
$^{298}\tau_R^{SS}$ / ps	59	30	–	9	–

For the parameters a, ^{298}D, E_R and E_v, values of 4.0 Å, 2.24×10^{-5}cm^2 s^{-1}, 17 and 1 kJ mol^{-1}, respectively, were used. Relaxivity ($^{298}r_{1p}^{20}$) at 298 K, 20 MHz. [a]Fixed in the fitting procedure.

Table 6 – Relaxation parameters of Gd–DO3AP^{DBAM} and the similar complexes (25 °C)

The Gd–DO3AP^{tBPAM} was also characterized by ^{1}H NMRD measurements (Appendix D). Its relaxivity is strongly depended on temperature as that for Gd–DO3AP^{DBAM}, thus, the water exchange rate has to be very fast.[139] Due to the micelle formation, VT ^{17}O NMR of Gd–DO3AP^{tBPAM} could not be carried out (~20 mM concentration is required).

The Gd–DO3AP^{DBAM}–HSA and Gd–DO3AP^{tBPAM}–HSA interactions were investigated in aqueous solutions at three different pH (Figure 64): (*i*) CA is fully protonated on the pendant arm amino group (pH 4.0 and 4.2, respectively), (*ii*) CA is deprotonated on the pendant arm amino group (pH 8.3 and 8.0, respectively), and (*iii*) at neutral / physiological pH (majority of CA is deprotonated on the pendant arm amino group). The data were fitted and the binding constants were obtained.

[138] Muller, R. N. Raduchel, B.; Laurent, S. *et al.* Physicochemical characterization of MS–325, a new gadolinium complex, by multinuclear relaxometry. *Eur. J. Inorg. Chem.*, 11, **1999**, 1949–1955.

[139] Botta, M. Personal communication. University of Eastern Piedmont, Alessandria, IT.

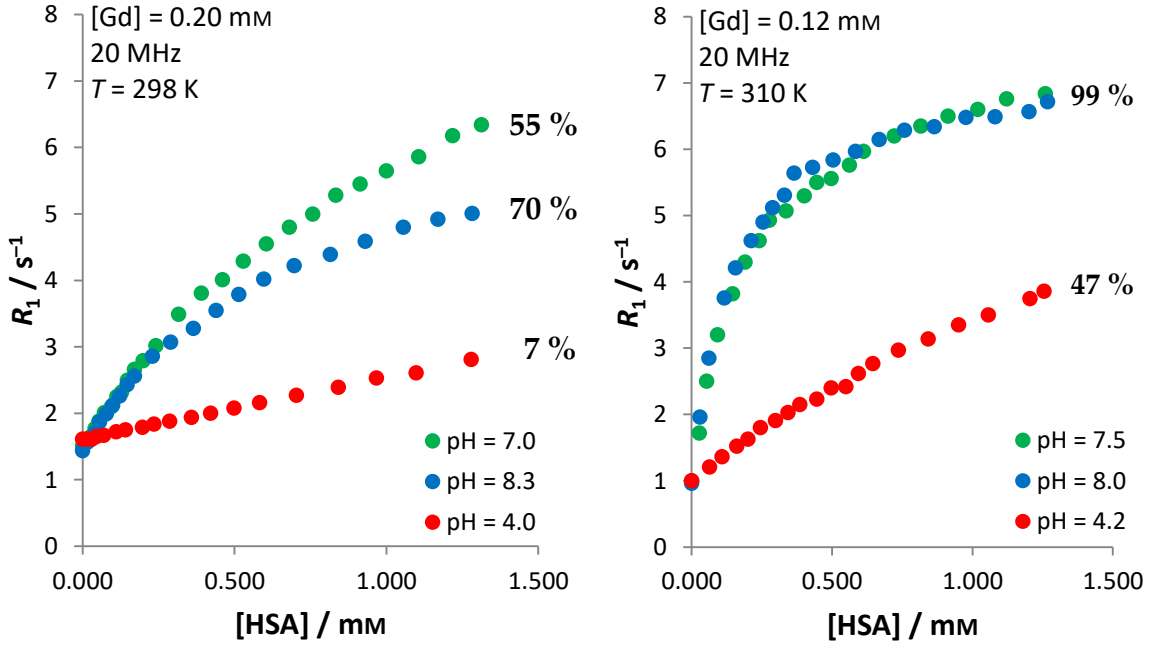

Figure 64 – Plots of relaxation enhancement of Gd–DO3AP^{DBAM} (left; 25 °C, 20 MHz, 0.20 mM of CA) and Gd–DO3AP^{tBPAM} (right; 37 °C, 20 MHz, 0.12 mM of CA) with a gradual addition of HSA; pH of the solutions was maintained as labelled. Amount of bound complex to HSA in 4.5% (w/w) HSA is given.

At the acidic pH, the interaction (*i.e.* binding constant, K_{Aff}, in 4.5% (w/w) HSA) of the Gd–DO3AP^{DBAM} complex was very weak (K_{Aff} ~10^2, 25 °C) and only ~7 % of CA was bound to HSA. The Gd–DO3AP^{tBPAM} with more hydrophobic pendant group (*i.e.* (4-*t*-butyl)benzyl) interacted with HSA, even at acidic pH, more efficiently (K_{Aff} ~$10^{2.5}$, 37 °C) and the fraction of CA bound to HSA increased to ~47 %. At neutral or physiological pH, the interaction of both Gd(III) complexes (in 4.5% (w/w) HSA) was increased: the HSA-bound Gd–DO3AP^{DBAM} fraction was ~55 % (K_{Aff} ~10^3, 25 °C) and the HSA-bound Gd–DO3AP^{tBPAM} fraction was ~99 % (K_{Aff} ~10^4, 37 °C). At acidic and neutral pH, theoretical relaxivities (20 MHz) of the fully bound complexes (r_{1p}^b, Appendices C and D) were calculated: (*i*) for the Gd–DO3AP^{DBAM}, r_{1p}^b ~47 and ~52 mM^{-1} s^{-1} (25 °C) at pH 4.0 and 7.0, respectively, (*ii*) for the Gd–DO3AP^{tBPAM}, r_{1p}^b ~55 mM^{-1} s^{-1} (37 °C) at both pH 4.2 and 7.5. The results point to that the CAs "rigidification" after binding to HSA is similar in both deprotonated and protonated forms. Therefore, the relaxivity change is mainly given by strength of the interaction (characterized by the affinity constant, K_{Aff}). For a comparison, DTPA derivative Ablavar® is bound to HSA by ~88 % (under the comparable conditions) and its r_{1p}^b ~50.8 mM^{-1} s^{-1} and K_{Aff} ~10^4 M^{-1} (37 °C).[96] Thus, Ablavar® interacts with HSA similarly to Gd–DO3AP^{tBPAM}.

^{1}H NMRD profiles of the Gd–DO3AP^{DBAM} and Gd–DO3AP^{tBPAM} in the presence of HSA (4.5% (w/w), see Appendices C and D) confirmed prolonged τ_R and its values depend on pH. The complexes in acidic solutions have smaller relaxation enhancement at ~20 MHz when compared with the complexes in neutral and alkaline solutions and, thus, it confirms that both differently protonated complexes interact with HSA but their bound fraction is different. Hence, the deprotonated complexes bind to HSA more efficiently. The observed relaxivities r_{1p} (20 MHz, 37 °C, pH ~7.4, 4.5% (w/w) HSA) are ~24.5 and ~55.3 mM^{-1} s^{-1} for Gd–DO3AP^{DBAM} and Gd–DO3AP^{tBPAM}, respectively.

The interaction sites of HSA–Gd–DO3AP^{DBAM} and HSA–Gd–DO3AP^{tBPAM} were determined by the relaxometric titration with inhibitors, warfarin and ibuprofen (pH ~7, Appendices C and D), which are specific for two major binding domains of HSA, I and II.[91] Whereas Gd–DO3AP^{DBAM} interacts only with HSA binding site II, Gd–DO3AP^{tBPAM} interacts with both main HSA binding sites. The results for Gd–DO3AP^{DBAM}–HSA interaction and its pH dependence were further confirmed by fluorescence spectroscopy measurements with specifically-binding dyes at pH ~7 and ~4 (see in Appendix C). In comparison, the interaction of Ablavar® with HSA (*i.e.* K_{Aff}) is similar to that of Gd–DO3AP^{tBPAM} and Ablavar® binding site(s) is similar to that of Gd–DO3AP^{DBAM}.[96]

The *t*-butyl group in Gd–DO3AP^{tBPAM} increased binding affinity to HSA (by one order of magnitude) in comparison with that of Gd–DO3AP^{DBAM} and, thus, the observed relaxivities are higher. However, Gd–DO3AP^{tBPAM} also interacts with HSA binding site I and the HSA interaction is also strong when the complex is protonated. Hence, ligands should be further tuned to expand the differences in binding interaction between protonated and deprotonated forms of such complexes. In addition, the data suggest the possible employment of drug–HSA interaction, which is dependent on the drug protonation, in design of drugs with altered pH-dependent pharmacokinetics.

5.2. The solid-state structures of Ln(III) complexes

In total, 15 X-ray structures of the Ln–DO3AP^{DBAM} complexes were obtained (four of them protonated on the pendant amino group). This is one of the largest data sets for Ln(III) complexes of a single DOTA-like ligand. Thus, dependence of structural parameter of the coordination cavity on Ln(III) size could be accurately evaluated and compared with the published parameters of Ln(III) complexes of similar DOTA-like ligands. More information is given in the reprinted paper[140] in the Appendix E. In addition, three X-ray structures of Ln–DO3AP^{tBPAM} complexes (all protonated on the pendant amino group) were also evaluated (see Appendix F).

In the solution, Ln–DO3AP^{R} complexes are present as two diastereoisomers, SA and TSA. However, in the case of Ln–DO3AP^{DBAM} and Ln–DO3AP^{tBPAM}, all the solid-state structures adopted the TSA / TSA' conformation (*i.e.* they are nona- or octa-coordinated, see Figure 65), that is common for of Ln–DO3AP^{R} complexes in the solid state.[140] The central ion in complexes of DOTA-like ligands is coordinated "*in-cage*" inside the macrocyclic cavity formed by four nitrogen atoms of macrocycle (N_4-plane) and by four oxygen anions of pendant carboxylates (O_4-plane). Centroids at the planes, QN_4 and QO_4 (Figure 65), are used to define distances of the central ion from N_4- and O_4-planes. The mutual distortion of these two planes is characterised by twist (torsion) angle φ and "the available space" above O_4-plane for additional water molecule coordination is characterized by opening angle ω (Figure 65).

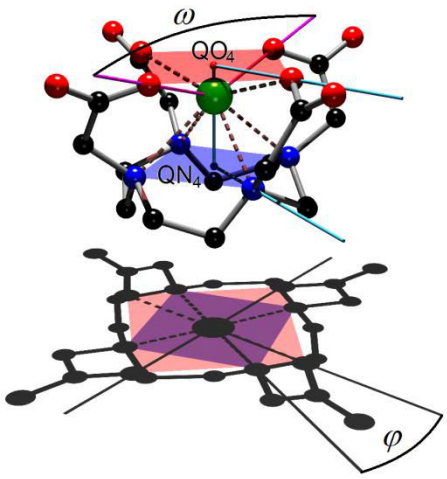

Figure 65 – Structure of TSA' diastereoisomer of Ln–DOTA with the highlighted key parameters, reprinted from[140]

All evaluated solid-state structures of Ln–DO3AP^{DBAM} and Ln–DO3AP^{tBPAM} adopted TSA / TSA' isomer conformation. Their twist angles (φ) were in a narrow range of ~25–27°. In comparison with the solid-state structures of Ln(III) complexes of DOTA-like ligands, the twist angles of TSA isomers are in a wider range than those for SA isomers (Figure 66). Thus, TSA isomers are less compact than SA isomers. The same trend was observed for distances between N_4- and O_4-planes (Figure 66). This is caused by presence of the bulky phosphorus acid pendant arm (*i.e.* the chelate ring

[140] Urbanovsky, P.; Kotek, J.; Cisarova, I.; Hermann, P. The solid-state structures and ligand cavity evaluation of lanthanide(III) complexes of a DOTA analogue with a (dibenzylamino)methyl-phosphinate pendant arm. *Dalton Trans.*, 49, **2020**, 1555–1569.

involving phosphinate / phosphonate is larger) and separation of N_4- and O_4-planes is proportionally larger for Ln(III) complexes of DOTA-like ligands with more phosphorus pendant arms. The Ln–DO3AP^{R} complexes have geometrically larger cavity than those of Ln–DOTA. The preference for TSA isomer and the larger cavity of Ln–DO3AP^{R} causes more internal movement freedom of the coordinated Ln(III) ion inside the ligand cavity.

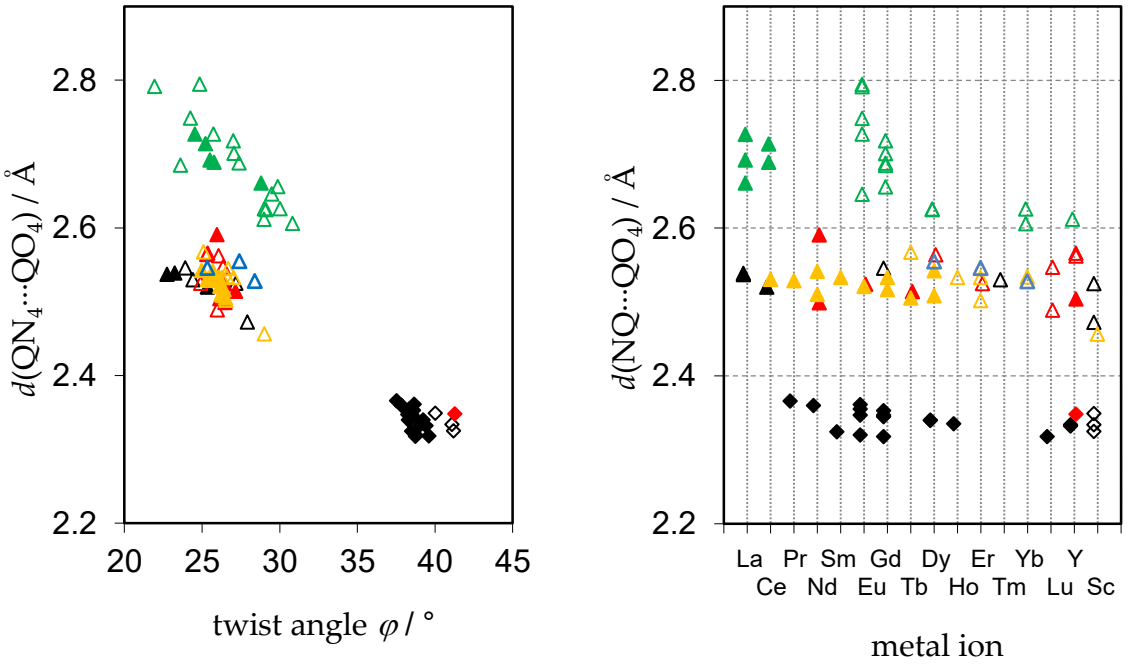

Figure 66 – Dependences of N_4- and O_4-planes separation on the mean twist angle φ (left) and on the coordinated Ln(III) ion (right). Ligand colour codes are: **black** for DOTA, **green** for DOTP^{R}, **red** for DO3AP^{R}, **orange** for DO3AP^{DBAM} and **blue** for DO3AP^{tBPAM}. Filled and empty symbols represent SA / TSA and SA' / TSA' isomers, respectively.

The position of the coordinated Ln(III) ion is defined by its distance from the plane centroids, QN_4 and QO_4. The large Ln(III) ions are closer to QO_4 than the smaller ones and *vice-versa* for the distance to QN_4 (Figure 67). The Ln(III)···QN_4 distance follows the trend of lanthanide contraction whereas its impact on the Ln(III)···QO_4 distance is minimal. Thus, Ln(III) moves "deeper into the cavity" with decreasing size of Ln(III) ion. At the same time, twist angle φ between N_4- and O_4-planes is larger which causes tighter wrapping of the Ln(III) ion by the pendant arms and moving pendant oxygen donor atoms closer. This results in decrease in opening angle ω.

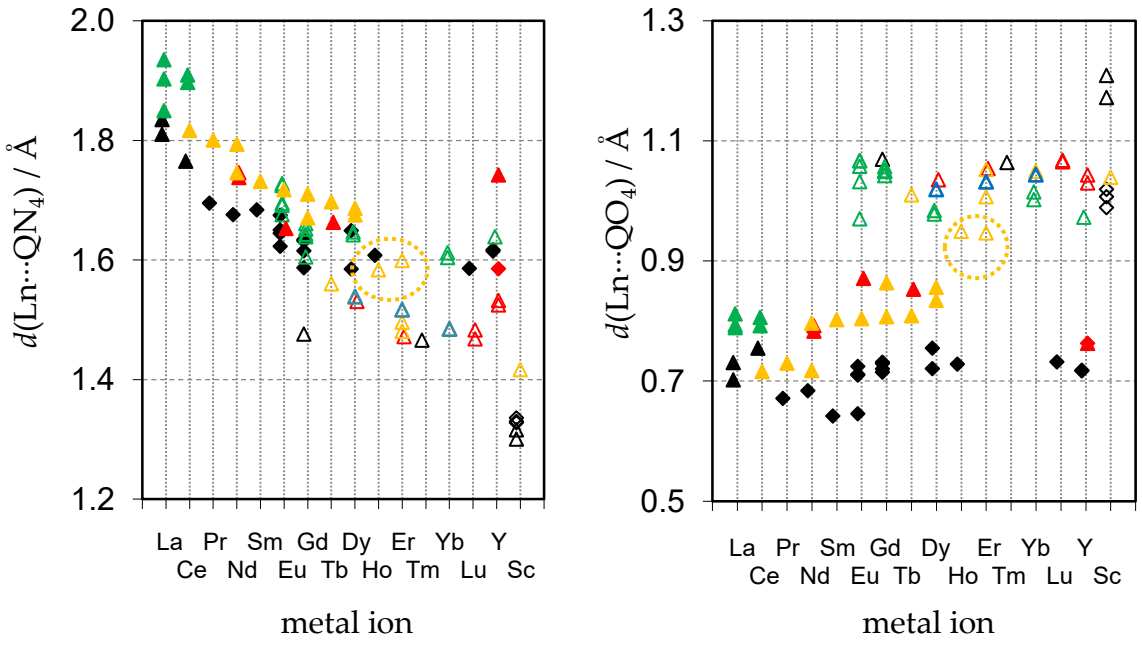

Figure 67 – Dependences of the distance Ln(III)···QN_4 (left) and Ln(III)···QO_4 (right) on the coordinated Ln(III) ion. Ligand colour codes are as in Figure 66. Orange oval highlights the structures with the "semi-coordinated" water to Ln–DO3AP^{DBAM}.

Opening angle ω of Ln(III) complexes of DOTA-like ligands is a measure of "available space" above the complex O_4-plane for a possible water coordination. The data for Ln–DO3AP^{DBAM} suggest limiting value to be ~133–134° (Figure 68) instead of 135° suggested earlier.[141] The smaller Ln(III) ions have shorter bond lengths to oxygen donor atoms (*e.g.* to the coordinated water molecule). However, decrease in opening angle ω and movement of Ln(III) ion closer to N_4-plane cause an opposite effect, prolongation of Ln(III)···OH_2, as "the available space" above O_4-plane reduces. This elongation of Ln(III)···OH_2 is connected with the hydration break in the series. The data on Ln–DO3AP^{DBAM} confirmed these trends (Figure 68) and a "semi-coordinated" water molecule (*i.e.* a crossover between TSA and TSA' isomers) to Ln(III) ion (bond length is ~2.75–2.80 Å) was identified for the Ho– and Er–DO3AP^{DBAM} complexes. These findings in the solid state correlate well with the solution data studies in which hydration break was found around Dy–DO3AP^{DBAM} (see also above).[137]

[141] (a) Vojtisek, P.; Cigler, P.; Kotek, J. *et al*. Crystal structures of lanthanide(III) complexes with cyclen derivative bearing three acetate and one methylphosphonate pendants. *Inorg. Chem.*, 44, **2005**, 5591–5599; (b) Lukes, I.; Kotek, J.; Vojtisek, P.; Hermann, P. Complexes of tetraazacycles bearing methylphosphinic / phosphonic acid pendant arms with copper(II), zinc(II) and lanthanides(III). A comparison with their acetic acid analogues. *Coord. Chem. Rev.*, 216–217, **2001**, 287–312.

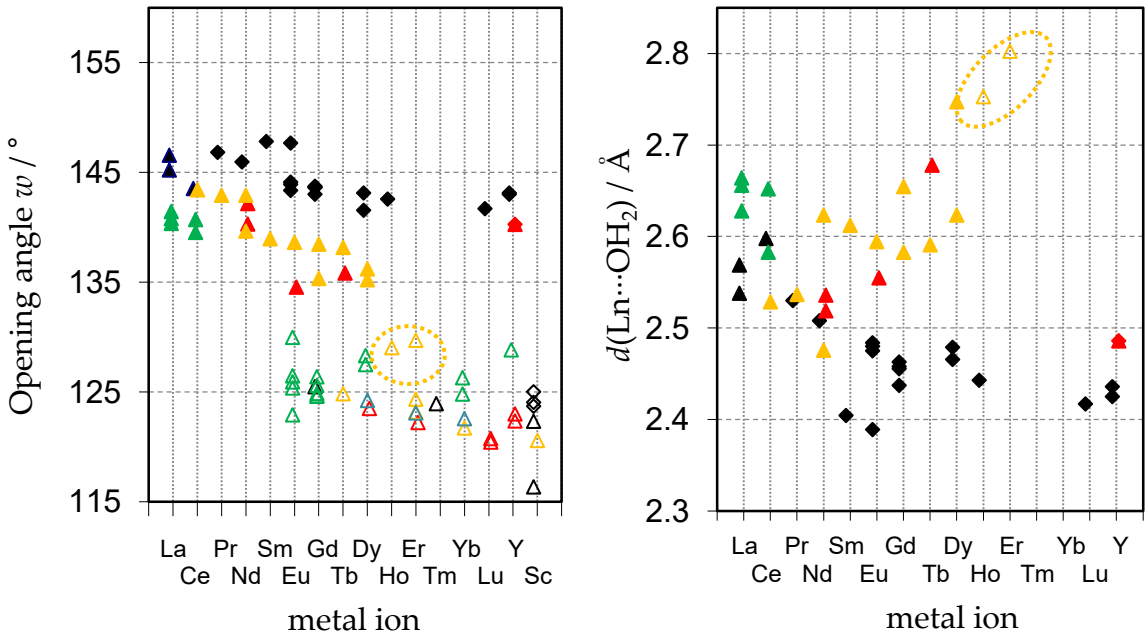

Figure 68 – Dependences of the opening angle ω (left) and the coordination bond length Ln(III)–OH_2 (right) on the coordinated Ln(III) ion. Ligand colour codes are as in Figure 66. Orange oval highlights the structures with the "semi-coordinated" water to Ln–DO3AP^{DBAM}.

Acquired information can be used to draw conclusions for the cyclen-based MRI CAs in general. TSA isomer coordination cavity is more "flexible" than that of SA isomer. The distance to the N_4-plane is shorter for smaller Ln(III) which increases "the tightness" of Ln(III) ion wrapping by the pendant arms. This causes decrease of opening angle ω and elongation of Ln(III)···OH_2 bond. The relaxivity of MRI CAs is dependent on ~$(r_{Gd–H})^{-6}$ (Gd–H is distance between Gd(III) and proton of the coordinated IS water molecule)[75] and, thus, even a small change in this length results in a great change of CA relaxivity. Moreover, the proximity of hydration break to Gd(III) in Ln(III) series accelerates IS water exchange of CA due to dominance of dissociative mechanism with octa-coordinated transient state in coordinated water exchange.[66] In the case of Gd–DO3AP^{DBAM}, hydration break is estimated just behind Tb(III) ion in Ln(III) series. Hence, water residence time is very short (τ_M ~5 ns for [Gd(do3ap^{DBAM})]$^-$, pH = 8.3, 25 °C) and we can speculate if the presence of the hydrophobic *N*,*N*-dibenzyl group also aids the water binding area in the complex.

5.3. Summary

- Two DO3AP^{R} ligands, DO3AP^{DBAM} and DO3AP^{tBPAM}, were prepared in a gram scale utilizing synthesis of amino-*H*-phosphinic acids in AcOH and Kabachnik–Fields reaction in pyridine.
- Ln(III) complexes of DO3AP^{DBAM} and DO3AP^{tBPAM} were prepared and pK_A's of their pendant amines are ~5.8 and ~6.8, respectively.
- Hydration break in their Ln(III) series was found after Dy(III) and Tb(III) in acidic and in alkaline solutions, respectively.
- Gd–DO3AP^{DBAM} and Gd–DO3AP^{tBPAM} complexes coordinate one inner-sphere water molecule which has one of the shortest residence times ($\tau_M \leq 15$ ns) observed for cyclen-based CAs with $q = 1$ till now.
- The solid-state structures of Ln–DO3AP^{DBAM} confirm the fast exchange of inner-sphere water in Gd–DO3AP^{DBAM} which adopts "flexible" TSA isomer, a proximity of hydration break to Gd(III) in the Ln(III) series, and the presence of hydrophobic *N*,*N*-dibenzyl moiety in proximity of the water-binding area of the complex.
- Gd–DO3AP^{DBAM} and Gd–DO3AP^{tBPAM} complexes bind to HSA, preferentially to the binding site II. The fraction bound to HSA is significantly larger when their pendant amine is deprotonated (*i.e.* there is likely an electrostatic repulsion of the protonated pendant amine group of the complex and positively charged amino acids around HSA binding sites).[93] Relaxivity of the fully bound complexes (both protonated and deprotonated species) is significantly increased because their complex–HSA interactions greatly decrease the complexes tumbling.

6 .The Ln–DO3AP^{AM} and Ln–DO3AP^{AcAM} complexes

The ligand DO3AP^{DBAM} (Chapter 5) is a precursor for a new bifunctional ligand with the free primary amino group on the pendant arm, DO3AP^{AM} (Figure 69). This compound serves as the simplest DO3AP^{R} ligand with a protonable pendant amine group. Additionally, this group can be also used for conjugation reactions. Properties of its Ln(III) complexes should be dependent on protonation state of the pendant amine group and, thus, on pH. To accurately evaluate this dependence, the ligand DO3AP^{AcAM} (Figure 69) with a non-protonable acetylated pendant amine was prepared for a comparison. The DO3AP^{AcAM} may also serve as a model compound for conjugates of the DO3AP^{AM} ligand.

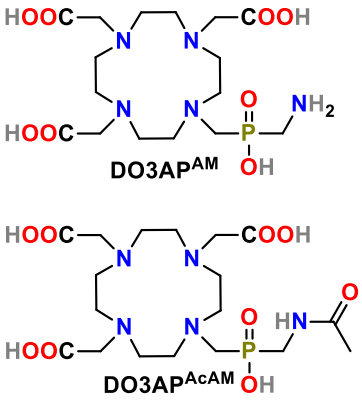

Figure 69 – Structures of the discussed ligands

The DO3AP^{AM} ligand was synthesized by a simple one-step *N*-benzyl groups removal from DO3AP^{DBAM} (Appendix G). Commonly used "hydrogenation protocols" (*e.g.* H_2 + Pd/C in MeOH, aq. HCl, or H_2O; or transfer hydrogenation with $NH_4(HCO_2)$, *etc.*) were not sufficient. The best results were achieved with Pd/C and H_2 (1 atm) at 50 °C in ~75% aq. AcOH which solubilizes hydrogen efficiently even at increased temperature.[142] The water presence prevented the free pendant amine acetylation. The isolated yield of hydrogenation was ~86 %. Ligand DO3AP^{AcAM} was prepared by acetylation of DO3AP^{AM} with an excess of LiOH and Ac_2O in a hot ~75% aq. dioxane (yield ~95 %, see Appendix G).

The Ln(III) complexes of DO3AP^{AM} and DO3AP^{AcAM} were prepared by a standard procedure (see Appendix G) and purified on neutral alumina to yield the complexes as viscous oils. The single crystals of Ln–DO3AP^{AM} and Ln–DO3AP^{AcAM} complexes were obtained by a slow diffusion of appropriate solvent into their aq. solutions (Appendix H).

Acid-base properties of the prepared ligands were investigated by ^{1}H and ^{31}P NMR titrations and potentiometry (Appendix G). The NMR titration of DO3AP^{AM} revealed unexpected protonation order (Appendix G) in which the most basic (logK_A 13.1) is the proton shared by all amines (in the macrocycle and on the pendant) of the ligand and the third constant (logK_A 8.3) corresponds to the second protonation of macrocycle amine. The second logK_A (9.4) is, surprisingly, assigned to the pendant amino group. The more acidic logK_A's (4.0, 1.4 and 0.6) were assigned to the

[142] Maxted, E. B.; Moon, C. H. The temperature coefficient of the solubility of the hydrogen in organic solvents. *Trans. Faraday Soc.*, 32, **1936**, 769–775.

carboxylates. The DO3AP^{AcAM} behaved like a typical DO3AP^{R} ligand with two basic logK_A's (12.6 and 9.3) for macrocycle amines, three acidic logK_A's (3.8, 2.9, 2.8) for pendant acetates and the last one (1.1) for macrocycle amine.

In the solution, Ln(III) complexes of DO3AP^{AM} and DO3AP^{AcAM} formed only two diastereoisomers, SA and TSA, as it was observed for Ln–DO3AP^{DBAM} (Chapter 5). Their abundance (^{31}P NMR) followed expected profile (Figure 70). For the Ln–DO3AP^{AM} complexes, there was almost no change of the isomers abundance with the pendant amine (de)protonation or with its acetylation. The maximum abundance of SA isomer was observed for Dy(III) complexes of both ligands. Abundance of TSA isomer in their Gd(III) complexes was ~30–45 %, *i.e.* smaller than that for Gd–DO3AP^{DBAM} or Gd–DO3AP^{tBPAM} (~45–75 %, Chapter 5) and two-to-three times higher than that for Gd–DOTA (~15 %).[101]

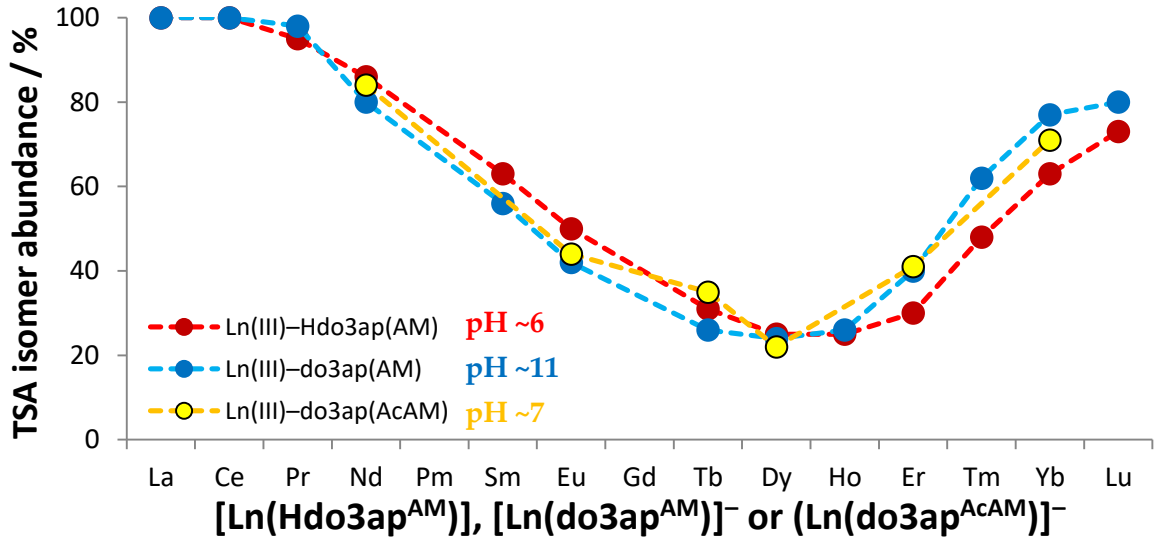

Figure 70 – The TSA(') abundance of Ln–DO3AP^{AM} (the fully protonated and fully deprotonated at pH ~6 and ~12, respectively) and Ln–DO3AP^{AcAM} (pH ~7) complexes (^{31}P NMR)

The ^{31}P NMR titrations confirmed that each isomer (SA and TSA) of the Ln–DO3AP^{AM} complexes has one pK_A (~8.3–8.6) which are mutually different (Figure 71). Two different pK_A's for SA and TSA isomers were also observed for Ln–DO3AP^{DBAM} (Chapter 5). The pK_A of the SA isomers increases along the Ln(III) series; however, the highest pK_A of TSA isomers was observed for the middle-sized Ln(III) (*i.e.* the smaller Ln(III) have smaller pK_A values than the middle-sized Ln(III)). For the Ln–DO3AP^{AM}, TSA isomers have always higher pK_A (by ~0.2) than the SA isomers. Moreover, there is a switch in order of pK_A values of SA / TSA isomers after Dy–DO3AP^{AM} – the pK_A's of SA isomers are higher than those of anhydrous TSA' isomers. The drop is probably due to a structural change in complexes – a possible consequence of the hydration break. In the case of DO3AP^{AcAM} complexes, no change in ^{1}H and ^{31}P NMR spectra with pH (~2–12) was observed during NMR titration.

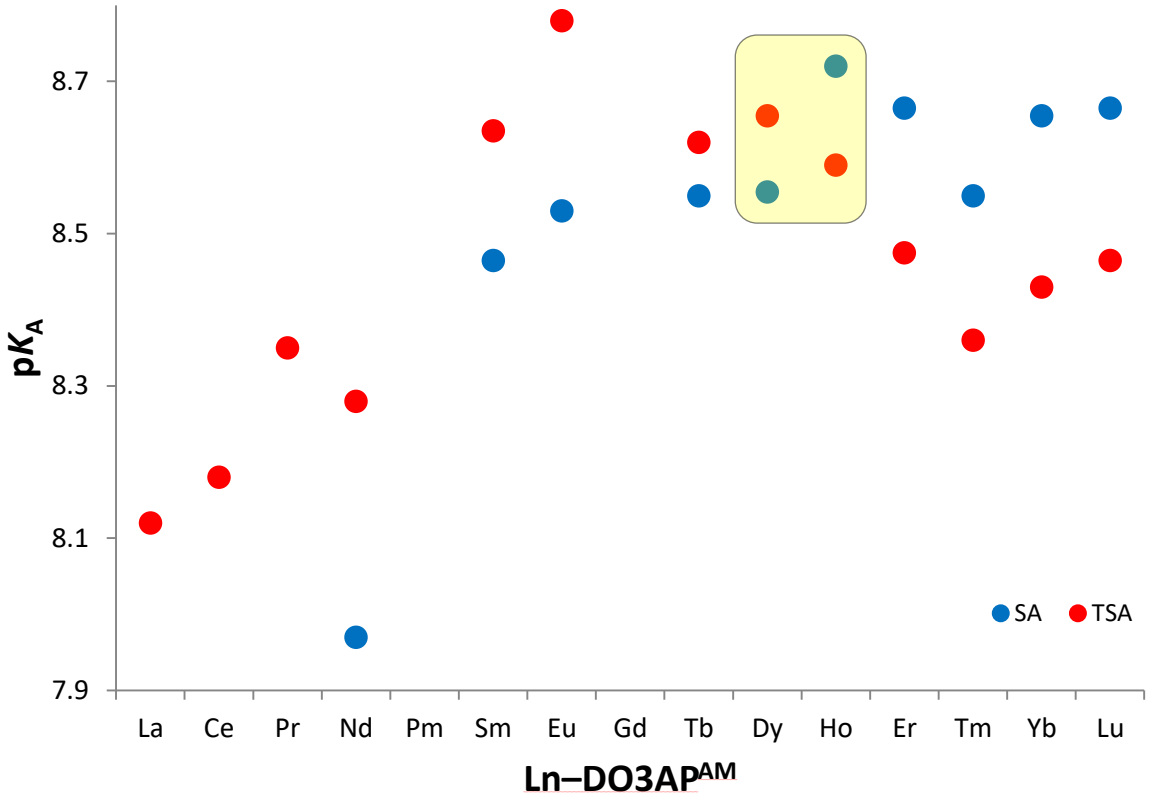

Figure 71 – The change of pK_A of the pendant amino group of the Ln–DO3AP^{AM} complexes along the Ln(III) series. In the highlighted area, pK_A values of TSA and SA isomers are reversed. It can be a consequence of the hydration break in the Ln(III) series.

The hydration break in the Ln(III) series of DO3AP^{AM} and DO3AP^{AcAM} at Dy(III) / Ho(III) is supported by several methods (TSA / SA isomer abundance of their Ln(III) complexes by ^{31}P NMR, luminescence lifetime of their Eu(III) complexes, variable-temperature (VT) high-resolution UV-VIS measurements of Eu–DO3AP^{AM}, and ^{17}O NMR Dy(III)-induced shift (DIS) measurements of their Dy(III) complexes). Moreover, the solid-state structures of TSA isomers of Ln–DO3AP^{AM} show presence of coordinated water molecule up to Dy–DO3AP^{AM} in TSA isomers (see Appendix H). All the measurements suggested q = 1 in Gd–DO3AP^{AM} and Gd–DO3AP^{AcAM} complexes and, in the case of Gd–DO3AP^{AM}, regardless of its pendant amine protonation.

6.1. Relaxivity investigations

Relaxivity of Gd–DO3AP^{AM} was expected to depend on pH, *i.e.* on protonation states of the pendant amino group. However, VT ^{1}H NMRD profiles were identical at three different pH (those for fully protonated, partially deprotonated and fully deprotonated species; see Appendix G). The same data were obtained from VT ^{17}O NMR measurements (Appendix G). Hence, no change of properties of Gd–DO3AP^{AM} with the pendant amino group (de)protonation was observed and the data were fitted and evaluated only for pH ~7 (Table 7).

Parameter	Gd–DO3AP^{AM} (pH ~7)	[Gd(do3ap^{AcAM})]$^{-}$ (pH ~7)	[Gd(do3ap^{DBAM})]$^{-}$ (pH = 8.3)[137]	[Gd(do3ap)]$^{2-}$ (pH = 7.0)[122]
$^{298}r_{1p}{}^{20}$ / mM^{-1}s^{-1}	4.1	4.9	5.5	4.6 (37 °C)
Δ^2/ 10^{19} s^{-2}	5.9	5.3	2.9	20.7
$^{298}\tau_V$ / ps	4.5	5.0	13	3.9
$^{298}\tau_M$ / ns	40	34	5	14
$^{298}\tau_R$ / ps	79	82	92	83
q	0.8	1[a]	1	1
$r_{Gd–H}$ / Å	3.1[a]	3.1[a]	3.1[a]	3.1
$\Delta H^{\#}_M$ / kJ mol^{-1}	47.0	50.6	34.1	76.0
$A/\hbar$ / 10^6 rad s^{-1}	–3.5	–3.2	–3.5	–3.3
q^{SS}	1[a]	1[a]	1[a]	1
$^{298}\tau_R{}^{SS}$ / ps	20	20	30	62

For the parameters *a*, ^{298}D, E_R and E_v, values of 4.0 Å, 2.24×10^{-5}cm^2 s^{-1}, 17 and 1 kJ mol^{-1}, respectively, were used. Relaxivity ($^{298}r_{1p}{}^{20}$) at 298 K, 20 MHz. [a]Fixed in the fitting procedure.

Table 7 – A set of relaxometric parameters (25 °C) for the Gd–DO3AP^{AM} and Gd–DO3AP^{AcAM} complexes and a comparison with parameters of the selected complexes in deprotonated forms

However, the Gd–DO3AP^{AM} had significantly lower relaxivity r_{1p} (4.1 mM^{-1} s^{-1}) than expected and the fitting was the best for q = 0.8, although all indirect determinations of hydration number pointed to q = 1 for the Gd–DO3AP^{AM}. In addition, the fitted parameter $A/\hbar$ (–3.5) is typical for the complexes of DOTA-like ligands with q = 1 (*i.e.* $A/\hbar$ approx. (–3.0)–(–3.7) × 10^6 rad s^{-1}). The main reason for the fitter q = 0.8 might be the fixation of $r_{Gd–H}$ distance to 3.1 Å (commonly used for other Gd(III) complexes).

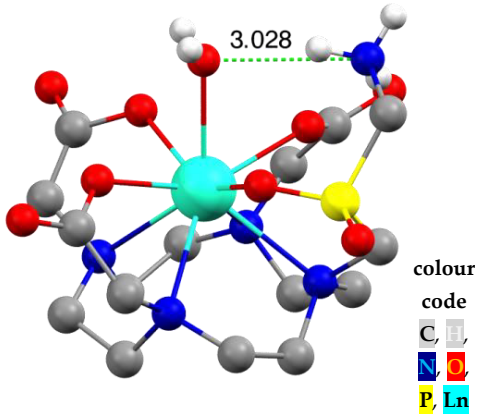

Figure 72 – The solid-state structure of Dy–DO3AP^{AM} with the highlighted N···OH$_2$ distance (in Å)

The "longer" r_{Gd-H} distance is supported by X-ray data of Ln–DO3AP^{AM} (17 structures, see Appendix H) in which the IS water molecule is always tilted away from the pendant amine and a relatively short N···OH_2 distance (Figure 72) was always found. In the solution, the geometry of the IS water molecule may be different due to a complicated hydrogen bond system involving the pendant amine group and, thus, the distance r_{Gd-H} may be longer (*i.e.* r_{Gd-H} > 3.1 Å). This is an unprecedented behaviour. The Gd–DO3AP^{AcAM} behaves as a common CA with slightly increased r_{1p} (~4.9 mM^{-1} s^{-1}) and q = 1. Its other relaxometric parameters reflect the typical Gd–DO3AP^{R} properties (*i.e.* q_{SS} = 1; Δ^2, τ_V and τ_R were in the expected range). Hence, upon acetylation of the pendant amine (*i.e.* formation of amide), the relaxivity r_{1p} has an expected value. This supports the idea of the geometry change of the IS water molecule due to its proximity to the pendant amino group in the Gd–DO3AP^{AM} complex.

Rotation correlation times τ_R of Gd–DO3AP^{AM} and Gd–DO3AP^{AcAM} are comparable with those of Gd–DO3AP as the complexes have similar size. The Gd–DO3AP^{DBAM} has a longer τ_R than the aforementioned complexes due to the presence of the bulky *N*,*N*-dibenzyl group.

Water residence times τ_M of the Gd–DO3AP^{AM} and Gd–DO3AP^{AcAM} complexes are shorter (40 and 34 ns, respectively) than that of Gd–DOTA (244 ns)[101] but longer by almost an order of magnitude when compared with that of Gd–DO3AP^{DBAM} (~5 ns, pH = 8.3). It agrees with the fast IS water exchange of Gd–DO3AP^{R} complexes. Slightly slower IS water exchange of Gd–DO3AP^{AM} and Gd–DO3AP^{AcAM} (when compared with Gd–DO3AP^{DBAM}, see above) may be a consequence of a more "distant" hydration break in the Ln(III) series.

The main contribution of IS water exchange acceleration in the investigated Gd–DO3AP^{R} seems to be a combination of several phenomena. The Gd(III) complexes have (*i*) large abundance of TSA isomer (when compared with that of Gd–DOTA) whose ligand cavity is more flexible than that in SA isomer (see Chapter 5.2) and water-binding site is more crowded (*i.e.* characterized by small opening angle ω).[140] Moreover, (*ii*) the Gd(III) complexes are closer to the hydration break in the Ln(III) series which stabilizes octa-coordinated transient state of Gd(III) in dissociative mechanism of coordinated water exchange. The Gd–DO3AP^{AM} complex shows that the pendant amino group can interact with IS water molecule by formation of hydrogen bonds and, in this case, it leads to a significant undesired relaxivity r_{1p} decrease likely due to elongation of the r_{Gd-H} distance.

6.2. The ^{31}P relaxation properties of the Ln–DO3AP^{AM} complexes

Magnetic resonance spectroscopy (MRS) offers many beneficial outputs (see Chapter 2.8.1) which can be utilized, *e.g.* in diagnostics. The ^{31}P MRS is currently used in determination of abundance of phosphorus-containing endogenous compounds (*e.g.* phosphocreatine, inorganic phosphate) in specific organs (*e.g.* brain).[111] Although this method is a powerful diagnostic tool, it is scarcely utilized due to necessity of a long data acquisition. It is scarcely used because of long ^{31}P relaxation times and overlapping signals. The most usefully, 3-APP with the protonable amino group (see Chapter 2.8.1), has already been used in ^{31}P MRS to determine the acidic pH of cancerous cells[114] but this CA lacks optimal ^{31}P relaxation properties (see above). Currently, there is no suitable CA which can be used for ^{31}P MRS and has properties dependent on pH.

The Ln–DO3AP^{DBAM} and Ln–DO3AP^{tBPAM} complexes with the (protonable) pendant amino group would greatly reduce measurement time of ^{31}P MRS due to the presence of paramagnetic Ln(III) but these complexes bind to HSA and, thus, are localized in bloodstream. Moreover, these complexes do not have suitable ^{31}P relaxation properties (*e.g.* they have a very short relaxation time T_2* when pH is close to pK_A of their pendant amine) and their SA / TSA isomer ratio greatly differ between species differently protonated on the pendant amine. Hence, the Ln–DO3AP^{AM} complexes were investigated as they do not bind to HSA. Their ^{31}P relaxation properties are suitable (see below), and their SA / TSA isomer ratio does not change significantly with (de)protonation on the pendant amine. Despite a non-ideal pK_A of their pendant amino group (pK_A ~8.3) making them not utilizable *in vivo*, the complexes can be used for a *proof-of-concept* studies. The pK_A of the pendant amino group can be tuned by a proper synthetic modification (*e.g.* alkylation).

The presence of paramagnetic Ln(III) ion (*i*) shifts ^{31}P NMR resonance frequency of the complexes away from those of "endogenous compounds", (*ii*) increases the ^{31}P resonance difference between the differently protonated species, and (*iii*) efficiently decreases ^{31}P relaxation times. The former two properties were already confirmed during the ^{31}P NMR characterization of Ln–DO3AP^{AM} complexes (see Appendix G). Ln(III) ions with the largest magnetic moment shifted ^{31}P NMR signal hundreds ppm away from the "diamagnetic" ^{31}P chemical shift region and a simple (de)protonation on the pendant amine caused change of ^{31}P signal frequency up to ~40 ppm (Figure 73) which was estimated from ^{31}P NMR titrations of these complexes. The T_2* relaxation times (estimated from ^{31}P NMR signal "half-width") remained almost the same at various pH, even at those close to pK_A of the complexes. It indicated none, or only a minor, structural changes in the first coordination sphere of Ln(III) with the

(de)protonation of the pendant amine. Moreover, only two isomers, SA and TSA, were observed and their abundance ratio is almost constant at different pH. Hence, change in pH would not produce an additional variable while measuring ^{31}P MRS and, thus, the Ln–DO3AP^{AM} complexes can be used for measurements of pH by MRS.

Relaxation times T_1(^{31}P) were measured at 25.0 and 37.0 °C at two pH values which correspond to the presence of the fully protonated and fully deprotonated (pH ~6 and ~11, respectively) complex species. Relaxation time T_1(^{31}P) is proportional to magnetic moments of Ln(III) ions (Appendix G): (*i*) the diamagnetic La(III) and Lu(III) with the longest T_1 (~2–3 s), (*ii*) the "slightly paramagnetic" Sm(III) and Eu(III) with shortened T_1 (~300–700 ms), (*iii*) Ce(III)–Nd(III) and Yb(III) with short T_1 (~40–100 ms), (*iv*) and Tb(III)–Tm(III) with very short T_1 (< ~5 ms). The relaxation time T_2* gradually decreased in the same order, from ~12 ms for La(III) to ~0.85 ms for Dy(III). More importantly, the T_2* / T_1 ratio should be as high as possible for MRS imaging but still with T_2* and T_1 values above ~8 and ~3 ms, respectively (due to technical limitations of the current scanners for imaging).[143] The Ln–DO3AP^{AM} complexes, in which Ln = Pr(III) and Yb(III), best fulfilled the given criteria (the ratio T_2*/T_1 were ~0.10 and ~0.11, respectively, at 25 °C) and they are the most suitable candidates for development of improved CAs for ^{31}P MRS based on the DO3AP^{R} skeleton.

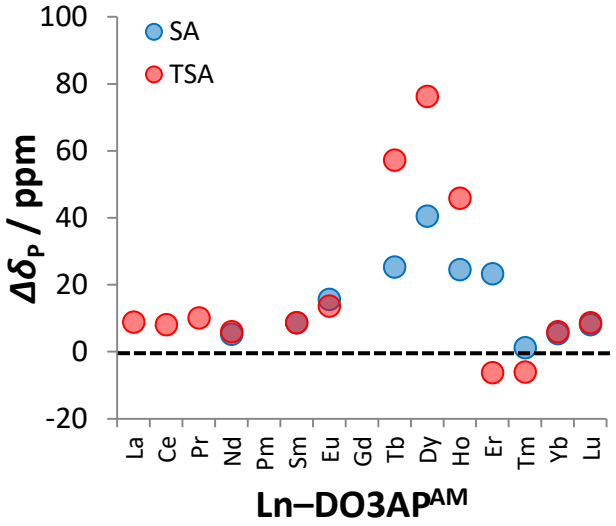

Figure 73 – The difference in δ_P between species fully deprotonated and fully protonated on the pendant amine group of the complexes for SA / TSA isomers

Temperature dependence of ^{31}P relaxation times of Ln–DO3AP^{AM} complexes was investigated to get data more accurate to conditions present *in vivo* (*i.e.* at 37 °C). The relaxation times T_1 increased and T_2* decreased with higher temperature, thus, the T_2* / T_1 ratio was significantly reduced. For some Ln(III) complexes, a reduction by up to ~50 % was observed (see Appendix G). Hence, elevated temperature decreases the T_2* / T_1 ratio and, thus, efficiency of the complexes for ^{31}P MRS.

[143] Jirak, D. Personal communication. Institute of Clinical and Experimental Medicine, Prague, CZ.

6.3. Summary

- Two ligands, DO3AP^{AM} and DO3AP^{AcAM}, were prepared by simple synthetic procedures. The DO3AP^{AM} is a bifunctional ligand and DO3AP^{AcAM} serves as a model compound for conjugates of DO3AP^{AM}.
- Some properties of the Ln–DO3AP^{AM} complexes are dependent on pH due to (de)protonation on the pendant amino group (pK_A ~8.3–8.5) and, thus, on pH of solution.
- Hydration break in Ln(III) series was estimated by various indirect methods (SA / TSA isomer ratio, luminescence, high-resolution UV-VIS, DIS, values of $A/\hbar$) and all methods suggested one IS water molecule in Gd–DO3AP^{AM} and Gd–DO3AP^{AcAM}.
- Relaxometric data of Gd–DO3AP^{AM} were fitted with lower effective hydration q ~0.8. However, it may be alternatively explained by a prolonged $r_{Gd–H}$ due to the complicated hydrogen bond system involving the IS water molecule and the pendant amine. Surprisingly, the Gd–DO3AP^{AM} has identical ^{1}H NMRD and VT ^{17}O NMR profiles at different pH and, thus, most of relaxometric parameters are not dependent on pH.
- The water residence times τ_M of Gd–DO3AP^{AM} and Gd–DO3AP^{AcAM} (40 and 34 ns, respectively) are longer than expected. It is likely caused by a more distant hydration break to Gd(III) in the Ln(III) series and by the lower TSA isomer abundance of the Gd(III) complexes when compared with those for Ln–DO3AP^{DBAM}.
- The Ln–DO3AP^{AM} complexes were investigated as model ^{31}P MRS probes. Despite the non-optimal pK_A of the pendant amine for utilization *in vivo*, the presence of paramagnetic Ln(III) was demonstrated to be useful. The most suitable candidates for ^{31}P MRS imaging are Pr– and Yb–DO3AP^{AM} complexes.

More experimental details and data can be found in Appendices G and H.

7 . Ditopic ligand DO3A–P–DO3A and its Ln(III) complexes

The investigations of K–F reaction in pyridine allowed preparation of a novel ditopic ligand, DO3A–P–DO3A (Figure 74), in which phosphinate group connects two DO3A fragments. The phosphinate group should serve as a bridge in its dimetallic complexes. Water residence time of its Gd(III) complexes should be short (due to employment of DO3AP^{R}-like moiety), tumbling of the dimetallic complexes should be fully coupled and, thus, the relaxation parameters of the dimetallic Gd(III) complex should be close to the optimal values. Moreover, the metal ions in the dimetallic complex would be separated from each other by only four bonds and their intramolecular distance should be short. It should lead to alteration of electron relaxation time T_{1e} of Gd(III) by the proximity of other paramagnetic ion. It is not fully known how change in T_{1e} alters the relaxivity. Hence, next investigations were partly focused on alteration of T_{1e} by a mutual interaction of two metal ions connected *via* the phosphinate bridge.

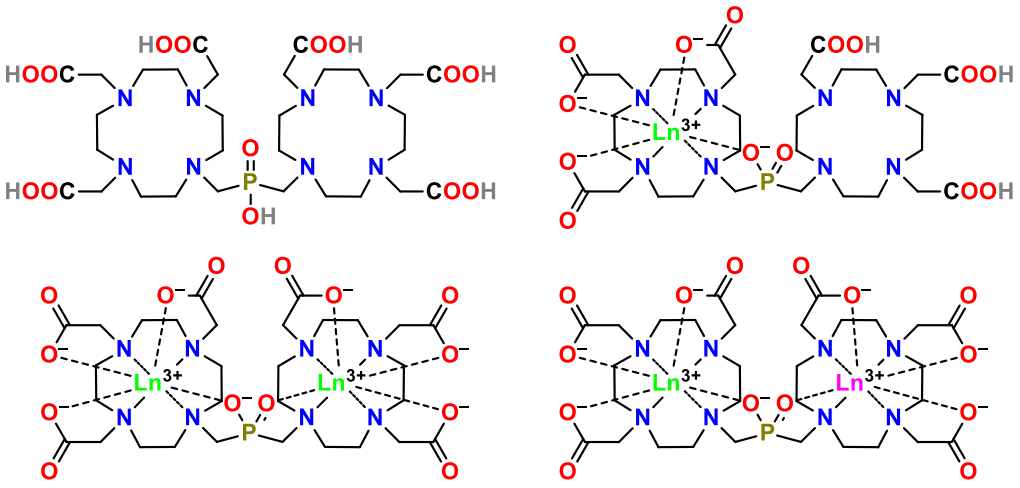

Figure 74 – Structure of the ditopic ligand DO3A–P–DO3A and its Ln(III) complexes with different coordination possibilities

The ligand possesses two (in)dependent macrocyclic cavities and it is able to coordinate one or two metal ions. Thus, the mono- and dimetallic complexes can be formed and they should be kinetically inert as each "half" resembles DO3AP fragment. Introduction of another metal ion to the monometallic complex should lead to hetero-dimetallic complexes. Hence, the second metal ion may be coordinated at will and it would lead to dimetallic complexes which should differ only in the total molecular mass. This might be used to evaluate effect of molecular mass on molecular tumbling and, thus, on relaxivity of the dimetallic complexes.

The synthesis of the ligand utilized K–F reaction in pyridine. Firstly, ethyl hypophosphinate, $H_2(O)P(OEt)$, was generated *in situ* from H_3PO_2, DCC and anhydrous EtOH (in molar ratio 1:3:2, respectively) in toluene. Then, *t*Bu$_3$DO3A · HBr and paraformaldehyde (in molar ratio 2.2:15, respectively, based on H_3PO_2 (1 equiv.)) were added and the mixture was diluted with dry pyridine to achieve ~1:5 (v/v) of toluene : pyridine mixture (see in Appendix B and Figure 75). Activated molecular sieves were added to the mixture to guarantee the fully anhydrous conditions. The reaction conversion was nearly quantitative (^{31}P NMR). However, the total hydrolysis of phosphinate ethyl ester was observed during the reaction. The crude intermediate was purified by extraction and silica column chromatography, *t*-butyl groups were removed in TFA, and the ligand was desalted on a strong cation exchanger. The ligand was isolated as a powder in its *zwitterionic* tetrahydrate form (yield ~70 %, see Appendix B).

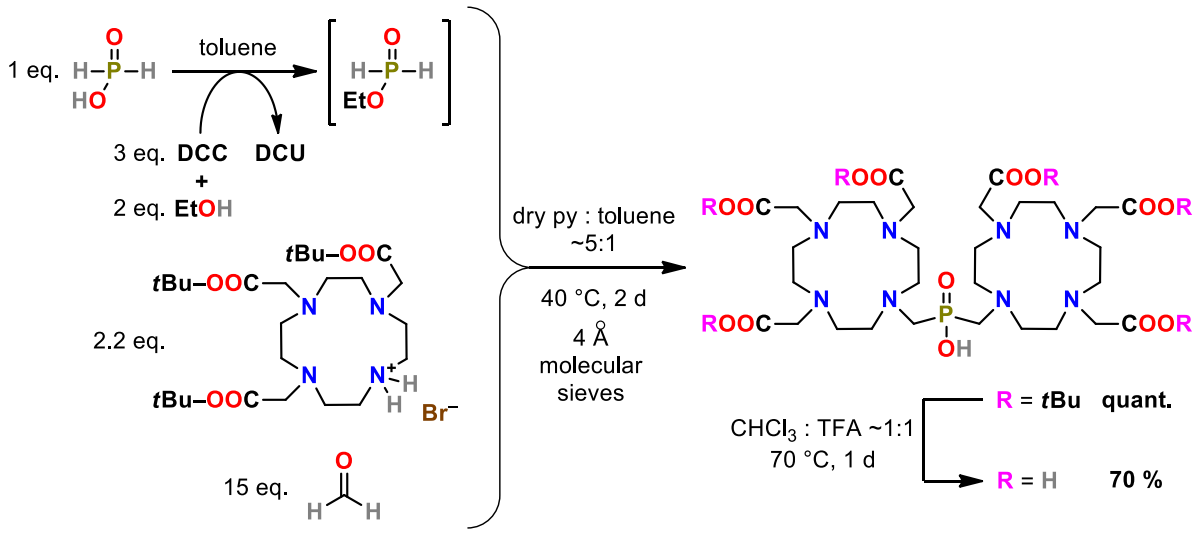

Figure 75 – The synthetic pathway of the ligand DO3A–P–DO3A

The acid-base properties of the ligand were investigated by the NMR titrations and potentiometry. Protonation constants of the ligand are similar to the other DO3AP^R ligands but they are "doubled" (Appendix I). The first four protonations were assigned to the macrocycle amines of each cavity (logK_A's 13.1, 12.4, 9.8, and 9.0) and the next five constants (logK_A's 4.8, 4.4, 3.6, 2.0, and 1.8) to the pendant acetates. Hence, the acid-base properties of the title ligand are similar to the "two interconnected" DO3AP^R ligands.

The DO3A–P–DO3A ligand coordination properties were investigated. Homo-dimetallic complexes were formed with an excess of Ln(III) salt. They were easily purified by precipitation of the excess Ln(III) as their hydroxides in the alkaline aq. solutions (pH ~12) and, finally, the solutions were desalted on strong cation exchanger in NH_4^+-form (Figure 76). The resultant complexes were precipitated in the MeOH / Et_2O mixture as the powdered ammonia salts.

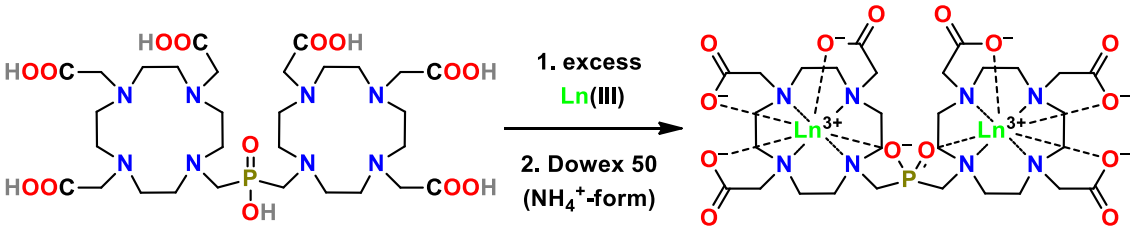

Figure 76 – Preparation of the homo-dimetallic complexes of the DO3A–P–DO3A ligand

Reaction of 1 equiv. of Ln(III) with DO3A–P–DO3A led to formation of the mixture of the desired monometallic (Figure 77) and the homo-dimetallic complexes, and the free ligand. The mixture containing mostly the monometallic complex (> 75 %) was separated by chromatography on neutral alumina. The purified complexes (mono- and dimetallic) were isolated as the powdered ammonia salts analogously as stated above. The mono- and dimetallic complexes were isolated in yields ~75 % and ~10 %, respectively.[144] Hence, the preference for formation of the monometallic complex can be explained by a fast "*out-of-cage*" coordination of carboxylates, which leaves almost no free Ln(III) in the solution, and the slow "descending" of the metal ion into one of the cavities. The monometallic complexes were observed to be stable in the solution with no metal ion exchange between the cavities and decomplexation was not observed (*i.e.* the complexes are kinetically inert). Hence, the monometallic complexes were used for the second ion coordination.

Hetero-dinuclear complexes were prepared by the reaction of the monometallic complexes with a slight excess of the second metal ion (Figure 77). The complexes were purified, as given above, on strong cation exchanger in NH_4^+-form and precipitated in the MeOH / Et_2O mixture as powdered ammonia salts.

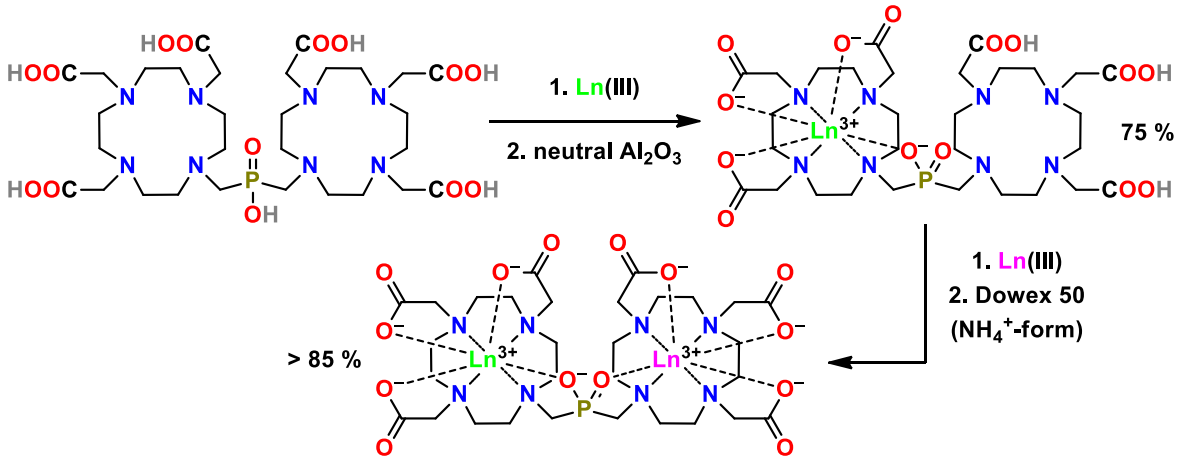

Figure 77 – Preparation of the monometallic and hetero-dimetallic complexes of the DO3A–P–DO3A ligand

[144] The remaining amount was assigned to the free ligand and to the mixed fractions.

As the main concern was relaxometric study of the Gd(III) complexes of the title ligand, hydration number of the Gd(III) complexes was estimated from luminescence measurements of the Eu(III) and Tb(III) complexes. The mono- and homonuclear dimetallic Eu(III) and Tb(III) complexes gave q = 1.0±0.2 and 0.6±0.2 for each Eu(III) and each Tb(III) in the complexes, respectively. Thus, it is likely that the Tb(III) complexes (mono- and dimetallic) are in the proximity of the hydration break in the Ln(III) series. The data suggest that the Gd(III) complexes (both mono- and dimetallic) should coordinate one IS water molecule and its residence time τ_M should be short as the hydration break is in proximity to Gd(III) in the Ln(III) series.

7.1. Structures of dinuclear complexes

In solution, Ln(III) complexes of the DO3AP^R ligands are commonly present as only two diastereoisomers, SA and TSA (Chapter 3.1). For the monometallic complexes of DO3A–P–DO3A, the "free" ligand cavity may be considered as a bulky pendant arm and these complexes should behave like Ln–DO3AP^R complexes in solution. However, the dimetallic complexes have four chiralities of Ln(III) complexes of the DOTA-like ligands (*i.e.* two complex cavities with their pendant arms rotation and macrocycle ethylenes conformation) and one chirality centre on phosphorus atom after coordination of the pendant phosphinate group (*i.e. R* or *S*).

By basic analysis of fluxionality of the isomers (*i.e.* the pendant arm rotation and the macrocycle ethylene conformation), the pendant arm rotation of one cavity affects the position of the second cavity and *vice-versa*. Thus, two fundamental types of isomerism involving fluxionality of the cavities were described by mutual position of their cavities (*i.e.* represented by orientation of their QN_4–QO_4 vectors). The results suggest: (*i*) if pendant arms of one cavity rotate into opposite direction (*i.e.* $\Delta \rightarrow \Lambda$ and, *vice-versa*, $\Lambda \rightarrow \Delta$, see Chapter 3.1), orientation of the QN_4–QO_4 vector of the second cavity rotates by ~90°, and (*ii*) if conformation of macrocycle changes (*i.e.* $\delta\delta\delta\delta \rightarrow \lambda\lambda\lambda\lambda$ and, *vice-versa*, $\lambda\lambda\lambda\lambda \rightarrow \delta\delta\delta\delta$, see Chapter 3.1), orientation of the QN_4–QO_4 vector of the second cavity does not change. In addition, change of chirality on phosphorus atom (*i.e.* $S \rightarrow R$ and, *vice-versa*, $R \rightarrow S$) flips the QN_4–QO_4 vector of the second cavity (*i.e.* ~180° rotation). Theoretically, these three types of isomerisms correspond to to five centres of chirality and, thus, to 2^5 = 32 possible isomers but some of them are enantiomers. Hence, 24 diastereoisomers are possible (see Appendix I) and, likely, not all are thermodynamically accessible.

From a practical point of view, the SA / TSA isomerism and mutual orientation of the cavities (*i.e.* orientation of their QN_4–QO_4 vectors) create 12 unique combinations (Appendix I) – the dimetallic complexes can accommodate four different isomer

combinations (= SA/SA, SA/TSA, TSA/SA, and TSA/TSA) and each of three different mutual orientations of their QN_4–QO_4 vectors (*i.e.* pointing (*i*) in the same direction, (*ii*) opposite to each other and (*iii*) orientated by ~90° mutually each other). In the case of homo-dimetallic complexes, SA/TSA is equal to TSA/SA isomer and, thus, 9 unique combinations could be theoretically observed (Appendix I). Analysis of the possible combinations of isomers showed that all four combinations of SA and TSA isomers can accommodate all three possible mutual orientations of their QN_4–QO_4 vectors. Hence, SA/SA as well as SA/TSA, TSA/SA, and TSA/TSA isomers can accommodate all three different mutual orientations of cavities (*i.e.* in the same or opposite direction, or rotated by ~90°). These unique combinations should be observable, *e.g.* by NMR. Two out of three QN_4–QO_4 vector orientations were found in the solid state, *i.e.* the vectors heading "against each other" and vectors pointing "in the same direction" (see below).

7.1.1. The solid-state structures of the Ln(III) complexes

Complexes of DO3A–P–DO3A were also studied in the solid state by X-ray diffraction on single crystals. The monometallic Eu(III) and Gd(III) complexes (Figure 78 and Appendix I) coordinate one Ln(III) ion "*in-cage*" and the second cavity is "unoccupied" and it does not interact with the other cavity. The Ln(III) ion coordinates one water molecule.

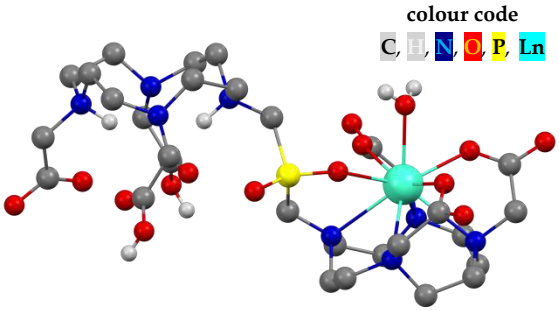

Figure 78 – A structure of the monometallic Gd(III) complex found in the solid state. Only one isomer (SA) is shown.

For the sake of clarity and simplicity, the complexes of the title ligand in the following text will be abbreviated only according to coordinated metal ions.

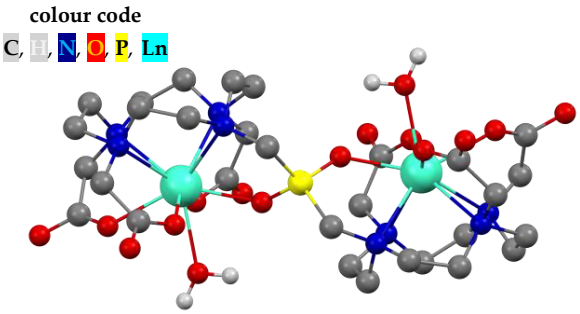

Figure 79 – A structure of the homonuclear dimetalic Gd(III) complex found in the solid state. The cavities are oriented into the opposite direction. Only one isomer (SA/SA) is shown.

The dimetallic complexes of the title ligand can be homo- and heteronuclear and both types were also investigated in the solid state. Each metal ion in the GdGd complex (Figure 79) coordinates one water molecule whereas no water molecule is directly coordinated to Ln(III) ions in the structures of TbTb, TmTm, and YbYb (Appendix I). In the structure of EuEr, one water molecule is coordinated to Eu(III) and none to Er(III) ion.

In all aforementioned complexes, the QN_4–QO_4 vectors have an identical orientation – in the opposite direction.

However, in the case of homonuclear dimetallic EuEu complex (Figure 80), the QN_4–QO_4 vectors are pointing into "the same direction" and, thus, the structure significantly differs from the previous ones. Moreover, the structure is stabilized by coordination of sodium(I) cations. No crystal structure of the complex with the third type of orientation of cavities (*i.e.* their QN_4–QO_4 vectors mutually rotated by ~90°) was obtained. More information about the isomerism of the complexes is given above.

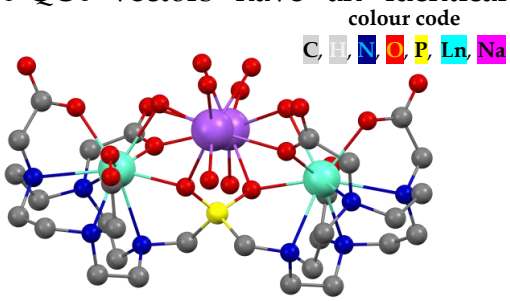

Figure 80 – A structure of the homonuclear dimetalic Eu(III) complex (TSA/TSA isomer) found in the solid state of its sodium salt. The QN_4–QO_4 vectors are pointing into the same direction. The structure is stabilized by coordination of two Na(I) cations (purple).

7.1.2. Solution structure of the Ln(III) complexes

The monometallic Ln(III) complexes of DO3A–P–DO3A behave in the solution as a standard Ln–DO3AP^R complex. Hence, in the ^{1}H and ^{31}P NMR spectra, only SA and TSA isomers were detected with the one preferential chirality of the coordinated phosphorus atom (*S* or *R*). ^{1}H NMR spectra were similar to those of Ln–DO3AP^R but with many signals of the other "free" cavity in the "diamagnetic" region (Figure 81).

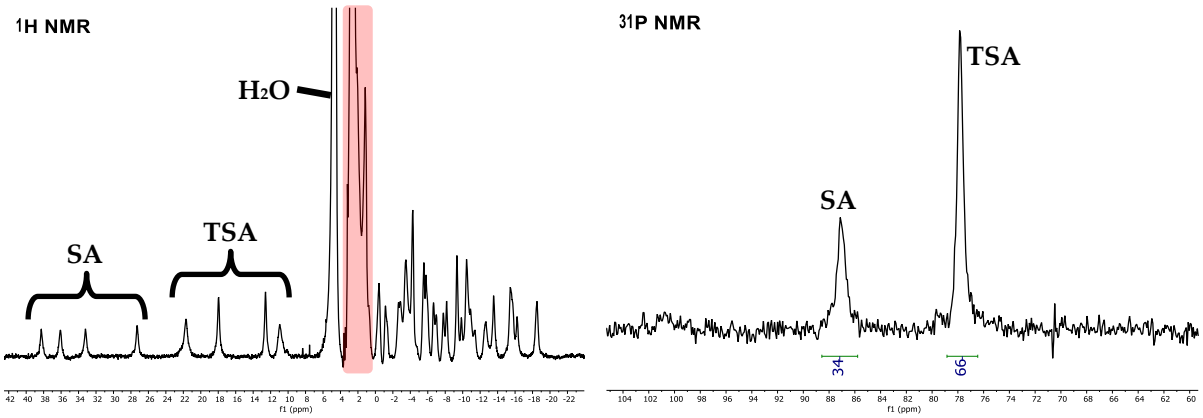

Figure 81 – ^{1}H (left, 300 MHz, "diamagnetic" region of the free macrocycle is in red, SA / TSA "axial" protons are labelled) and ^{31}P (right, 121 MHz) NMR spectra (pH ~7, H_2O, 25.0 °C) of the monometallic Eu(III) complex

The dimetallic complexes can be present as numerous diastereoisomers and some of them were observed, *e.g.* in NMR spectra of EuEu (Figure 82). In the ^{1}H NMR spectrum of the EuEu complex, two major sets of signals corresponding to the "axial"

protons of SA and TSA isomers were observed. They can be assigned to several diastereoisomers which originate from isomerism of each complex unit (see Chapter 7.1). Moreover, several minor sets of signals assignable to the "axial" protons of other diastereoisomers were observed. ^{1}H–^{1}H EXSY confirmed that all ^{1}H signals belong to only one compound (see Appendix I). The ^{31}P NMR spectrum showed three major signals and four-to-five minor ones partially overlapped. Hence, at least seven diastereoisomers of nine unique combinations are observed in solution of the EuEu complex. The major NMR signals of the EuEu complex were assigned to SA/SA (~15 %), SA/TSA (~46 %) and TSA/TSA (~22 %) diastereoisomers.

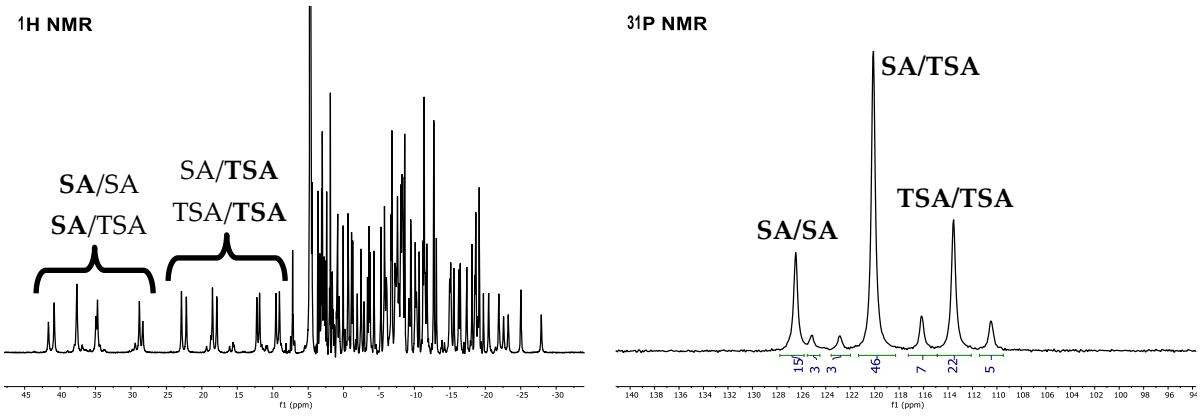

Figure 82 – ^{1}H (left, 600 MHz) and ^{31}P (right, 243 MHz) NMR spectra (pD ~7, D_2O, 5.0 °C) of the homonuclear dimetallic EuEu complex. SA / TSA "axial" protons are labelled.

Analogously, ^{1}H and ^{31}P NMR spectra of EuYb complex show many diastereoisomers (Figure 83). In this case, SA / TSA isomerism can be distinguished and assigned to the particular Ln(III) ion due to different ^{1}H NMR chemical shifts of "axial" protons in the complex "halves" with the particular Ln(III) ion. The signals from ^{31}P NMR can be also assigned due to the different LIS contributions (*e.g.* the SA diastereoisomer of cavity with Yb(III) ion shifts ^{31}P NMR signal to the more negative resonance frequencies than the TSA diastereoisomer of cavity with Yb(III) ion). The major signals were assigned to TSA(Eu)/TSA(Yb) (~53 %), SA(Eu)/TSA(Yb) (~30 %), SA(Eu)/SA(Yb) (~5 %) and TSA(Eu)/SA(Yb) (~7 %) diastereoisomers. Together, four major signals were observed in ^{31}P NMR and four minor ones out of the possible twelve unique combinations for the EuYb complex. The chirality of the phosphorus atom could not be assigned.

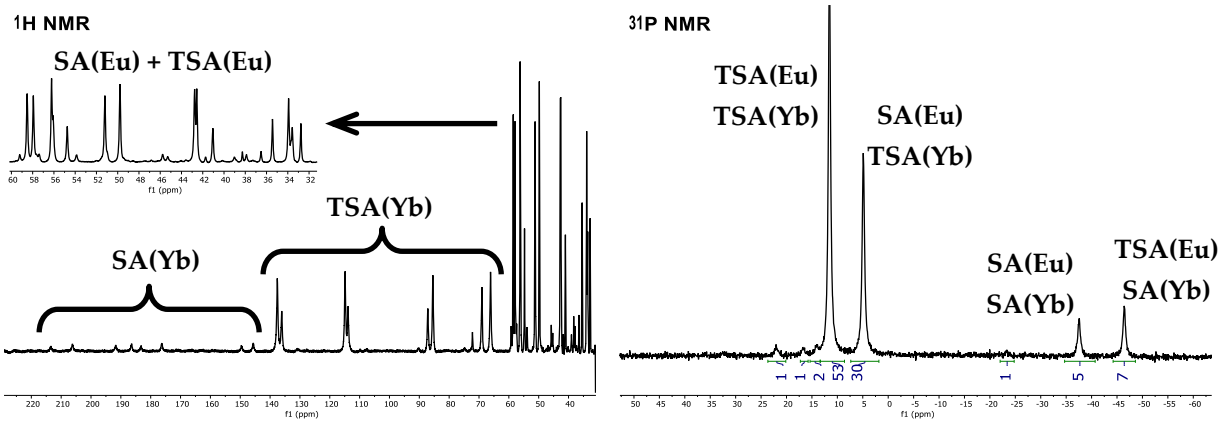

Figure 83 – ^{1}H (left, 600 MHz, region above 30 ppm) and ^{31}P (right, 243 MHz) NMR spectra (pD ~7, D_2O, 5.0 °C) of the heteronuclear dimetallic EuYb complex. SA / TSA "axial" protons are labelled.

There is an interesting remark. The monometallic complexes with Eu(III) or Yb(III) ions have SA / TSA diastereoisomer ratios equal to ~1:2 and ~1:9, respectively. For the EuYb complex, the SA / TSA diastereoisomer ratios of two cavities, with Eu(III) and with Yb(III) ions, are ~1:2 and ~1:8, respectively. Hence, some approximations can be made from the isomerism data. The final SA / TSA diastereoisomer ratio of a particular hetero-dimetallic complex may be estimated from the SA / TSA diastereoisomer ratios of its individual monometallic Ln(III) complexes. However, this estimation cannot be applied on the homo-dimetallic complexes (*e.g.* on EuEu).

7.2. The relaxometry of the Gd(III) complexes

7.2.1. The monometallic Gd complex

The main goal was the relaxometric evaluation of the Gd(III) complexes of the title ligand. The relaxometric data for monometallic Gd(III) complex suggested the presence of one IS water molecule and a rich SS hydration (r_{1p} = 6.0 mM^{-1} s^{-1}, 40 MHz, 25 °C, pH ~7.5; Appendix I). A weak pH dependence (the change of r_{1p} < 10 %) likely resulted from an alteration in the SS hydration and the prototropic exchange contribution due to proximity of many protonable groups of the other "free" DO3A unit. The VT ^{1}H NMRD profiles (Appendix I) are typical for a CA with a significant changes in relaxivity with temperature, thus, the Gd(III) complex should have a fast IS water exchange rate.[139] TSA isomer abundance of the Gd(III) complex should be similar to that of Eu(III) complex of the ligand and, thus, it should have ratio of SA / TSA isomers ~1:2 (^{31}P NMR). Hence, TSA isomer should govern the relaxivity properties of the Gd(III) complex. For a comparison, Gd–DOTA has only ~15 % of TSA isomer in the solution.[101]

7.2.2. The homonuclear dimetallic GdGd complex

The GdGd complex possesses the pH independent relaxivity (25 °C) of r_{1p} 12.4 / 11.4 mM^{-1} s^{-1} (at 20 / 40 MHz) *i.e.* ~6.2 / ~5.7 mM^{-1} s^{-1} per Gd(III) ion, respectively. The introduction of the second Gd(III) into the monometallic Gd(III) complex doubled relaxivity. The results suggest the presence of two "Gd–DO3AP-like" units independent on each other but with a highly coupled tumbling. The VT ^{1}H NMRD and VT ^{17}O NMR measurements (Appendix I and Table 8) were carried out and evaluated. The GdGd has an extremely short IS water residence time (τ_M ~7 ns, 25 °C). Its τ_R is twice as high as that of the half-sized Gd–DOTA, and $A/\hbar$ suggests one IS water molecule per Gd(III). The investigated complex looks like two rigidly bridged Gd–DO3AP units tumbling together with the accelerated IS water exchange due to closely located hydration break. The TbTb X-ray structure (TSA'/TSA' isomer, Appendix I) showed no IS water molecule and the GdGd X-ray structure (SA/SA isomer, see above) showed one water molecule per Gd(III) ion. Hence, the GdGd might have an easily accessible octa-coordinated "anhydrous" transient state during the coordinated water exchange. The GdGd relaxivity is likely significantly affected by a high TSA isomer abundance as the EuEu complex has overall SA / TSA isomer ratio ~1:1.2 (^{31}P NMR).

Surprisingly, the electronic relaxation parameters (Δ^2 and τ_V) have not been affected significantly despite the proximity of two Gd(III) to each other (~6.6 Å from the X-ray structure of the GdGd, see Appendix I) and the bridging phosphinate group.

Parameter	**[GdGd]$^-$**	**[Gd(do3ap)]$^{2-}$** [122]	**[Gd(dota)]$^-$** [101]
$^{298}r_{1p}^{20}$ / mM^{-1} s^{-1}	2× 6.2	5.1	4.7
$^{298}\tau_M$ / ns	7	14	244
$^{298}\tau_R$ / ps	132	83	77
q	*1.0*[a]	*1.0*	*1.0*
Δ^2 / 10^{19} s^{-1}	1.3	20.7	1.6
$^{298}\tau_V$ / ps	24	3.9	11
$A/\hbar$ / 10^6 rad s^{-1}	–3.6	–3.3	–3.7
M_w / g mol^{-1}	1091.2	594.6	558.6

For the parameters a, ^{298}D, E_R and E_v, values of 4.0 Å, 2.24×$10^{-5}$$cm^2$ s^{-1}, 17 and 1 kJ mol^{-1}, respectively, were used. Relaxivity ($^{298}r_1^{20}$) at 298 K, 20 MHz. [a]Fixed in the fitting procedure.

Table 8 – The relaxation data set (20 MHz, 25 °C, pH ~7) of the GdGd complex and a comparison with similar Gd(III) complexes

7.2.3. *The heteronulear dimetallic GdM complexes*

One of the goals was to study a change in relaxivity with the change of total molecular mass of the complex. The complexes of DO3A–P–DO3A are suitable candidates as metal ions of different molecular weight can be coordinated together with Gd(III) ion. Several heteronuclear dimetallic complexes were prepared (ordered by the ascending molecular weight): GdSc, GdY, GdLa, GdEu, and GdBi. All of the mentioned complexes have negative charge 1–, the same volume (thus, molecular tumbling) but different molar mass (differing by ~5–15 %, Table 9). However, the ^{1}H NMRD profiles showed no simple relaxivity dependence on the molecular mass (Figure 84). The results suggest a significant change of τ_M for different metal ions (see Appendix I). It could be caused by change of SA / TSA isomers abundance. However, the determination of the SA / TSA isomers abundance is impossible due to presence of Gd(III) ion. Hence, alteration of relaxivity in the series of complexes is more complicated than originally expected and it cannot be explained by a simple change of molecular mass of whole complex.

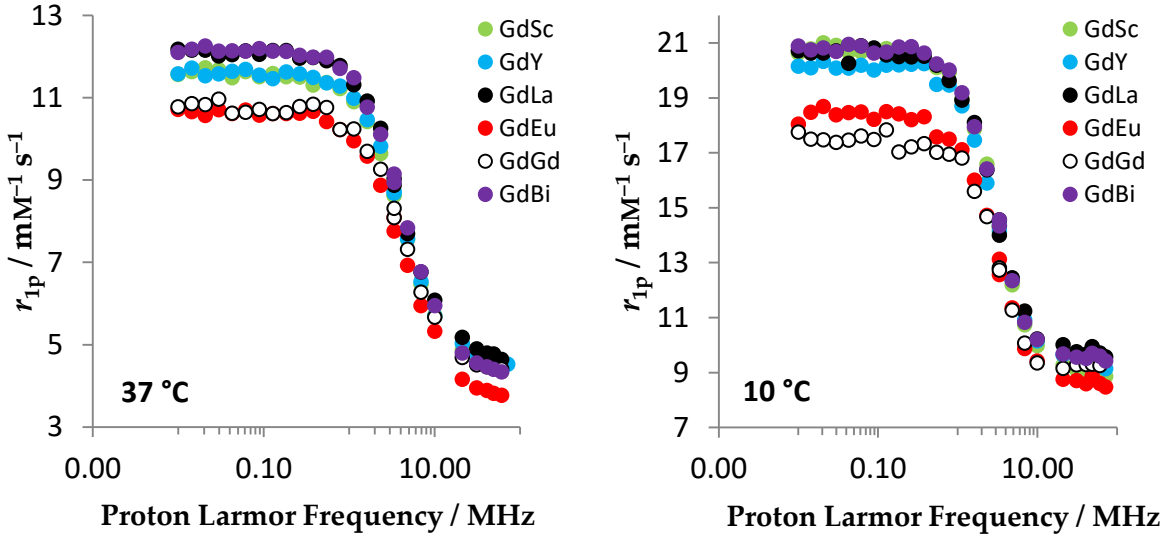

Figure 84 – The ^{1}H NMRD profiles (at 37 °C and 10 °C, left and right, respectively) of the GdM complexes

Parameter	GdSc	GdY	GdLa	GdEu	GdGd	GdBi
M_w / g mol^{-1}	979	1023	1073	1086	1091	1143
M_w / M_w(GdBi)	86 %	90 %	94 %	95 %	95 %	100 %
$^{298}r_{1p}^{20}$ / mM^{-1} s^{-1}	6.29	6.50	6.70	5.43	6.27	6.25

Table 9 – Comparison of the molar masses and relaxivities (20 MHz, 25 °C, H_2O, pH ~7, ~1.6 mM of complexes) of the GdM complexes

7.3. Summary

- The novel ditopic ligand DO3A–P–DO3A was prepared in the multi-gram scale by a simple three-step synthesis utilizing Kabachnik–Fields reaction in pyridine.
- The mono- and the dimetallic Ln(III) complexes of the title ligand were prepared. The dimetallic complexes were formed with both identical and different metal ions.
- Complicated isomerism of the complexes was investigated by NMR in solution and by X-ray diffraction in the solid state. Two out of the three possible mutual orientations of the macrocycle cavities were identified in the solid state.
- Bridging character of phosphinate group was confirmed in the dimetallic complexes.
- The relaxivity-related properties of the mono- and the dimetallic Gd(III) complexes were evaluated. The inner-sphere water residence time of the GdGd complex is very short (τ_M ~7 ns, 25 °C); and the GdGd complex can be described as two rigidly connected Gd–DO3AP units.
- The relaxometric parameters of the heteronuclear dimetallic GdM complexes could not be fully evaluated due to different SA / TSA isomer ratios in the complexes. Water exchange is strongly dependent on the SA / TSA abundance and it dominates over a possible relaxivity change with the total molecular mass of the heteronuclear dimetallic complexes.

More experimental details and data can be found in Appendices B and I.

Conclusions

The main aim of this Thesis was to evaluate effect of (de)protonation of the pendant amine group on properties of Gd(III)-based MRI contrast agents. The amino group was located near the phosphorus atom of phosphinic acid pendant arm as the group is an electron-withdrawing group and it can effectively decrease basicity of the amine group down to physiological pH. Hence, properties of compounds with such pendant amine should change with pH *in vivo*.

To synthesize the corresponding ligands, the appropriate *H*-phosphinic acids have to be accessible as well as a procedure to attach these precursors onto cyclen skeleton. Thus, a new synthetic protocol to obtain the amino-*H*-phosphinic acids (AHPAs) was devised. The reaction of aq. H_3PO_2 and paraformaldehyde with nucleophilic primary or secondary amines (pK_A > 7–8) in AcOH under the mild conditions (40 °C, 1 d) gives AHPAs in moderate-to-excellent yields without extensive purification. Secondary polyamines can be used but the amine groups have to be separated by at least three carbon atoms. Presence of ethylene-diamine fragment leads to the extensive *N*-methylation of the amine group(s) coupled with oxidation of the phosphorus acids. Thus, the synthetic protocol is not suitable for common polyazamacrocycles such as cyclen. A small library of ~40 AHPAs, alkylamino-bis(*H*-phosphinic acids) and their derivatives was prepared. Some of them are hardly accessible by other methods. The reaction mechanism was investigated. Initially formed *N*-hydroxymethyl derivative of the amine is then presumably acetylated. It is likely followed by trans-esterification with H_3PO_2 (either in P(V) or in its P(III) tautomeric form) and the intermediate re-arranges to the desired AHPA.

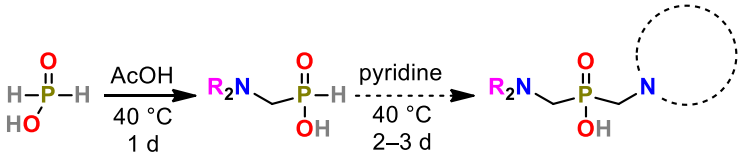

As the AcOH-based protocol cannot be used for synthesis of polyaza-macrocycles with phosphorus acid pendant arms, a new synthetic strategy was sought. Commonly used Kabachnik–Fields (K–F) reaction employing a rather unusual solvent, pyridine, and alkyl esters of *H*-phosphorus acids leads to a very clean reaction (*i.e.* almost no by-products were detected). Reaction is performed in anhydrous solvent under the mild conditions (40 °C, 2–3 d) and requires a strong acid as a catalyst. The best results were achieved with HBr in a form of pyridine hydrobromide. This synthetic strategy accessed the target macrocylic ligands with *P*-aminomethyl group as well as several DOTA derivatives with phosphorus acid pendant arm(s) which are otherwise unavailable. The reaction mechanism follows

the "generally accepted mechanism" of the K–F reaction. Thus, the amine and formaldehyde give the appropriate aminal which is decomposed by the strong acid to the iminium cation and free amine. The final product if formed after the addition of *H*-phosphorus ester (*e.g.* of alkyl *H*-phosphinate) to the iminium cation double bond. This variant of K–F reaction represents the most efficient and general synthesis of polyazamacrocycles with phosphorus acid pendant arms described till now.

Having synthesized the desired ligands, their complexes with Ln(III) ions were prepared and investigated. Firstly, the complexes of ligands with hydrophobic amine pendant arm, Ln–DO3AP^{DBAM} and Ln–DO3AP^{tBPAM}, were studied to elucidate effect of protonation of the amine group on interaction of the complexes with HSA. Properties of the complexes depend on the pendant amine protonation because of the proximity of the pendant amine group to the ligand cavity. The Gd(III) complexes of both ligands are monohydrated regardless of their protonation state and they have a large abundance of the TSA isomer. The hydration breaks in the Ln(III) series are just behind Gd(III); closer to Gd(III) for the complexes with the deprotonated pendant amine group. It leads to a very short water residence times (down to τ_M ~5 ns at 25 °C for the [Gd–do3ap^{DBAM}]$^-$ complex). The Gd(III) complexes non-covalently bind to HSA (mainly to the binding site II). At physiological pH where deprotonated complexes are present, binding of the *N*,*N*-dibenzyl- and *N*-(4-*t*-Bu-benzyl)-containing complexes is ~55 % and ~100 %, respectively. The protonated forms of the complexes have much lower binding affinity than the deprotonated complexes. After binding to HSA, the complexes induce several-fold increase of water proton relaxivity. The observed water proton relaxivities (37 °C, 20 MHz, ~4.5 % (w/w) HSA, pH ~7.4) of Gd–DO3AP^{DBAM} (0.20 mM) and Gd–DO3AP^{tBPAM} (0.12 mM) complexes are ~24.5 mM^{-1} s^{-1} and ~55.3 mM^{-1} s^{-1}, respectively. The latter one is one of the highest relaxivities achieved for a small-sized Gd(III) complex bound to HSA observed till now. The relaxivity enhancement is caused mainly by the quantitative binding of the complex to HSA as well as by the optimally fast water exchange. For the first time, it was proven that interaction of molecules with HSA can be modified by protonation of the molecules. The study shows that pharmacokinetics of drugs (*e.g.* their bloodstream elimination time or their targeted delivery) can be altered by the drug protonation and, thus, by pH of tissues.

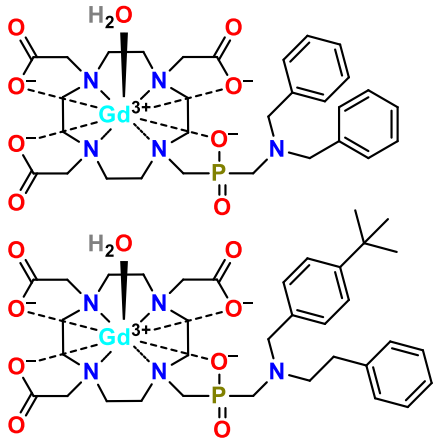

Additionally, one of the largest sets of solid-state structures of Ln(III) complexes of DOTA-like ligands (15 Ln–DO3AP^{DBAM} and 3 Ln–DO3AP^{tBPAM} complexes) was evaluated. The data confirm the expected structural trends in Ln(III) structures with the

DOTA-like ligands (*e.g.* gradually shorter distance Ln(III)–QN_4 with smaller Ln(III) ion as well as "closing" of the opening angle ω and prolongation of the Ln(III)···OH_2 distance). The structures suggest that the pendant *N*,*N*-dibenzylamine group in the Gd–DO3AP^{DBAM} complex can interfere with the water binding site in the complex. Thus, combination of high abundance of the TSA isomer, proximity of the hydration break in the Ln(III) series to Gd(III) and the presence of the hydrophobic group highly increase the water exchange (τ_M ~5 ns; 25 °C).

The simplest DOTA derivative with a nearby amine group to the pendant phosphorus atom is DO3AP^{AM} with the *P*-aminomethyl group. It is also a bifunctional ligand which can be further conjugated to a (bio)vector by the amide bond. The DO3AP^{AcAM} was used as the amide bond-containing model compound which also lacks a protonable amine group. The Gd(III) complexes of the ligands have properties as complexes of common DO3AP^{R}-like ligands with a high TSA isomer abundance and a rather distant hydration break (around Dy(III)). It results in short water residence times (~40 and ~34 ns for Gd–DO3AP^{AM} and Gd–DO3AP^{AcAM}, respectively; 25 °C, pH ~7); however, they are significantly longer than that for Gd–DO3AP^{DBAM}. Surprisingly, properties of Ln–DO3AP^{AM} (*e.g.* SA / TSA isomer ratio) and relaxometric properties of Gd–DO3AP^{AM} are only insignificantly altered with (de)protonation of the pendant amino group. The protonable pendant amine group of DO3AP^{AM} is close to the phosphorus atom. Therefore, the ^{31}P NMR properties of the Ln–DO3AP^{AM} complexes depend on the amine protonation. The presence of Ln(III) ion has several advantages. The ^{31}P resonance frequencies in the complexes are shifted tens-to-hundreds ppm away from the ^{31}P shifts of the endogenous phosphorus-containing compounds. The ^{31}P chemical shift differences between the differently protonated species are significantly increased (the largest observed till now). The ^{31}P relaxation times are significantly shortened. These ^{31}P NMR properties may be very useful for ^{31}P MRS currently lacking a desired sensitivity and reasonable acquisition times. The complexes can be used for ^{31}P MRS pH imaging as their ^{31}P NMR shifts are highly pH sensitive. For the use in MRS, T_2*/T_1 ratio is an important parameter. The best T_2*/T_1 ratio and the ^{31}P NMR properties were found for the Pr– and Yb–DO3AP^{AM} complexes. However, the pK_A of the pendant amine group is ~8.3 and, thus, the Ln–DO3AP^{AM} complexes are not suitable for pH sensing *in vivo*. Thus, the investigations can be considered as *proof-of-concept* studies. As pK_A of the pendant amine group can be tuned (decreased) by its derivatization, future research can lead to ^{31}P MRS contrast agents useful for pH imaging *in vivo*.

The new K–F reaction protocols allowed synthesizing a new ditopic ligand in which two DO3A units are connected by the phosphinic acid group. As the phosphinate group can easily bridge two metal ions, the ligand permits a fully rigid connection of both metal-DO3A units. Thus, properties of the ligand, DO3A–P–DO3A, and its mono- and dimetallic complexes (both homo- and heteronuclear ones) were investigated. The monometallic Ln(III) complexes were characterized in solution and in the solid state. They behave as complexes of a DOTA-like ligand having a bulky pendant arm, and only a simple SA / TSA isomerism was observed. As the monometallic complexes are kinetically inert, there is no exchange between the cavities and / or with an excess of other metal ion. Therefore, the complexes were used for synthesis of heteronuclear dimetallic complexes. Homodimetallic complexes were obtained by a simple reaction of the ligand with excess of a metal ion. Solution and solid-state structural studies confirmed that the phosphinate group serves as a bridge in the dinuclear complexes. In these complexes, combination of independent fluxionality (SA / TSA isomerism) of each formal Ln–DO3AP unit and chirality on the phosphorus atom leads to a complicated isomerism (analogous mutually "knotted" system has not been investigated before). The best description of the isomers employs three different mutual orientations of the macrocycle cavities (represented by their QN_4–QO_4 vectors) and *S* / *R* configuration on the phosphorus atom; two orientations of ligand cavities were observed in the solid state (six structures). Out of 32 possible isomers, approx. eight diastereoisomers were distinguished in solution by ^{1}H / ^{31}P NMR spectroscopy and out of which three-to-four were the major diastereoisomers with overall abundance > 85 %. The homodinuclear GdGd complex has a very short water residence time (τ_M ~7 ns; 25 °C) likely due to the hydration break in the Ln(III) series just behind Gd(III). The GdGd complex has one of the highest relaxivities per Gd(III) (6.2 mM^{-1} s^{-1}; 20 MHz, 25 °C) achieved for a small-sized molecule. Likely, it is result of a highly rigid structure of the dinuclear GdGd complex. Hetero-dimetallic complexes (combination of Gd(III) with Sc(III), Y(III), Eu(III), Lu(III), or Bi(III)) show no significant change of relaxivity with molecular mass of the complexes. The relaxivity is more affected by a different SA / TSA isomer ratio of the complexes due to a strong effect of the other metal ion on the SA / TSA isomerism of the Gd(III) "half" of the molecules.

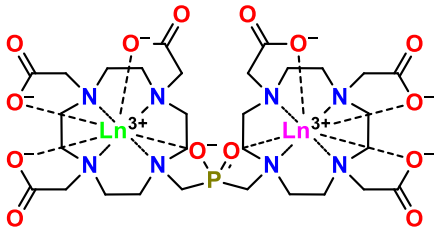

Overall, the Thesis confirms that protonation of the closely located amino group affects various properties of Ln(III) complexes of macrocyclic ligands. The new synthetic protocol has allowed investigation of the entirely rigidly linked dinuclear complexes of DOTA-like ligands for the first time.

List of Abbreviations

General:

CA – contrast agent
DIS – Dysprosium(III)-induced shift
EWG – electron-withdrawing group
EXSY – exchange spectroscopy
FDA – Food and Drug Administration
flexiTPI – flexible twisted projection imaging
IS – inner-sphere
K–F – Kabachnik–Fields
LD_{50} – median lethal dose
LIS – lanthanide(III) induced shift
M–I – Moedritzer–Irani
MI – molecular imaging
MRA – magnetic resonance angiography
MRI – magnetic resonance imaging
MRS – magnetic resonance spectroscopy
N.D. – not determined
NCS – isothiocyanide group (*i.e.* the N=C=S fragment)
NFS – nephrogenic systemic fibrosis
NMRD – nuclear magnetic resonance dispersion
NT – number of scans
OS – outer-sphere
PET – positron emission tomography
QN_4 – centroid of N_4-plane
QO_4 – centroid of O_4-plane
RT – room / laboratory temperature
SA and **SAP** – square antiprism(atic)
SBM – Solomon–Bloembergen–Morgan
SNR – signal-to-noise ratio
SPECT – single-photon emission computed tomography
SS – second-sphere
TMS – trimethylsilyl
TSA and **TSAP** – twisted square antiprism(atic)
TSA′ – "anhydrous" twisted square antiprism(atic) (*i.e.* TSA isomer with $q = 0$)
VT – variable-temperature

Ligand pendant arm abbreviations:

^{ABn} – 4-aminobenzyl
^{AcAM} – (*N*-acetyl)aminomethyl
^{AM} – aminomethyl
^{BP} – ethyl-2,2-bis(phosphonic acids)

Chemical compounds:

2-AEP – (2-aminoeth-1-yl)phosphonic acid
3-APP – (3-aminoprop-1-yl)phosphonic acid
AAZTA – 1,4-bis(carboxymethyl)-6-[bis(carboxymethyl)]amino-6-methylperhydro-1,4-diazepine
AHPA – amino-*H*-phosphinic acid
APA – aminophosphonic acid
ATP – adenosine triphosphate
BSA – *N*,*O*–bis(trimethylsilyl)acetamide
CD – cyclodextrin
DCC – *N*,*N*′-dicyclohexyl-carbodiimide / dicyclohexyl-carbodiimine
DCU – *N*,*N*′-dicyclohexyl-urea
DEP – diethyl phosphite
DO3A – 1,4,7,10-tetraazacyclododecane-1,4,7-triacetic acid
DO3AP – 1,4,7,10-tetraazacyclododecane-4,7,10-tetraacetic-1-methylphosphonic acid
$DO3AP^R$ – 1,4,7,10-tetraazacyclododecane-4,7,10-tetraacetic-1-[(alkyl)methylphosphinic] acid
DOA3P – 1,4,7,10-tetraazacyclododecane-10-acetic-1,4,7-tris(methylphosphonic) acid
DOTA – 1,4,7,10-tetraazacyclododecane-1,4,7,10-tetraacetic acid
DOTAM – 1,4,7,10-tetraazacyclododecane-1,4,7,10-tetraacetamide
DOTP – 1,4,7,10-tetraazacyclododecane-1,4,7,10-tetrakis(methylphosphonic acid)
DTPA – diethylene-triamine-*N*,*N*,*N*′,*N*′′,*N*′′-pentaacetic acid
HMDS – hexamethyldisilazane, bis(trimethyldisilyl)azane
HSA – human serum albumin
IDA – imino-diacetic acid
MS–325 – Ablavar®, Vasovist®
MsOH – methanesulfonic acid
PAMAM – poly(amido-amine), [dendrimer]
PCTA – 3,6,9,15-tetraazabicyclo[9.3.1]pentadeca-1(15),11,13-triene-3,6,9-triacetic acid
PEP – 2-phosphoenolpyruvate
PIN – phosphinic acid
PON – phosphonic acid
py – pyridine
TACN – 1,4,7-triazacyclononane
TFA – trifluoroacetic acid
$TRAP^H$ – 1,4,7-triazacyclononane-1,4,7-tris(methyl-*H*-phosphinic acid)
Z – Cbz, benzyloxycarboxymethyl

^{CE} – 2-carboxyethyl
^{DBAM} – (*N*,*N*-dibenzyl)aminomethyl
^{PrA} – *P*-propionic acid
^{tBPAM} – *N*-[(4-*t*-butyl)-benzyl]-*N*-(2-phenyl-ethyl)aminomethyl

Author's Contributions

Data presented in this Thesis are multidisciplinary and some of them were obtained through collaborations. However, Author declares the vast majority of the work was conducted by himself. It means he elaborated all the synthetic strategies, synthetic work (preparation of precursors, ligands and their complexes) as well as samples preparation for advanced measurements. Author also did all the 1D / 2D NMR measurements, NMR titrations, luminescence measurements and variable-temperature (VT) UV-VIS experiments, and all interpretation of the data measured by others (*e.g.* MS and some advanced NMR spectra). Moreover, author acquired the VT ^{1}H NMRD profiles and VT ^{17}O NMR data during his scientific stays and directly participated in the fittings of the data. All single crystals were obtained by Author. Author also interpreted the measured / fitted data.

Nevertheless, some of the measurements and evaluations were conducted by others who are gratefully acknowledged as follows. The honest gratitude belongs to Dr. Ivana Císařová and Doc. Jan Kotek who measured and refined, respectively, all the single-crystal X-ray data on crystals prepared by the Thesis author. Another appreciation belongs to Mgr. Zuzana Böhmová and RNDr. Jana Havlíčková for all the potentiometric titrations. The final fittings of relaxometric data, and a small part of their measurements, were done by Prof. Mauro Botta and Dr. Fabio Carniato (both at University of Eastern Piedmont, Alessandria, Italy) during / shortly after the Author's scientific stays. Luminescence data acquisition of complexes of the "dimer" ligand DO3A–P–DO3A was done under supervision of Prof. Stephen Faulkner during Author's scientific stay at University of Oxford (Oxford, UK). Author prepared manuscripts for the hereby presented publications and actively contributed to finalization of the manuscripts.

_____

Peter Urbanovský

Acknowledgements

Whom would I express my sincere gratitude more than to my supervisor, prof. Petr Hermann? It would not be possible to finish this Thesis without his help and guidance, and without him making me constantly motivated and scientifically curious. I also thank him for (trying to) "keep me on a leash" and not starting a new project before completing the previous one. It took me several years to understand the importance of the conscientious enclosing (*i.e.* publishing) of the current ongoing project. Let it be a lesson for me and a serious warning for others…

From the scientific world, let me thank the co-supervisor, officially labelled as my advisor, doc. Jan Kotek, who essentially contributed to all "my" crystallographic publications as well as to my reckless path to have a real challenge for my PhD degree. Furthermore, it must not be forgotten who measured and solved all the single-crystal structures, Dr. Ivana Císařová, "my hat is off"! Many more contributed to finishing of the work presented in this Thesis, namely: Ondřej Zemek (MS service), Dr. Zdeněk Tošner (advanced NMR), Zuzana Böhmová and Dr. Jana Havlíčková (potentiometry service), doc. Vojtěch Kubíček (advices), Adam Svítok (advanced NMR), Dr. Fabio Carniato and prof. Mauro Botta (help with ^{1}H NMRD and VT ^{17}O NMR acquisition and the data evaluation), Dr. Robert Edkins and prof. Stephen Faulkner (help with advanced luminescence data acquisition and supervising).

From the workplace, my honest gratitude goes to the "malý lab 313" – to the previous, the current and, surely, the future colleagues, friends – many interesting topics were discussed and, only because of them, I could stay positive and happy to return there every day / night. One very special thanks goes to Adam Svítok who did the last English corrections of this Thesis in a swift rush.

Last but not least, my gratefulness goes to my parents without whom I would not achieve any of "this", to my family for supporting me in my scientific path, and to my "beloved half" for keeping me in the "alert mode" regarding research chemistry topics and being with me in this unforgettable journey through life.

Appendices

Content:

Appendix A – Synthesis of amino-*H*-phosphinic acids.
The published paper (Urbanovsky, P. *et al*. Selective and clean synthesis of aminoalkyl-*H*-phosphinic acids from hypophosphorous acid by phospha-Mannich reaction. *RSC Adv.*, 10, **2020**, 21329–21349.) about synthesis of AHPAs (see Chapter 4.1)

Appendix B – Reactions of *H*-phosphites and *H*-phosphinates with amines.
Data on Kabachnik–Fields reaction in pyridine (see Chapter 4.2)

Appendix C – Interaction of protonable MRI CAs (with *N*-benzyl groups) with HSA.
The published paper (Urbanovsky, P. *et al.* Lanthanide complexes of DO3AP–(dibenzylamino)methylphosphinate: effect of protonation of the dibenzylamino group on the water-exchange rate and the binding of human serum albumin. *Inorg. Chem.*, 58, **2019**, 5196–5210.) about Ln–DO3AP^{DBAM} complexes and interaction with HSA (see Chapter 5.1)

Appendix D – Interaction of protonable MRI CAs (with (4-*t*-butyl)benzyl group) with HSA.
Data on Ln–DO3AP^{tBPAM} complexes and their interaction with HSA (see Chapter 5.1)

Appendix E – X-ray structures of complexes with *N*-benzyl groups.
The published paper (Urbanovsky, P. et al. The solid-state structures and ligand cavity evaluation of lanthanide(III) complexes of a DOTA analogue with a (dibenzylamino)methyl-phosphinate pendant arm. *Dalton Trans.*, 49, **2020**, 1555–1569.) about evaluation of the solid-state structures of Ln–DO3AP^{DBAM} complexes (see Chapter 5.2)

Appendix F – X-ray structures of complexes with *N*-((4-*t*-butyl)benzyl) group.
Data on the solid-state structures of Ln–DO3AP^{tBPAM} complexes (see Chapter 5.2)

Appendix G – Complexes of DO3AP^{R} with aminomethyl- and acetyl-amidomethyl-phosphinic acid pendant arms.
Data on solution behaviour, and relaxometric and ^{31}P MRS evaluations of Ln–DO3AP^{AM} and Ln–DO3AP^{AcAM} complexes (see Chapter 6)

Appendix H – X-ray structures of DO3AP^{R} with aminomethyl- and acetyl-amidomethyl-phosphinic acid pendant arms.
Data on the solid-state structures of Ln–DO3AP^{AM} and Ln–DO3AP^{AcAM} complexes (see Chapter 6.1)

Appendix I – Mono- and dimetallic complexes of the DO3A–P–DO3A.
Data on the ligand and its mono- and dimetallic homo- and heteronuclear complexes (see Chapter 7)